9. Supplements

9.1. Publication I

Chuman, T., Oulehle, F., Zajícová, K., Hruška, J., 2021. The legacy of acidic deposition controls soil organic carbon pools in temperate forests across the Czech Republic. European Journal of Soil Science 72, 1780–1801. https://doi.org/10.1111/ejss.13073

Received: 3 June 2020 | Revised: 8 September 2020 | Accepted: 11 November 2020

DOI: 10.1111/ejss.13073

ORIGINAL ARTICLE

European Journal of Soil Science WILEY

The legacy of acidic deposition controls soil organic carbon pools in temperate forests across the Czech Republic

Tomáš Chuman[1,2] | **Filip Oulehle**[1,3] | **Kateřina Zajícová**[2] | **Jakub Hruška**[1,3]

[1]Czech Geological Survey, Prague 1, Czech Republic

[2]Faculty of Science, Department of Physical Geography and Geoecology, Charles University, Prague 2, Czech Republic

[3]Global Change Research Institute, Brno, Czech Republic

Correspondence
Tomáš Chuman, Czech Geological Survey, Klárov 3, 118 21 Prague 1, Czech Republic.
Email: tomas.chuman@email.cz

Funding information
Czech Geological Survey, Grant/Award Number: 331700; The Czech Science Foundation (GACR), Grant/Award Number: 18-17295S; Ministry of Education, Youth and Sports of the Czech Republic, Grant/Award Number: PROGRES; National Sustainability Program I, Grant/Award Number: LO1415

Abstract

Temperate forest ecosystems store most of the organic carbon in soils (SOC), and changes in the soil carbon stock due to climate change or land management can potentially have a large influence on carbon balance. The most important factors controlling the SOC pool on a global scale are generally agreed upon; however, estimations of SOC pools differ significantly among studies at regional and local scales due to different sampling protocols and local scale variability. This study evaluates the SOC pool in the forest floor and mineral soil sampled down to a depth of 80 cm in 14 forested catchments with variable environmental conditions and soil acidification and eutrophication legacies, and determines the best explanatory variables of the SOC pool. The average SOC pool of 34 t ha^{-1} measured in the forest floor (O horizon) was best explained by measures of historical sulphur (S) deposition (i.e., soil acidification legacy) and forest type (conifer vs. broadleaf forest). An average total SOC pool of 132 t ha^{-1}, combining both the carbon pool in the mineral soil down to 80 cm and the carbon pool in forest floor, was best explained solely by elevation, which reflects temperature and precipitation gradients. However, when considering the coupled SOC pool in the forest floor and upper half of the sampled mineral soil (down to 40 cm), natural environmental factors were outweighed by anthropogenic ones (soil acidification legacy and forest type). This has important implications for understanding potential SOC pool changes under ongoing global climate change, especially in regions currently or historically affected by soil acidification caused by acid deposition. The acidification effect on the SOC accumulation and subsequent soil recovery after acidification retreat might affect carbon balance.

Highlights

- The SOC pool is dependent on soil acidification legacy, forest type and climatic gradient.
- Anthropogenic factors outweigh the natural ones if shallow sampling is carried out.

- Shallow sampling commonly carried out in forest soils underestimates the SOC pool.
- Soil acidification caused SOC accumulation and subsequent soil recovery might lead to carbon loss.

KEYWORDS

acidification recovery, broadleaf forest, Cambisols, coniferous forest, forested catchments, Podzols, soil carbon content

1 | INTRODUCTION

Forest ecosystems play significant roles in the terrestrial carbon cycle due to the land-atmosphere CO_2 exchange (Lorenz & Lal, 2010). In temperate forest ecosystems, more than 60% of the total carbon is stored in the forest floor and mineral soil (Watson et al., 2000) (hereafter soil organic carbon [SOC]). At a global scale, climate (reflecting temperature and moisture gradients) is the principal factor explaining spatial SOC variability due to its influence on forest productivity and decomposition activity (Bellamy, Lovejoy, Bradley, Lark, & Kirk, 2005; Chiti, Díaz-Pinés, & Rubio, 2012; Liski, Perruchoud, & Karjalainen, 2002; Lorenz & Lal, 2010). At local scales, SOC pools can vary significantly due to the influence of other environmental factors such as soil parent material (Barré et al., 2017), soil properties (texture, bulk density and soil type) (Callesen et al., 2003; Conforti, Lucà, Scarciglia, Matteucci, & Buttafuoco, 2016; Schöning, Morgenroth, & Kögel-Knabner, 2005) and topography (slope, slope curvature and landscape position) (Callesen et al., 2003; Conforti et al., 2016; Garcia-Pausas et al., 2007). Topography has been identified as an important variable explaining SOC pool variability due to influences on the soil moisture regime (Buczko et al., 2017; Callesen et al., 2003). Furthermore, one of the main processes leading to the stabilization of organic matter in well-drained soils is the association with minerals with large specific surface areas (clays, short-range order and amorphous inorganic phases such as imogolite, allophane, ferhydrite and other poorly defined Al and Fe phases) (Grand & Lavkulich, 2011; Schöning et al., 2005; Spielvogel, Prietzel, & Kögel-Knabner, 2008).

Besides natural environmental factors, SOC pools can vary significantly due to the influence of anthropogenic factors such as land use or forest management practices (Achat, Fortin, Landmann, Ringeval, & Augusto, 2015; Chiti et al., 2012; Hofmeister, Oulehle, Krám, & Hruška, 2008; Lal, 2005; Liptzin & Seastedt, 2010; Lützow et al., 2006; Mou, Jones, Guo, & Lister, 2005; Nabuurs et al., 2008; Schulp, Nabuurs, & Verburg, 2008; Tan et al., 2004), and can also be altered by anthropogenic influences through the input of acidifying compounds such as sulphur (S) or growth-limiting nutrients such as nitrogen (N) (Moldan, Kjønaas, Stuanes, & Wright, 2006; Oulehle et al., 2008).

Besides the above-mentioned studies showing variability of environmental factors controlling the SOC pool, there are also differences in the SOC pool size independent of environmental factors. This fact can be attributed to different sampling protocols, especially sampling depth, and methods of SOC assessments, for instance whether the bulk density is directly measured or is calculated by using pedotransfer functions. A majority of studies assessing SOC pools in forest soils and determining driving factors have considered only the upper 20–30 cm (including the forest floor) where the highest SOC concentrations usually occur, often neglecting the deeper mineral soil horizons (Baritz, Seufert, Montanarella, & Van Ranst, 2010; Burke et al., 1989; Conen et al., 2005; Homann, Bormann, & Boyle, 2001; Innangi, d'Alessandro, & Fioretto, 2015; IPCC, 2003; Janssens et al., 2005; Jones, Hiederer, Rusco, & Montanarella, 2005; Taylor, Wang, & Chen, 2007; Yanai et al., 2003). However, the amount of SOC stored in the lower mineral soil (below the top 30 cm) often exceeds 50% of the total SOC in most ecosystems (Harrison, Footen, & Strahm, 2011; Jobbágy & Jackson, 2000; Rumpel & Kögel-Knabner, 2011; Wang, Li, Ye, Chu, & Wang, 2010). For instance, Batjes (1996) showed that measuring SOC only from the depth of 0–30 cm underestimates the content of SOC, especially in forest ecosystems. This issue was also addressed by Schmidt et al. (2011), who additionally pointed out that the response of lower mineral SOC to changes (e.g. land-use changes) can equal that from the top 30 cm of soil. Despite this, only shallow depths are still explicitly represented in some studies (e.g., Baritz et al., 2010; Innangi et al., 2015; Morais, Teixeira, & Domingos, 2019) modelling the SOC pools. Furthermore, SOC stored in deeper mineral soils often represents the most recalcitrant part of soil C with long turnover times (Lorenz, Lal, & Shipitalo, 2011; Schmidt et al., 2011; Schöning et al., 2005), and its pool is controlled by other factors than those in the topsoil SOC (Chen et al., 2018; Rumpel & Kögel-Knabner, 2011;

Salomé, Nunan, Pouteau, Lerch, & Chenu, 2010; Schmidt et al., 2011).

When used for modelling of the effects of ecosystem transitions under climate change (potential carbon sequestration and emission) such significant differences in estimated SOC pools and their driving factors can generate very inconsistent results. This is especially true for temperate forest soils, which are one of the largest terrestrial carbon stores (Watson et al., 2000). Small variations in this pool caused, for instance, by changes in biomass productivity controlled by climate and nutrient availability or changes in forest management, can significantly affect soil properties (nutrient retention, water holding capacity, etc.), and consequently the carbon balance (potential carbon sequestration).

Therefore, the specific objectives of this study were: (a) to determine SOC pools in the forest floor and in mineral soil down to the 80-cm depth in 14 temperate forest catchments representing climate and acidification gradients; (b) to specifically examine relationships between SOC pools and environmental variables (elevation, geology, mean annual temperature, mean annual precipitation, forest type, historical sulphur and nitrogen deposition, bulk density and soil texture); and (c) to assess the sensitivity of environmental explanatory variables to changing sampling depth.

This study is unique in that it covers soils recovering from acidification within the temperate forest zone in central Europe, where an unprecedented high deposition of sulphur (Kopáček & Veselý, 2005), especially in the region of the so called "Black Triangle" on the German-Polish-Czech border, led to severe soil and surface water acidification (Hruška, Moldan, & Krám, 2002; Kopáček & Veselý, 2005; Navrátil, Kurz, Krám, Hofmeister, & Hruška, 2007; Oulehle, Hofmeister, Cudlín, & Hruška, 2006), forest declines and vegetation changes (Schulze, Lange, & Oren, 1989; Vávrová, Cudlín, Vavříček, & Cudlín, 2009). The results are also relevant to other regions of temperate forest soils recovering from acidification, such as in North America and elsewhere in Europe (Norton, Kopáček, & Fernandez, 2013; Oulehle et al., 2017), or currently threatened by ongoing acidification in Asia (Bouwman, Van Vuuren, Derwent, & Posch, 2002; Duan et al., 2016; Vet et al., 2014).

2 | MATERIALS AND METHODS

We sampled soils in 14 long-term monitored catchments across the Czech Republic (GEOMON; Oulehle et al., 2017) (Figure 1). To capture most of the carbon stored in the soil, sampling was based on quantitative soil pits by excavating the forest floor mass and then the soil mass to a depth of

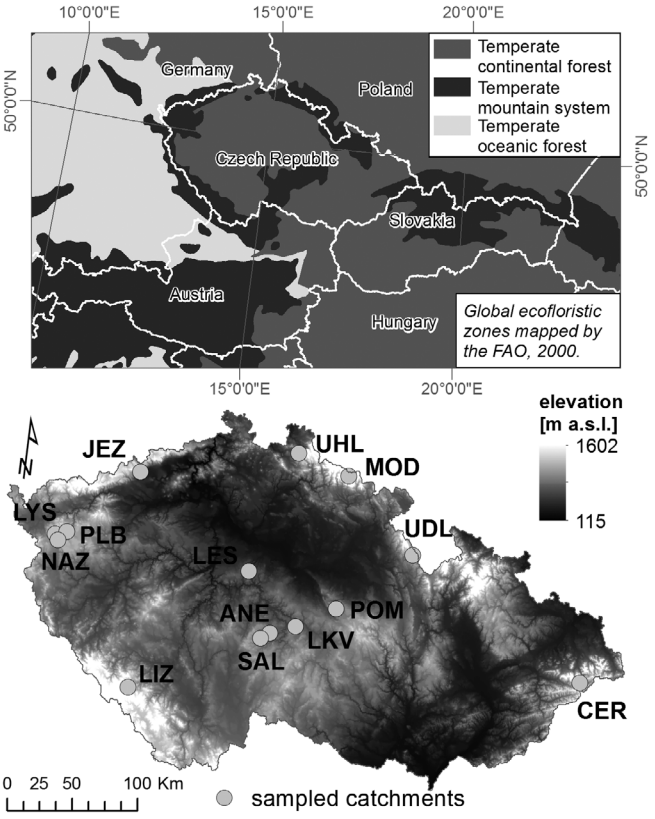

FIGURE 1 Location of studied catchments. ANE, Anenský potok; CER, Červík; JEZ, Jezeří; LES, Lesní potok; LIZ, Liz; LKV, Loukov; LYS, Lysina; MOD, Modrý potok; NAZ, Na zeleném; PLB, Pluhův Bor; POM, Polomka; SAL, Salačova Lhota; UDL, U dvou louček; UHL, Uhlířská

80 cm of mineral soil within a 0.5 m^2 reference frame (according to Huntington, Ryan, & Hamburg, 1988). Within this reference frame each soil profile was excavated in several horizons as follows: Oi (L)-layer, Oe (F)-layer + Oa (H)-layer, and the mineral soil in horizons specified by the depths 0–10 cm, 10–20 cm, 20–40 cm and 40–80 cm. The sampling depth was set arbitrarily following the method proposed by Huntington et al. (1988).

In the field, excavated material from each horizon was weighed, sieved through a 1-cm sieve, and separated into stones, soil <1 cm and coarse roots. Each separated fraction was weighted; 2 kg of bulk soil <1 cm was then taken to the laboratory, where moisture was determined (as the difference between the fresh weight and after 24 hr of oven-drying at 105°C). Samples were air-dried and sieved through a 2-mm sieve to allow determination of the soil skeleton content (stones >1 cm + stones >2 mm), fine earth (<2 mm) and roots (>1 cm, + >2 mm), enabling the quantification of the total weight of fine earth and soil skeleton, and the calculation of the SOC pool without the need for using pedotransfer functions. We also described soil profiles in excavated pits according to FAO guidelines (FAO, 2006) and

TABLE 1 Environmental characteristics of the studied catchments and number of soil pits

Catchment code	Mean elevation (m a.s.l)	Mean annual temperature (°C)	Mean annual precipitation (mm)	Mean stand age category Years	Bedrock	Coefficient of alkalinity	Vegetation cover (%)			Number of soil pits	Area (ha)
							Clearcuts, open spaces	Conifers	Broadleaf		
ANE	523	8	651	41–60	Gneiss	Low Calk	12	87	1	5	27
CER	805	6	1,293	41–60	Sandstone	Very low Calk	3	88	10	10	185
JEZ	746	6	773	61–80	Gneiss	Low Calk	7	50	43	13	261
LES	478	8	625	41–60	Granite	Low Calk	3	39	58	8	70
LIZ	926	5.5	894	61–100	Gneiss	Low Calk	9	85	6	10	99
LKV	606	7.5	737	41–80	Granite	Low Calk	3	90	7	7	66
LYS	880	5	972	41–60	Granite	Low Calk	1	99	0	5	27
MOD	1,188	3	1778	101–120	Mica schist	Low Calk	63	40	0	9	262
PLB	754	6	913	61–100	Serpentinite	Very high Calk	19	81	0	5	22
POM	612	7	696	61–80	Gneiss	Low Calk	13	71	16	7	69
SAL	646	7	630	61–80	Gneiss	Low Calk	7	92	1	10	168
UDL	912	5	1726	21–40	Gneiss	Low Calk	5	90	5	6	33
UHL	818	5.5	1,181	21–40	Granite	Low Calk	16	84	0	10	187
NAZ	779	5.5	770	21–60	Amphibolite	High Calk	12	85	3	7	53

Note: Coefficient of alkalinity is showing the bedrock alkali and alkaline-earth metal content, based on silicate rock analysis, calculated as follows: Calk = (Na + K + Li + Ca + Mg + Ba + Sr)/(Si + Ti + Al + Fe + Mn + Na + K + Li + Ca + Mg + Ba + Sr). The concentrations of elements are in mol kg^{-1}. Categories in the table are: very high Calk >0.4, high Calk = 0.25–0.4, low Calk = 0.1–0.2, very low Calk = 0.05–0.1. ANE, Anenský potok; CER, Červík; JEZ, Jezeří; LES, Lesní potok; LIZ, Liz; LKV, Loukov; LYS, Lysina; MOD, Modrý potok; NAZ, Na zeleném; PLB, Pluhův Bor; POM, Polomka; SAL, Salačova Lhota; UDL, U dvou louček; UHL, Uhlířská.

classified soil types according to WRB 2014 (IUSS Working Group WRB, 2015). Air-dried soil samples were then analysed for organic carbon and texture. All SOC concentrations were determined by dry combustion with a CNS FLASH 2000 Elemental Analyser (Thermo Fisher Scientific, Waltham, MA). Soil texture was analysed by a hydrometer method (ISO 11277, 2009) and textural classes were defined according to USDA particle sizes.

Soil samples were taken during the vegetation season from June to September in 2015 except for the Uhlířská and Červík catchments sampled 1 year earlier. The number of soil pits varied according to the catchment size, from 5 to 13 soil pits (Table 1). Positions of soil sampling pits within catchments were chosen by stratified random sampling as follows: each catchment was divided into homogeneous units based on the forest stand age and the ecological category of the forest sites (so-called forest-site complexes reflecting edaphic conditions; see Viewegh, Kusbach, & Mikeska, 2003). The position of soil sampling pits was then generated randomly within these homogeneous units.

The resulting comprehensive dataset of 112 soil profiles (669 soil samples) across 14 long-term monitored catchments was used to calculate the SOC stock in the forest floor (O horizon), and the mineral soil down to 80 cm, both in total and separately for different depths. In most catchments mineral soils were at least 80 cm deep, thus samples from all six defined soil layers were collected. Only in the Uhlířská catchment, were soils shallower, with an average mineral soil depth of 47 cm. Most of the soils were classified as Cambisols (60%) and Podzols (22%), whereas 8% of soils showed stagnic properties and were classified as Stagnosols. Out of 112 soil pits, there were 11 soil profiles classified as hydromorphic soils (Histosols or Gleysols).

Potential explanatory variables were either determined in the field (forest type; i.e., the proportion of broadleaf trees and conifers assessed in a 400 m^2 circular plot surrounding each soil pit), in the laboratory (soil texture), by performing spatial analysis in ArcGIS, or extracted from long-term measurements. Spatial analysis in ArcGIS was used to determine elevation (derived from the Digital Elevation Model with 25-m pixel size), the geochemical reactivity of rocks (showing the bedrock alkali and alkaline-earth metal content and susceptibility to weathering, according to Chuman, Gürtlerová, Hruška, and Adamová (2014)) and mean annual temperature (Tolasz, Míková, Valeriánová, & Voženílek, 2007). The amount of annual precipitation was derived from monthly measurements of bulk precipitation available from GEOMON catchments since 1994. Sulphur and nitrogen depositions from the 1980s were extracted from grid maps produced by Oulehle et al. (2016). We used calculated S and N depositions for the year 1980, when the depositions peaked in central Europe (Kopáček & Veselý, 2005; Mylona, 1996), to capture the legacy of soil acidification and eutrophication. We also used forest age, derived from forest management inventories, as an explanatory variable. These inventories record the year of planting of every forest stand and are regularly updated.

2.1 | Comprehensive catchment characteristics

The sampled catchments (Figure 1) covered a range of environmental characteristics (Table 1). Mean catchment elevation ranged from 523 to 1,188 m a.s.l., mean annual temperatures from 3 to 8°C and mean annual precipitation from 630 to 1780 mm. Most catchments were underlain by metamorphic rocks (gneiss or schist), whereas Pluhův Bor consisted of serpentinite, Uhlířská, Lysina and Lesní potok were underlain by granite, Na zeleném by amphibolite and Červík by tertiary sandstone (Table 1). Except for Pluhův Bor and Na zeleném, these soil parent materials were low in alkali and alkaline-earth metal contents. Catchments were completely forested by managed forests; the only exception was Modrý potok, where the catchment extends above the alpine tree line, but the alpine part of the Modrý potok catchment was not sampled. The dominant tree species were Norway spruce (*Picea abies* (L.) Karst) and European beech (*Fagus sylvatica* L.), which was present at Jezeří, Lesní potok and Červík. Scots pine (*Pinus sylvestris* L.) was frequent at Pluhův Bor. The humus form was mull at the beech-dominated stands and mor at the spruce or pine-dominated stands. The age of forests ranged from planted young seedlings to more than 120-year-old stands. The area-weighted average stand age for catchments was between 40 and 80 years. The oldest stands were in the Modrý potok catchment, at more than 120 years old. The catchments have never been deforested to our knowledge over the last 200 years. There were only small historical meadows in the Anenský potok, Modrý potok and Pluhův Bor catchments found on the old maps (second military survey of the Habsburg Empire at scale 1:28,800 and Cadastral maps of the Habsburg Empire at scale 1:2,880) from the middle 19th century, but the soils were not sampled at these particular plots.

2.2 | Statistical analysis

We applied a linear mixed effect model for analysis of the relationship between the soil organic carbon stock and environmental variables. The analysis was run in the R program (R Development Core Team, 2013) with the package "nlme" (Pinheiro et al., 2017). The individual catchments were set as random effects and the

TABLE 2 Spearman rank order correlation coefficients among explanatory variables used to find best explanatory variables of the soil organic carbon pool

	Mean elevation	Mean annual temperature	Mean annual precipitation	S_{tot} deposition 1980	N_{tot} deposition 1980	Fine earth content	Sand	Silt	Clay	Conifers	Broadleaf
Mean elevation (m a.s.l.)	1	**−0.94**	**0.83**	0.57	**0.81**	−0.44	0.22	−0.03	−0.43	0.12	−0.27
[a] Mean annual temperature (°C)	**−0.94**	1	**−0.83**	**−0.63**	**−0.82**	0.49	−0.20	0.00	0.45	−0.10	0.23
[a] Mean annual precipitation (mm)	**0.83**	**−0.83**	1	**0.72**	**0.93**	−0.42	0.11	0.06	−0.34	−0.01	−0.17
S_{tot} deposition 1980 (kg ha^{-1})	0.57	**−0.63**	**0.72**	1	**0.91**	−0.35	0.06	0.17	−0.44	−0.17	0.06
[a] N_{tot} deposition 1980 (kg ha^{-1})	**0.81**	**−0.82**	**0.93**	**0.91**	1	−0.41	0.10	0.11	−0.44	−0.08	−0.07
Fine earth content (t ha^{-1})	−0.44	0.49	−0.42	−0.35	−0.41	1	−0.28	0.19	0.31	0.07	−0.02
[a] Sand (%)	0.22	−0.20	0.11	0.06	0.10	−0.28	1	**−0.91**	**−0.64**	0.03	−0.14
Silt (%)	−0.03	0.00	0.06	0.17	0.11	0.19	**−0.91**	1	0.25	−0.08	0.15
Clay (%)	−0.43	0.45	−0.34	−0.44	−0.44	0.31	**−0.64**	0.25	1	0.08	0.04
[a] Conifers (%)	0.12	−0.10	−0.01	−0.17	−0.08	0.07	0.03	−0.08	0.08	1	**−0.86**
Broadleaf (%)	−0.27	0.23	−0.17	0.06	−0.07	−0.02	−0.14	0.15	0.04	**−0.86**	1

[a]Marked variables were excluded from statistical analysis due to strong correlation. Correlation is significant at the 0.05 level. S_{tot}- total sulphur deposition, N_{tot}

environmental variables were set as fixed effects. Data on soil organic carbon pools were either square root or log transformed prior to analysis to meet normal distribution. Highly correlated explanatory variables (Spearman rank order correlation coefficient >0.6) were excluded from the analysis (Table 2). This applied to the mean annual precipitation, mean annual temperature and historical nitrogen deposition, which were all strongly correlated with elevation. Historical N deposition was also correlated with historical S deposition. We included only historical S deposition, which was less strongly correlated with elevation in comparison with N deposition, in the analysis. Of the forest type variables, only the proportion of broadleaf trees was used. We calculated the AIC (Akaike information criterion) values for every possible combination of explanatory variables (mean elevation, S deposition, proportion of broadleaf trees, fine earth content, percentage of silt and percentage of clay) using the MuMIn package (Bartoń, 2013), and the most parsimonious model was selected based on the lowest AIC value. The piecewiseSEM (Lefcheck, 2015) package was run to obtain marginal variability and the marginal R ̂2 (based on fixed effects only). All statistical tests were performed with a significance level of 5% ($\alpha \leq 0.05$).

3 | RESULTS

Sampled soils showed high variability in physical characteristics as well as soil organic carbon pools (Table 3). The average fine earth mass (soil particles <2 mm) across all soil pits was 6,348 t ha^{-1} (standard deviation. ± 2,458) (dry mass) and the mass of soil skeleton (rock fragments) was 5,611 t ha^{-1} (standard deviation ± 2,728). The average dry mass weight of roots was 18.6 t ha^{-1} (standard deviation ± 27.4). The lowest average mass of the fine earth fraction was in the Uhlířská catchment (3,096 t ha^{-1}), where the soils were the shallowest, and the highest was in the Lesní potok catchment (10,560 t ha^{-1}), where the soils had a very low content of soil skeleton. Soil texture was comparable among the catchments and showed rather low variability (Figure 2). Most samples were determined as sandy loam and loam (Figure 2). The average clay content across all samples was 11.1% (standard deviation ± 4.5), ranging from 6.5% (standard deviation ± 1.9) in the Modrý potok catchment to 18.1% (std. ± 5.9) in the Salačova Lhota catchment.

TABLE 3 Average values of determined soil parameters across all soil pits and all catchments

	Mean	Standard deviation
O horizon thickness (cm)	6.7	3.0
O horizon mass (t ha^{-1})	86.4	55.9
Fine earth mass (t ha^{-1})	6,348.0	2,458.2
Root mass (t ha^{-1})	18.6	27.4
Soil skeleton mass (t ha^{-1})	5,611.1	2,728.2
SOC pool in O horizon (t ha^{-1})	34.0	20.2
SOC pool in 0–80 cm of mineral soil	97.8	35.4
SOC pool in O horizon + 0–80 cm of mineral soil	131.9	41.2

The SOC pools were calculated separately for the forest floor (organic O horizon) and mineral soil horizons (Tables 3, 4). Hydromorphic soils (Histosols and Gleysols found in 11 pits) were excluded from the analysis due to their specific soil properties, for example high carbon stocks due to anaerobic conditions which impede decomposition of soil organic matter. The soils from all pits could be characterized as follows (Tables 3, 4). (a) The forest floor (O horizon) thickness ranged from 1.5 to 15 cm with an average value of 6.7 cm. (b) The average forest floor dry mass was 86 t ha^{-1} with an SOC pool of 34 t ha^{-1} (mean C concentration of 39.5%). The dry mass of the forest floor varied substantially, with the lowest mass (36 t ha^{-1}) in the Loukov catchment and the highest mass of 156 t ha^{-1} in the Uhlířská catchment. (c) The average SOC pool in mineral soil was almost three times higher (98 t ha^{-1}) compared to the forest floor. The SOC pool in the mineral soil was lowest in the Salačova Lhota catchment (60 t ha^{-1}) and

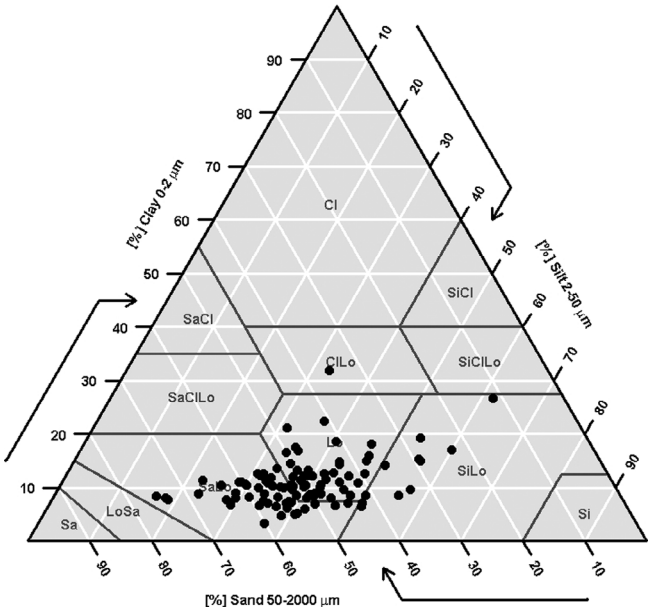

FIGURE 2 Soil texture diagram of sampled soils based on mean values of clay, silt and sand for the whole profile (created by using the "soiltexture" package for R). Abbreviations: Cl, clay; Lo, loam; Sa, sand; Si, silt. The arrows indicate the direction of reading of the percentages of sand, silt and clay (e.g., clay percentages are read from left to right across the triangle, silt percentages are read from the upper right to lower left)

TABLE 4 Average values of determined soil parameters across catchments[1]

				Catchment												
				ANE	CER	JEZ	LES	LIZ	LKV	LYS	MOD	PLB	POM	SAL	UDL	UHL	NAZ
Number of soil pits				5	10	12	8	9	6	4	9	4	5	9	5	8	7
O horizon thickness (cm)			Mean	3.9	7.5	7.4	5.3	5.9	4.3	8.3	8.5	6.7	5.9	5.8	8.0	2.6	4.3
			Std	1.5	3.5	2.7	1.7	3.0	1.8	4.2	3.5	2.7	1.3	1.5	0.8	2.1	1.9
Fine earth (t ha^{-1})	Depth layer	0–10 cm	Mean	772	490	322	954	346	688	544	498	678	837	570	487	466	521
			Std	77	214	138	110	126	234	273	151	88	68	192	153	121	173
		10–20 cm	Mean	1,054	672	427	1,254	460	776	677	601	1,077	878	790	822	616	726
			Std	107	229	166	177	154	216	351	149	441	148	263	296	153	162
		20–40 cm	Mean	2,436	1,254	1,174	2,739	1,260	1,517	1802	1,556	1,468	2061	2009	3,805	1,353	1719
			Std	206	236	398	480	324	332	480	437	381	339	433	4,401	507	469
		40–80 cm	Mean	5,183	2,505	2,816	5,614	3,573	3,549	4,138	3,400	2,177	4,073	4,338	2,915	1762	3,769
			Std	680	677	690	913	1780	853	2,326	969	989	640	1,472	1,239	313	1,343
Soil skeleton (t ha^{-1})	Depth layer	0–10 cm	Mean	154	508	876	104	568	384	528	679	241	164	586	355	333	356
			Std	57	339	599	72	350	62	169	401	75	46	186	237	153	206
		10–20 cm	Mean	306	503	913	230	743	482	523	693	496	341	812	469	356	666
			Std	117	270	348	157	281	101	294	225	64	64	342	202	134	238
		20–40 cm	Mean	736	951	1,788	535	1,442	1,137	1,362	1,483	2,123	915	1,625	2,169	779	1,378
			Std	208	490	481	399	554	260	311	351	649	533	552	1,069	362	587
		40–80 cm	Mean	2,430	2,185	4,372	2,899	4,086	2,709	3,110	4,207	6,238	2,592	3,460	4,549	1,176	3,293
			Std	929	1,120	760	3,415	1,274	823	1,175	1,138	712	480	1,489	1,654	205	1,539
Roots (t ha^{-1})	Depth layer	0–10 cm	Mean	12.8	26.7	2.8	22.0	8.5	15.8	11.5	3.1	23.5	6.1	17.4	2.4	5.7	32.6
			Std	6.6	43.6	4.9	9.8	4.4	9.6	12.2	5.0	14.7	3.9	11.6	2.9	7.8	40.0
		10–20 cm	Mean	1.3	6.0	0.3	4.6	3.9	1.8	0.1	0.8	11.1	0.6	2.0	0.0	1.1	1.3
			Std	1.5	6.6	0.8	2.7	6.5	1.7	0.2	1.8	18.0	0.8	2.1	0.0	1.9	2.0
		20–40 cm	Mean	0.8	6.6	2.1	1.9	3.0	1.6	0.0	0.4	0.0	0.2	1.1	0.0	0.7	2.2
			Std	1.0	6.2	4.2	1.5	4.7	1.2	0.0	1.3	0.0	0.4	2.4	0.0	1.8	3.7
		40–80 cm	Mean	0.2	6.5	0.8	1.0	0.1	0.3	0.0	0.0	0.0	0.0	0.0	0.0	0.0	0.0
			Std	0.4	9.5	2.3	1.8	0.3	0.8	0.0	0.0	0.0	0.0	0.0	0.0	0.0	0.0
		O horizon	Mean	22.3	35.3	43.5	23.6	23.0	16.0	36.5	36.7	47.8	32.6	32.4	43.5	58.7	21.3
			Std	13.4	10.3	23.9	18.2	8.7	7.8	15.9	19.0	33.6	11.9	11.3	11.1	17.8	12.6

(Continues)

TABLE 4 (Continued)

				Catchment												
				ANE	CER	JEZ	LES	LIZ	LKV	LYS	MOD	PLB	POM	SAL	UDL	UHL	NAZ
SOC pool (t ha^{-1})	Depth layer	0–10 cm	Mean	34.3	27.8	28.0	35.4	35.2	28.8	33.9	33.6	36.2	35.4	23.2	42.1	35.1	41.2
			Std	3.7	9.7	13.6	7.6	10.0	9.3	5.4	10.3	16.2	5.2	4.2	9.4	7.9	12.4
		10–20 cm	Mean	14.2	15.8	18.2	14.4	20.6	12.0	13.2	22.9	14.0	15.8	10.0	21.5	21.9	19.7
			Std	2.9	4.4	10.4	1.7	6.2	4.1	7.2	9.4	5.9	3.6	4.0	10.8	7.9	3.9
		20–40 cm	Mean	17.3	23.3	30.1	14.1	31.4	13.4	24.1	32.3	28.9	20.5	11.9	59.4	26.1	20.3
			Std	6.1	8.4	18.9	4.3	7.4	5.3	11.4	7.0	31.7	6.5	2.3	71.2	12.9	7.8
		40–80 cm	Mean	21.9	36.0	36.7	14.4	40.6	14.2	41.8	25.6	8.1	21.8	15.1	20.1	12.8	20.7
			Std	8.7	14.1	24.2	3.9	22.1	5.9	20.9	10.2	2.2	7.2	3.8	2.2	17.4	7.8
		0–80 cm	Mean	87.7	103.0	113.0	78.1	127.7	68.3	113.0	114.3	87.2	93.5	60.1	143.1	95.9	102.0
			Std	20.6	22.3	52.3	12.2	28.2	22.5	29.0	28.4	11.5	19.4	8.7	64.3	39.9	25.8
		O horizon + 0–10 cm	Mean	56.7	63.1	71.5	59.0	58.1	44.7	70.4	70.2	83.9	68.0	55.6	91.8	93.8	62.5
			Std	13.2	15.0	20.5	21.9	15.7	10.8	23.6	26.1	47.9	14.4	13.6	14.6	14.5	19.0
		O horizon + 0–20 cm	Mean	70.9	78.9	89.7	73.3	78.7	56.7	83.7	93.1	98.0	83.8	65.6	107.2	115.7	82.3
			Std	11.5	15.7	22.5	21.9	14.9	13.7	22.2	29.9	44.1	15.2	13.1	26.3	9.7	19.9
		O horizon + 0–40 cm	Mean	88.2	102.2	119.8	87.4	110.1	70.1	107.8	125.4	126.9	104.2	77.5	139.9	141.8	102.6
			Std	13.0	18.3	35.6	23.5	16.5	18.6	21.0	35.1	29.4	18.7	15.1	34.7	14.3	25.8
		O horizon + 0–80 cm	Mean	110.0	138.3	156.4	101.8	150.7	84.3	149.5	151.0	135.0	126.1	92.6	186.6	154.6	123.3
			Std	18.0	27.3	51.3	24.3	33.2	24.3	41.7	40.0	27.7	25.2	17.7	60.9	28.8	32.4
SOC pool (% of SOC pool in mineral soil)	Depth layer	0–10 cm	Mean	40.2	27.8	26.9	45.1	27.6	42.4	31.9	29.1	44.3	38.4	38.6	34.9	41.2	40.5
			Std	4.6	8.4	12.2	5.5	5.2	7.5	9.7	3.9	22.0	3.9	5.2	12.5	12.6	7.0
		0–20 cm	Mean	56.5	43.3	43.3	63.8	44.8	60.1	43.2	48.9	61.2	55.3	55.2	51.9	64.7	60.5
			Std	5.1	10.4	14.5	6.0	8.3	6.1	7.0	8.8	28.9	4.4	4.6	18.0	15.0	8.0
		0–40 cm	Mean	75.8	65.8	69.0	81.6	70.2	79.8	64.8	77.8	90.8	76.8	75.0	83.4	91.1	79.9
			Std	3.8	8.2	13.4	3.5	10.6	2.9	8.6	6.4	2.2	6.2	4.7	6.2	11.6	4.6

highest in the Liz catchment (128 t ha^{-1}). (d) The average total SOC pool from both the mineral soil organic carbon and forest floor organic carbon pools was 132 t ha^{-1}. (e) The proportion of forest floor SOC represented only 25% of the total SOC pool, with the lowest value in the Liz (15%) and Na zeleném (17%) catchments and highest in the Uhlířská (38%), Pluhův Bor (35%) and Salačova Lhota (35%) catchments. (f) Vertical variation of the mineral soil SOC pools among horizons was large, as was the variation among catchments (Figure 3, Table 4). The first 10 cm of mineral soil contained on average 33% of the total mineral soil SOC pool across all soil pits, with a maximum value of 45% in the Lesní potok catchment and minimum of 25% in the Jezeří catchment. The first 20 cm of the mineral soil contained up to 50% of the mineral soil SOC pool, with a maximum of 64% in the Lesní potok catchment. Thus, a substantial proportion of the SOC pool (50% of soil pit average, representing 50 t ha^{-1}) was located below the first 20 cm of the mineral soil. Below the top 40 cm of mineral soil there was still a substantial pool of carbon (25 t ha^{-1}, about one-quarter of the total SOC pool in the mineral soil).

The results of statistical analyses revealed that SOC pools in temperate forests were significantly influenced either by anthropogenic factors (historical S deposition and forest type) or natural environmental factors (elevation and soil texture), depending on the soil horizons (Tables 5, 6). Based on the AIC criterion, determining which model among a set of models is the most parsimonious, the model containing historical S deposition and the proportion of broadleaved trees best fitted the SOC pool in the forest floor, explaining 27% of the variability (Figure 4). The higher the catchment's historical S deposition and the lower the proportion of broadleaved trees, the higher the SOC pool in the forest floor was, although the influence of tree type was much lower than that of S deposition (Table 5, Figure 4). The same set of variables also best fitted the SOC pools when considering the coupled SOC pool in the forest floor and in mineral soil down to either 10, 20 or 40 cm (i.e., SOC pool in the forest floor + 0–10 cm of mineral soil; forest floor + 0–20 cm of mineral soil; forest floor + 0–40 cm of mineral soil), explaining 24, 26 and 29% of the variability, respectively (Table 5, Figure 5). The historical S deposition was the main factor explaining the thickness of the forest floor (Table 5, Figure 6). However, for the total SOC pool (combined pools in the mineral soil down to 80 cm and the forest floor) these anthropogenic factors were outweighed by natural environmental factors, and the best model based on the AIC was the one containing solely elevation, accounting for 24% of the variability (Table 5, Figure 7). The higher the catchment's elevation was, the higher the total SOC pool was (Figure 7).

The SOC pool in mineral soil sampled to different depths was best explained by soil texture, but its influence changed with the depth of sampling (Table 6, Figure 8). For the uppermost mineral soil layer (0–10 cm) we did not find any variable explaining the SOC pool. The mineral soil SOC pool down to 20 cm was best explained by clay and silt concentrations, accounting for 10% of the variability. The SOC pool down to 40 cm was best explained by clay, silt and elevation, together explaining 27% of the variability, but the importance of texture diminished for the SOC pool down to 80 cm. The SOC pool down to 80 cm was best explained solely by elevation, accounting for 19% of the variability (Figure 8).

4 | DISCUSSION

4.1 | The vertical distribution of SOC in forest soils

Our analysis of 101 forest soil pits across 14 long-term monitored catchments found a wide range of the SOC

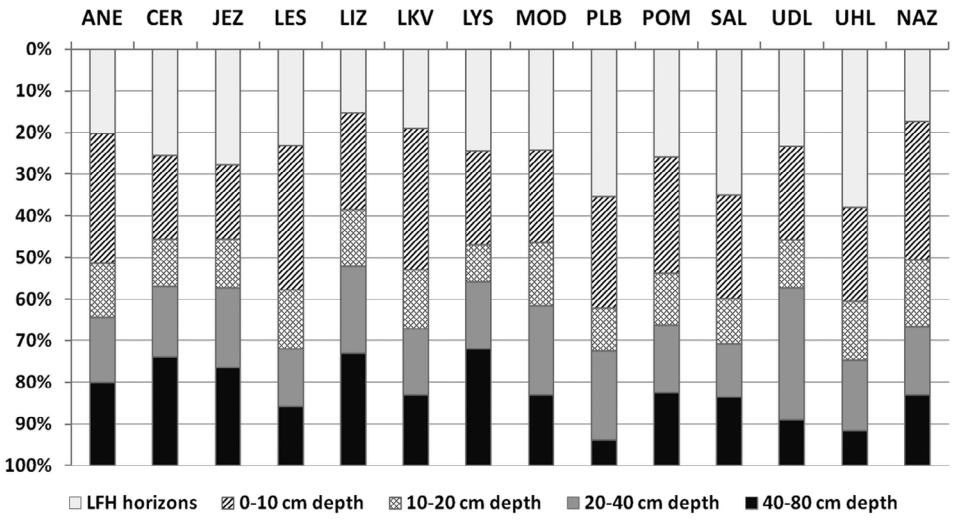

FIGURE 3 The average percentage of the soil organic carbon (SOC) pool in the forest floor and at certain depth horizons out of the total SOC pool (forest floor + mineral soil) for individual catchments

TABLE 5 Statistics of the most parsimonious linear mixed effects models assessing the explanatory variables of the total SOC pool sampled to different depths and explanatory variables of the O horizon thickness

		Fixed effects:	Value	SE	df	t-value	*p*-value	Marginal R^2	Conditional R^2
SOC pool	O horizon	(Intercept)	3.77	0.70	84	5.38	0.00	0.27	0.41
		Broadleaved trees	−1.16	0.38	84	−3.09	0.00		
		S_{tot} dep.1980	0.03	0.01	84	3.19	0.00		
	O horizon + 0–10 cm	(Intercept)	1.65	0.05	84	32.37	0.00	0.24	0.32
		Broadleaved trees	−0.08	0.03	84	−2.51	0.01		
		S_{tot} dep.1980	0.00	0.00	84	3.65	0.00		
	O horizon + 0–20 cm	(Intercept)	1.74	0.05	84	36.83	0.00	0.26	0.35
		Broadleaved trees	−0.06	0.03	84	−2.15	0.03		
		S_{tot} dep.1980	0.00	0.00	84	3.97	0.00		
	O horizon + 0–40 cm	(Intercept)	1.85	0.06	84	32.29	0.00	0.29	0.47
		Broadleaved trees	−0.08	0.03	84	−2.66	0.01		
		S_{tot} dep.1980	0.00	0.00	84	3.37	0.00		
	O horizon + 0–80 cm	(Intercept)	1.81	0.07	85	25.54	0.00	0.24	0.38
		Elevation	0.00	0.00	85	4.10	0.00		
O horizon thickness (cm)	(Intercept)	1.72	0.18	85.00	9.73	0.00	0.25	0.28	
	S_{tot} dep.1980	0.01	0.00	85.00	4.79	0.00			

Note: The proportion of broadleaved trees was arcsine square root transformed. *df*, degree of freedom; *SE*, standard error.

TABLE 6 Statistics of the most parsimonious linear mixed effects models assessing the explanatory variables of the SOC pool in mineral soil sampled to different depths

Mineral soil	Fixed effects:	Value	*SE*	*df*	t-value	*p*-value	Marginal R^2	Conditional R^2
SOC pool 0–20 cm	(Intercept)	1.63	0.08	84	20.65	0.00	0.10	0.16
	Clay 0–20 cm	−0.01	0.00	84	−2.49	0.01		
	Silt 0–20 cm	0.00	0.00	84	2.27	0.03		
SOC pool 0–40 cm	(Intercept)	1.62	0.10	83	16.47	0.00	0.27	0.31
	Elevation	0.00	0.00	83	2.72	0.01		
	Clay 0–40 cm	−0.01	0.00	83	−2.75	0.01		
	Silt 0–40 cm	0.00	0.00	83	2.68	0.01		
SOC pool 0–80 cm	(Intercept)	1.69	0.08	85	22.16	0.00	0.19	0.29
	Elevation	0.00	0.00	85	3.66	0.00		

Note: df, degree of freedom; *SE*, standard error.

pool in the whole soil profile of 84–187 t ha^{-1} in the O horizon + 0–80 cm of mineral soil, which corresponded to data reported from adjacent regions in central Europe, for example by Wiesmeier et al. (2013) for soils sampled down to 100 cm from a Bavarian forest and Meier and Leuschner (2010) for central Germany. Buczko et al. (2017) reported higher SOC pools in a temperate forest in Poland, but these higher values were reported for hydromorphic soils in which stagnic/gleyic soil properties (seasonally high soil moisture) slow down decomposition. Buczko et al. (2017) reported average SOC pool values exceeding 300 t ha^{-1} down to 1 m. Such a high value was reached only in three soil pits showing hydromorphism in our study. The rest of the hydromorphic soils (there were only 10 soil profiles classified as Gleysosls and one soil profile classified as a Histosol) showed a lower SOC pool. The average SOC pool down to 80 cm for these 11 soil pits was 186 t ha^{-1} (std. ± 111), which is 40% more than the average total SOC pool of well-drained soils. Due to the small number of

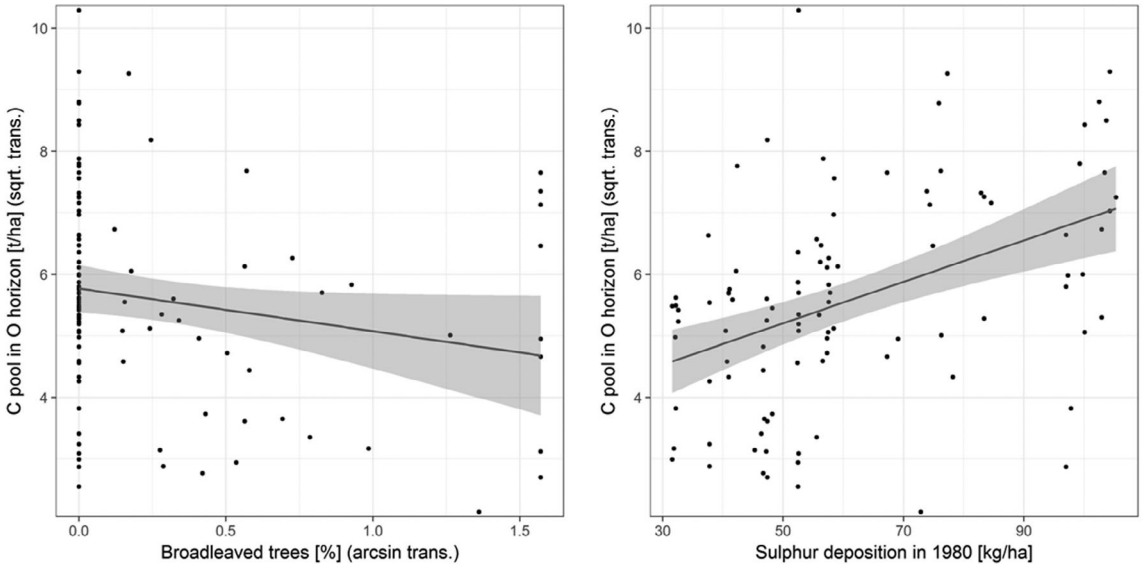

FIGURE 4 The relationship between the soil organic carbon (SOC) pool (t ha^{-1}) in the forest floor (O horizon) and proportion of broadleaved trees and historical S deposition (kg ha^{-1}) that best fit the data using linear mixed effect models. The C pool was square root transformed; the proportion of broadleaved trees was arcsine transformed

observations and specific factors, that is, high soil water content induces anaerobic conditions, which impede decomposition of soil organic matter, resulting in humus accumulation, hydromorphic soils were excluded from the analysis. However, Gleysosls and Histosols cover 5.3 and 6.5% of the land surface of the European Union, respectively (Tóth et al., 2008), and in some areas of temperate climate forest, such as in northern Germany (Buczko et al., 2017), these soils' contribution to the SOC pool can be substantial.

The total forest SOC pool (O horizon + 0–80 cm of mineral soil) of well-drained soils significantly deviated from published soil C pools in the Czech Republic based on a recommended depth of sampling (30 cm) for forest soils (IPCC, 2003) (Landscape Atlas of the Czech Republic, 2009; Marková et al., 2016). Below the top 40 cm of mineral soil there was still a substantial pool of carbon in our catchments, about one-quarter of the total SOC pool in the mineral soil. Surprisingly, even though the issue of shallow sampling has been addressed by many studies (e.g., Batjes, 1996; Chiti et al., 2012; Harrison et al., 2011; Jandl et al., 2014; Jobbágy & Jackson, 2000), shallow sampling still prevails when reporting SOC pools. This may be due to high stone contents, which are often encountered in the subsoil of forest soils, or labour costs. However, shallow soil sampling has major implications for modelling of changes in SOC pools. Harrison et al. (2011) pointed out that due to shallow soil sampling we may not be able to adequately measure the impacts of vegetation management, climate change or changes in atmospheric deposition. This may have been due to factors controlling the SOC pool in the topsoil that differ from those in the subsoil (Schmidt et al., 2011), as suggested by our results and discussed in the following paragraphs. Other studies also conclude that SOC stored in deeper mineral soils often represents the most recalcitrant part of soil C, controlled by other factors than those in the topsoil SOC (Chen et al., 2018; Rumpel & Kögel-Knabner, 2011; Salomé et al., 2010; Schmidt et al., 2011).

4.2 | The influence of environmental factors on the vertical SOC pool distribution

Our study showed that when considering the SOC pool in the forest floor and in the mineral soil down to the 10, 20 or 40-cm depths separately, controlling factors differed from those controlling the total SOC pool (forest floor + mineral soil). Similarly, for the mineral soil SOC pool, factors varied from an exclusive soil texture effect, combined effects of both soil texture and elevation, to elevation only for the total mineral soil. The forest floor SOC pool as well as the combined SOC pool in the forest floor and mineral soil down to 10, 20 or 40 cm was dependent on forest type (expressed as the percentage of broadleaves) and historical S deposition. The influence of the two two main factors controlling the forest floor SOC pool (forest type and S deposition) also dominated when considering the SOC pool in the forest floor coupled with the shallow depths of mineral soil. However, for the total

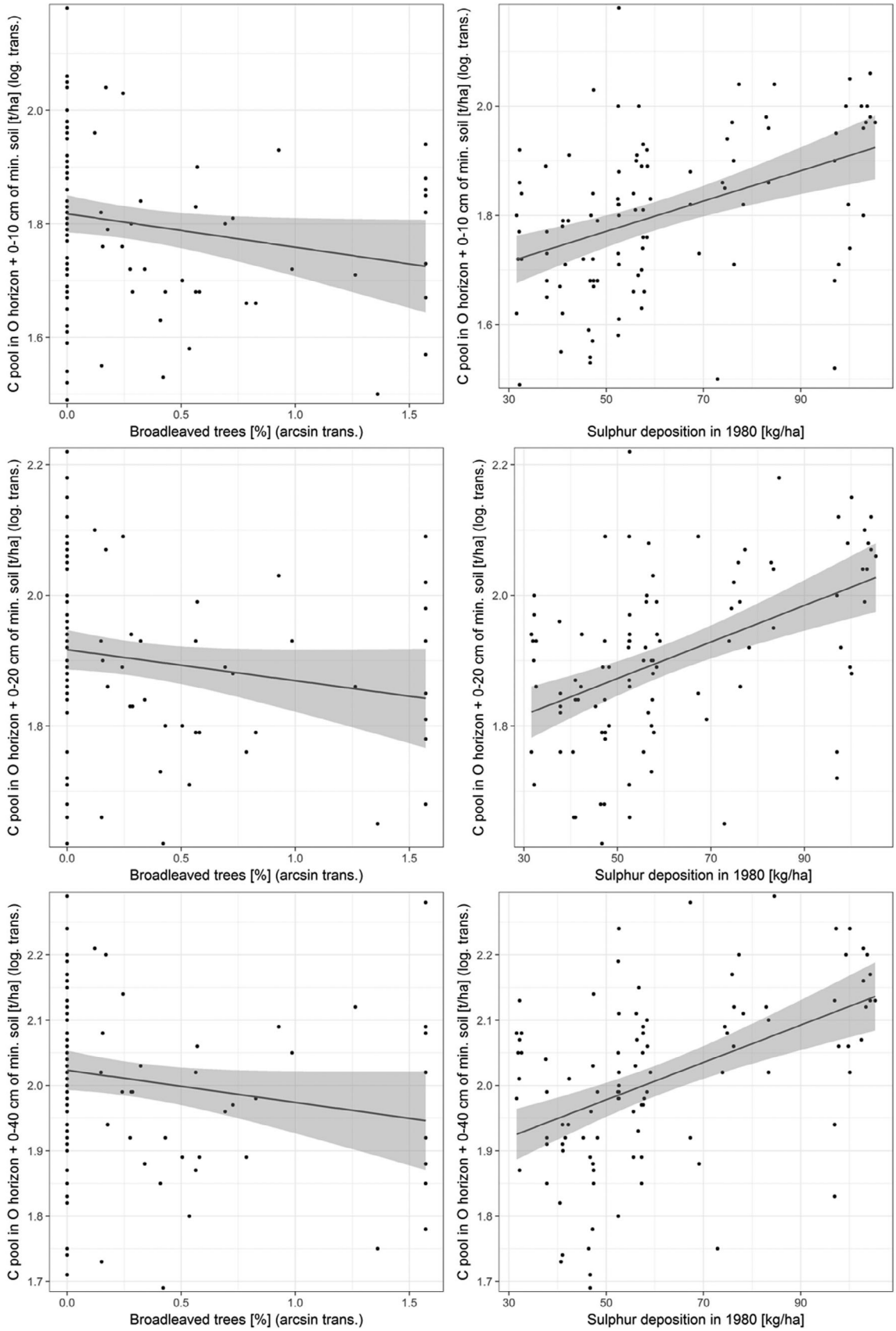

FIGURE 5 The relationship between the coupled soil organic carbon (SOC) pool (t ha^{-1}) in the forest floor and mineral soil down to a certain depth (C pool in the forest floor + C pool in the mineral soil) and explanatory variables that best fit the data using linear mixed effect models. The SOC pool was log-transformed; the proportion of broadleaved trees was arcsine transformed

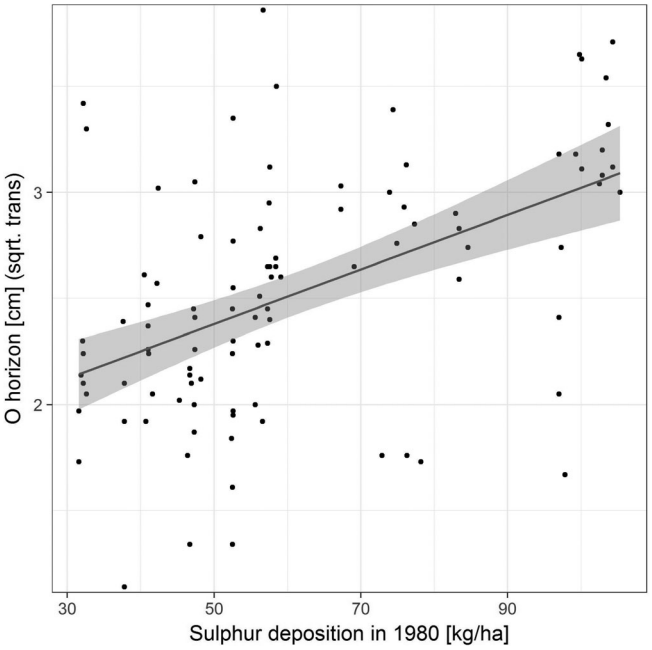

FIGURE 6 The relationship between the forest floor thickness (O horizon) (cm) and historical S deposition (kg ha^{-1}) that best fit the data using linear mixed effect models. The O horizon thickness was square root transformed

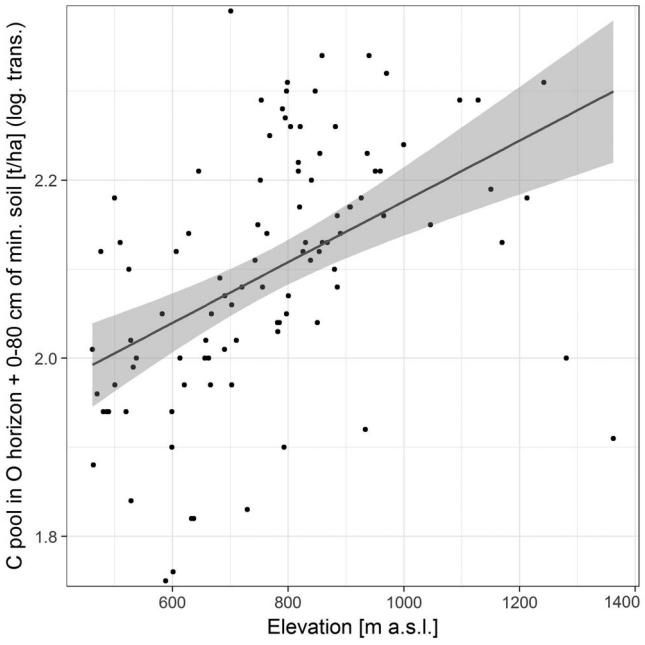

FIGURE 7 The relationship between the total soil organic carbon (SOC) pool (t ha^{-1}) (C pool in the forest floor + C pool in the mineral soil) and elevation (m a.s.l.) that best fits the data using linear mixed effect models. The SOC pool was log-transformed

SOC pool (O horizon + 0–80 cm of mineral soil) the significant factors changed from anthropogenic to natural environmental, and the principal variable controlling the total SOC pool turned out to be elevation. The separate analyses for aggregated soil depths illustrate that factors change with sampling depth. This should be carefully considered when modelling SOC pool changes or when extrapolating the SOC pool, especially in areas with soil acidification legacy.

The influence of tree species on the SOC pool has been shown by other studies as well. Cremer, Kern, and Prietzel (2016), Vesterdal, Schmidt, Callesen, Nilsson, and Gundersen (2008), Vesterdal, Clarke, Sigurdsson, and Gundersen (2013) and Jonard et al. (2017) all found significant differences in SOC pools among broadleaf tree species and conifers, with the highest values being reported for the Norway spruce and Scots pine. The influence of tree species was most pronounced in the forest floor, whereas in the mineral soil it was only in some layers down to 30 cm (Vesterdal et al., 2008, 2013). Our data also suggest that the influence of the forest type on the SOC pool diminished with the soil depth and was not significant either for the total SOC pool (forest floor + mineral soil pool down to 80 cm) or solely for the mineral soil pool at any depth. On the contrary, Gurmesa, Schmidt, Gundersen, and Vesterdal (2013) found a significantly higher C pool under conifers than under broadleaf trees also in mineral soil down to 30 cm and hypothesized that the reason for this could be the differences in belowground root litter input in nutrient-poor sandy soils, because the aboveground litterfall input did not differ.

A larger C pool under conifers is often explained by the recalcitrant litter, due to high lignin and polyphenol content, and due to annual carbon input. However, Vesterdal (1999) showed that lignin content in beech foliage does not differ from that in spruce foliage. There is also no clear evidence that annual C input differs among tree species. Hansen et al. (2009), for example, found that annual carbon input from litterfall is higher in spruce forest than in beech forest, but Oulehle, Růžek, Tahovská, Bárta, and Myška (2016), on the contrary, reported higher annual carbon input from litterfall in the beech forest. Trum, Titeux, Ranger, and Delvaux (2011) reported that C-input from litterfall was similar whatever the tree species (oak, beech, spruce or Douglas-fir). Litter inputs therefore are more likely to correspond to actual forest productivity, influenced by forest age and stand fertility rather than specific species present. Thus different rates of litter decomposition under spruce and beech trees are more likely to be due to different adaptations of decomposers, as shown for example in the study by Oulehle et al. (2018).

Our study, however, suggested that the influence of tree species is much less than that of historical S deposition or elevation. S deposition in the Czech Republic,

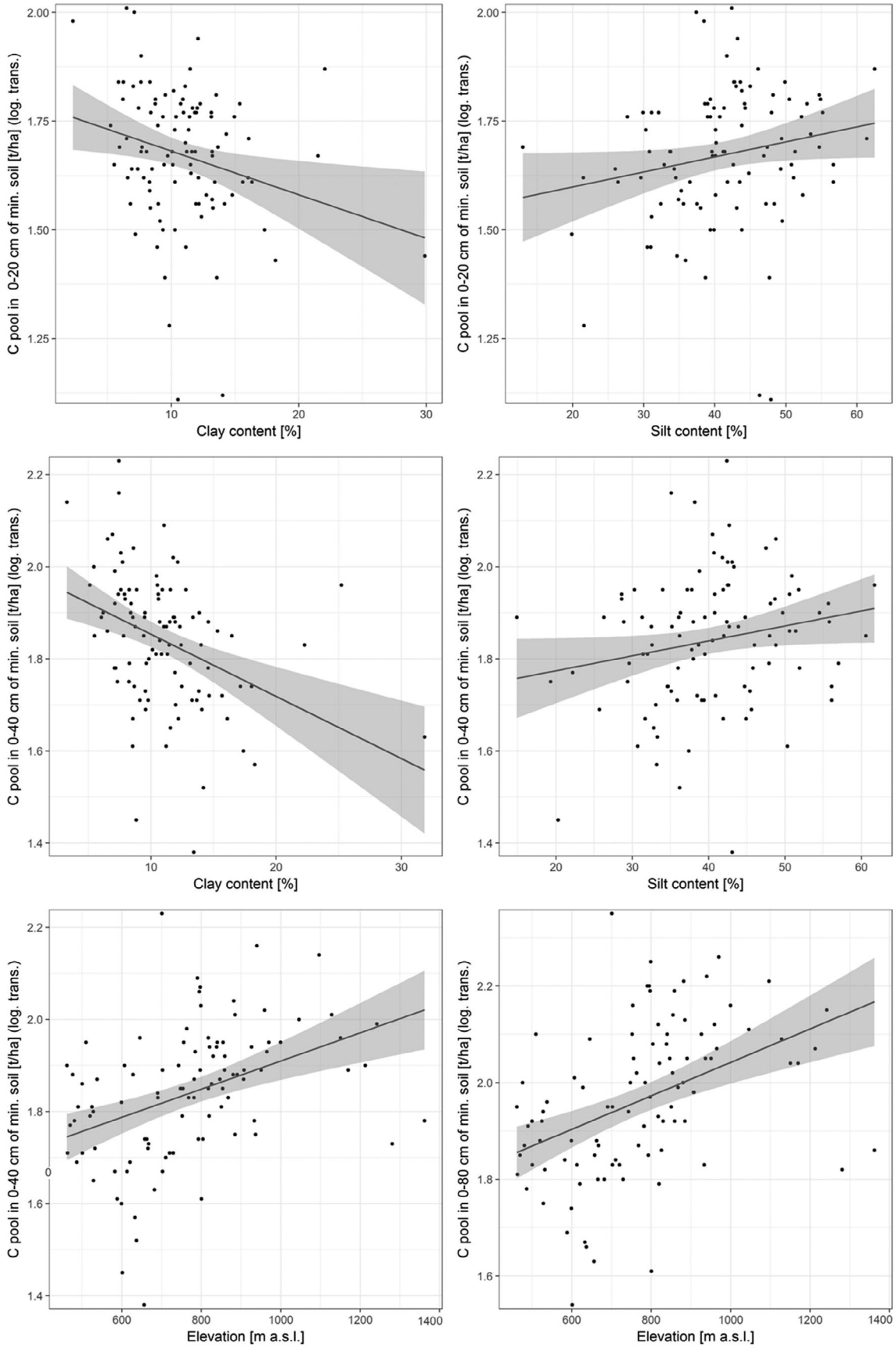

FIGURE 8 The relationship between the soil organic carbon (SOC) pool (t ha^{-1}) in the mineral soil down to a certain depth and explanatory variables that best fit the data using linear mixed effect models. The SOC pool was log-transformed

as well as in central Europe, represents to some extent, due to the correlation structure of environmental variables (Table 1), climatic gradient (temperature and precipitation) and positively correlates also with N deposition. The separate effect of each variable is a real conundrum.

The relation between elevation and the SOC pool has been demonstrated in other studies in Europe (Meier & Leuschner, 2010; Wiesmeier et al., 2013) and also in other regions of the world (Dieleman, Venter, Ramachandra, Krockenberger, & Bird, 2013; Du et al., 2014; Tashi, Singh, Keitel, & Adams, 2016), and has been interpreted as a climate factor that is explained by a build up of a thicker organic layer at higher elevations, related mainly to decreasing temperatures and increasing precipitation with elevation, resulting in decreased litter decomposition at high-elevation sites. The significant positive relationship between the SOC pool and elevation (i.e., climate - decreasing temperature and increasing precipitation) found in our study was valid for both the total and mineral soil SOC pools. However, when shallow sampling is performed this influence is outweighed by anthropogenic factors and/or soil texture. Wiesmeier et al. (2013) reported that the dependence of the SOC pool and climate seemed to be slightly stronger in the subsoil (B horizon), and supposed that the subsoil SOC mirrors the continuous impact of climate over several centuries, whereas the climate effect in the topsoil is masked by, for example, land use. However, on a global dataset from different biomes, Jobbágy and Jackson (2000) showed a significant consistent influence of climate (temperature and precipitation) for all depth layers.

A higher subsoil SOC pool with increased elevation could be also attributed to more intensive podzolization and translocation of organic complexes down the soil profile. In our studied catchments, the proportion of podzolized soils increased with elevation, as did the SOC concentration in the mineral soil (Table S1 in the supplementary materials). Thus higher precipitation and lower temperature do not only decrease litter decomposition at high-elevation sites, but also lead to advanced soil podzolization and translocation of organic complexes. We hypothesize that translocation of organic processes was intensified by soil acidification caused by high S deposition.

On the other hand, a study of the SOC pool in the forest floor and mineral soil to a depth of 1 m in Nordic forest soils conducted by Callesen et al. (2003) showed that the SOC pool increased with both mean annual temperature and mean annual precipitation, and was explained by higher net primary production (NPP). The positive relationship of the SOC pool to mean annual temperature is in contrast to our results, as well as to the results of Wiesmeier et al. (2013) from an environment similar to sampled catchments in the Czech Republic. Callesen et al. (2003) elaborated on this issue and concluded that the negative relation of SOC pools and temperature generally found in analyses of global databases is probably the result of a high frequency of hydromorphic soils in humid areas of boreal forest and in arctic tundra. The negative relation between SOC pools and temperature was reversed when the analyses were restricted to well-drained soils (Callesen et al., 2003). However, in our study the positive relation of SOC pools and elevation (thus increasing precipitation and decreasing temperature) was found for well-drained soils after the exclusion of all hydromorphic soils.

As has been already mentioned, the elevation gradient in our study does not represent only precipitation (positive correlation) and temperature (negative correlation), but also length of growing season (negative correlation) as well as S and N deposition (both positive correlation). The N deposition was omitted from the analysis due to strong correlation with S deposition and because S deposition was also less strongly correlated with elevation. Nevertheless, the S deposition gradient represents also the N deposition gradient, to some extent. Increase of N availability may increase NPP and/or decrease decomposition of N-rich litter, as concluded in several studies (Janssens et al., 2010; Liu & Greaver, 2010; Šantrůčková, Tahovská, & Kopáček, 2009). It has been shown by Berg and Matzner (1997) that initially fast decomposition of N-rich substrates slows down in the later phases of the decomposition relative to N-poor substrates and over a longer time produces more remaining recalcitrant organic matter. A negative effect of increased N availability on decomposition rates was suggested by many experimental N addition studies (e.g., Hobbie, 2008; Olsson, Burleigh, & Van Aarle, 2005; Waldrop, Zak, & Sinsabaugh, 2004). Furthermore, S deposition to European forests has changed more rapidly and more dramatically over the last 50 years than N deposition, implying that S may have had a greater influence on the soil C cycle during this period, and also raising the possibility that some observed changes may have been incorrectly attributed to N deposition. The significant relation of the SOC pool and historical soil acidification was suggested by Oulehle, Evans, and Hofmeister (2011). The relation of the carbon pool to historical S deposition was significant for both the forest floor SOC pool and forest floor thickness in our study as well. The higher the historical S deposition was, the thicker the forest floor was and the larger the forest floor SOC pool. A positive relation between S deposition and the forest floor SOC pool was reported also, for example, by Mulder, De Wit, Boonen, and Bakken (2001) and Oulehle et al. (2008). Oulehle et al. (2018) studied the effect of soil acidification

on SOC dynamics in a field S addition experiment, in which soil respiration decreased in both coniferous as well as broadleaved forest. They conclude that slow down of litter decomposition in forest soils affected by high S deposition might have led to accumulation of soil organic matter in the forest floor. The rate of soil C decomposition is likely to decrease due to elevated soil acidity and subsequent mobilization of Al^{3+}, with a toxic effect on plant roots (de Wit, Eldhuset, & Mulder, 2010) and changes in the soil biota (Persson, Lundkvist, Wirén, Hyvönen, & Wessén, 1989) leading to an increase of the fungal to bacterial ratio due to decreases of bacterial abundance (Oulehle et al., 2018). Furthermore, the abundance of soil fauna, especially the presence of earthworms, which have a significant effect on litter decomposition, is low in acid soils (Frouz, 2018; Lavelle, Chauvel, & Fragoso, 1995), which is an additional limitation to litter decomposition.

Most of the studied catchments are underlain by bedrock with low or very low alkali and alkali earth metal contents (gneises, granites, phylites and sandstones), and thus their soils have a low buffering capacity and are susceptible to soil acidification (Chuman et al., 2014). Because these catchments experienced high S deposition and soil acidification (Oulehle et al., 2017) in the past we hypothesize that the S deposition (i.e., the soil acidification legacy) further suppressed litter decomposition naturally following the elevation gradient (increasing precipitation and decreasing temperature), and led to the SOC accumulation mainly in the forest floor. However, our data do not allow us to disentangle what is the separate effect of N and S depositions or the effect of climate, as there were no catchments with high S and N deposition, high precipitation and low temperature in the lowlands and vice versa in the mountains.

4.3 | SOC pools and soil texture

Although soil texture is considered an important factor controlling SOC pools (e.g., Grand & Lavkulich, 2011; Martin et al., 2011), our study found a less pronounced influence of soil texture on the SOC pool in forest soils, probably because of low texture variability. Most samples were sandy loam and loam, with average clay content across all samples of 11.1% (std. ± 4.5), ranging from 6.5% (std. ± 1.9) in the MOD catchment to 18.1% (std. ± 5.9) in the SAL catchment. The SOC pool was significantly influenced by texture only in the 0–20 cm and 0–40 cm layers of mineral soil, and its influence diminished with sampling depth. Nonetheless, the negative relation of the SOC pool to clay content (Table 6) was surprising and it is contrary to published research. Chiti et al. (2012) demonstrated that even though the high influence of climate on the SOC stock exceeded the effect of soil texture, there was a positive correlation between clay content (varying approximately between 2 and 60%) and the SOC stock. Barré et al. (2017) found a significant positive relation between SOC concentrations and clay concentrations (varying approximately between 15 and 42%) for forest soils but no correlation between the SOC pool and clay content. Similarly, Meier and Leuschner (2010) reported from Germany that the estimated clay content of the upper mineral soil layers had no significant influence on the SOC pool either in the organic layer or mineral soil. This study did not report clay content, but the soil texture varied between loamy-silty sand and clay loam; thus, the clay content is likely to have ranged from a few percent up to 40%. Wiesmeier et al. (2013) in Germany also found a strong positive correlation between clay content and the SOC pool in the topsoil (median topsoil clay content was 17%, varying between 10 and 22%, and median subsoil clay content was 21%, varying between 13 and 32%), but when analysing the total SOC pool down to 100 cm he concluded that the total storage of SOC did not depend on soil texture. Vesterdal et al. (2008) reported a strong positive relation of mineral soil OC to clay content (varying between 8 and 30%) in the 50–100-cm depth. The studies by Martin et al. (2011), Hassink (1997) and Grand and Lavkulich (2011) also found that SOC of forest soils depends strongly on clay content, although the first two studies also had higher soil texture variability compared to our dataset.

The correlation structure of our data shows that clay content is negatively correlated to elevation, and thus higher precipitation, lower temperature and higher S and N deposition. All these factors, together with organic acids developed through decomposition processes in the forest floor, lead to soil podzolization, with the destruction of clay minerals and translocation of iron and aluminium organic complexes (Lundström, Van Breemen, & Bain, 2000; Sauer et al., 2007), which then leach downward through the soil profile and precipitate in the spodic B horizons. Coniferous forests have been shown to speed up forest soil acidification compared to broadleaved forests because conifers have higher interception of dry deposition (i.e., are able to more efficiently scavenge atmospheric compounds such as SO_4^{2-}, which are then rinsed to the soil during subsequent rainfall) (Oulehle & Hruška, 2005), and spruce litter leaches more organic acids compared to beech (Augusto, Ranger, Binkley, & Rothe, 2002; Ružek, Myška, Kučera, & Oulehle, 2019). The proportion of acid soils such as dystric Cambisols and Podzols increased with elevation in our study, but as the clay content decreased, the SOC pool increased. This may suggest a greater role of Al and Fe hydroxides in SOC stabilization, as suggested by Rumpel and Kögel-Knabner (2011) and Kleber, Mikutta, Torn, and Jahn (2005) or Rasmussen et al. (2018). Those studies

concluded that in acid soils poorly crystalline minerals represented by Al and Fe hydroxides preferentially stabilize the SOC. This is further supported by the conclusions of Doetterl et al. (2015) showing that reactive Al and Fe hydroxides are more important in stabilizing SOC than clay content.

4.4 | Implications for SOC calculations

Our sampled soil types (Cambisols and Podzols) cover 67 and 15%, respectively, of the forested land in the Czech Republic, and are dominant soils, each representing approximately one-quarter of the forest soils in Europe (Vanmechelen, Groenemans, & Ranst, 1997). We therefore believe that this study has important implications for understanding potential SOC pool changes under ongoing global climate change over a large area of temperate forests, especially in regions currently or historically affected by soil acidification caused by acidic deposition. The large-scale acidification of soils affected not only Europe but also North America, and more recently has also been recognized as a potential threat to ecosystems in Asia (Bouwman et al., 2002; Duan et al., 2016; Vet et al., 2014). Our results suggest that substantial SOC pools have accumulated due to soil acidification caused by high sulphur deposition suppressing microbial activity, and subsequent soil recovery might lead to carbon loss as a result of increases in microbial activity. Additionally, forest management might trigger the release of accumulated SOC via unsuitable management practices such as clear-cut harvesting or tree species conversion. The tree species conversion from spruce monocultures to deciduous and mixed forests, which is inevitable in central Europe as an adaptation to climate change, will very likely lead to loss of SOC. In the Czech Republic or other central European countries the predominance of spruce was the result of forest management oriented at maximum timber production and converting natural deciduous forest to spruce monocultures even in low elevations. Such stands are nowadays very sensitive to drought and subsequent bark beetle attack and the Czech national authorities plan to convert spruce stands back to deciduous or mixed forests.

5 | CONCLUSIONS

This study found soil acidification legacy (historical S and N depositions) and elevation (temperature and precipitation) to be the most important factors controlling SOC pools in Podzols and Cambisols. The great the historical deposition of acidifying compounds and the higher the elevation were, the larger the SOC pool was. The forest floor stored 34 t ha^{-1} of SOC on average, three times as much as is located in the first 80 cm of the mineral soil, of which only 50% is located in the first 20 cm of the soil profile. We further illustrate that the selected sampling method has major implications when interpreting changes in the SOC pool, because factors controlling the SOC pool change with sampling depth and natural environmental factors are outweighed by anthropogenic factors. Thus, when modelling SOC pool changes in soils that exhibited anthropogenic acidification and/or tree species conversion, such factors should be considered. These confounding factors are not directly related to climate change. It is possible that SOC pools in such areas may not be in a long-term steady state (C inputs vs. decomposition) as a consequence of the legacy of acidic deposition rather than ongoing climate change.

ACKNOWLEDGEMENTS

The authors acknowledge the Czech Science Foundation Grant no. 18-17295S and internal project of the Czech Geological Survey 331700. This work was supported by the Ministry of Education, Youth and Sports of the Czech Republic for the support of science and research, and within the National Sustainability Program I (NPU I), grant number LO1415.

AUTHOR CONTRIBUTIONS

Tomas Chuman: Conceptualization; formal analysis; investigation; methodology; writing-original draft; writing-review and editing. **Filip Oulehle:** Conceptualization; funding acquisition; investigation; methodology; writing-original draft; writing-review and editing. **Katerina Zajicova:** Data curation; formal analysis; investigation. **Jakub Hruska:** Conceptualization; funding acquisition; methodology; project administration; writing-original draft; writing-review and editing.

CONFLICT OF INTEREST

The authors declare no competing financial interest.

AUTHOR CONTIBUTIONS

Study concept and design: T. Chuman, F. Oulehle and J. Hruška. Aquisition, analysis and interpretation of data: T. Chuman and K. Zajícová. Drafting the manuscript: T. Chuman and F. Oulehle. Critical revision of the manuscript: F. Oulehle and J. Hruška.

DATA AVAILABILITY STATEMENT

The data that support the findings of this study are available from the corresponding author upon request.

ORCID

Tomáš Chuman https://orcid.org/0000-0003-2525-5379

REFERENCES

Achat, D. L., Fortin, M., Landmann, G., Ringeval, B., & Augusto, L. (2015). Forest soil carbon is threatened by intensive biomass harvesting. *Scientific Reports*, *5*, 1–10. https://doi.org/10.1038/srep15991

Augusto, L., Ranger, J., Binkley, D., & Rothe, A. (2002). Impact of several common tree species of European temperate forests on soil fertility. *Annals of Forest Science*, *59*, 233–253. http://www.scopus.com/inward/record.url?eid=2-s2.0-21244502256&partnerID=40&md5=bbe5799f53da1f737ee7a31c40a4109f

Baritz, R., Seufert, G., Montanarella, L., & Van Ranst, E. (2010). Carbon concentrations and stocks in forest soils of Europe. *Forest Ecology and Management*, *260*, 262–277. https://doi.org/10.1016/j.foreco.2010.03.025

Barré, P., Durand, H., Chenu, C., Meunier, P., Montagne, D., Billiou, D., & Cécillon, L. (2017). Geo-pedological control of soil organic carbon and nitrogen stocks at the landscape scale. *Geoderma*, *285*, 50–56. https://doi.org/10.1016/j.geoderma.2016.09.029

Batjes, N. H. (1996). Total carbon and nitrogen in the soils of the world. *European Journal of Soil Science*, *47*, 151–163.

Bellamy, P. H., Lovejoy, P. J., Bradley, R. I., Lark, R. M., & Kirk, G. J. D. (2005). Carbon losses from all soil across England and Wales 1978-2003. *Nature*, *437*, 245–248.

Berg, B., & Matzner, E. (1997). Effect of N deposition on decomposition of plant litter and soil organic matter in forest systems. *Environmental Reviews*, *5*, 1–25.

Bouwman, A. F., Van Vuuren, D. P., Derwent, R. G., & Posch, M. (2002). A global analysis of acidification and eutrophication of terrestrial ecosystems. *Water, Air, and Soil Pollution*, *141*, 349–382.

Buczko, U., Köhler, S., Bahr, F., Scharnweber, T., Wilmking, M., & Jurasinski, G. (2017). Variability of soil carbon stocks in a mixed deciduous forest on hydromorphic soils. *Geoderma*, *307*, 8–18.

Burke, I. C., Yonker, C. M., Parton, W. J., Cole, C. V., Schimel, D. S., & Flach, K. (1989). Texture, climate, and cultivation effects on soil organic matter content in U.S. grassland soils. *Soil Science Society of America Journal*, *53*, 800–805. https://doi.org/10.2136/sssaj1989.03615995005300030029x

Callesen, I., Liski, J., Raulund-Rasmussen, K., Olsson, M., Tau-Strand, L., Vesterdal, L., & Westman, J. (2003). Soil carbon stores in Nordic well-drained forest soils relationships with climate and texture class. *Global Change Biology*, *9*, 358–370.

Chen, S., Martin, M. P., Saby, N. P. A., Walter, C., Angers, D. A., & Arrouays, D. (2018). Fine resolution map of top- and subsoil carbon sequestration potential in France. *Science of the Total Environment*, *630*, 389–400.

Chiti, T., Díaz-Pinés, E., & Rubio, A. (2012). Soil organic carbon stocks of conifers, broadleaf and evergreen broadleaf forests of Spain. *Biology and Fertility of Soils*, *48*, 817–826.

Chuman, T., Gürtlerová, P., Hruška, J., & Adamová, M. (2014). Geochemical reactivity of rocks of the Czech Republic. *Journal of Maps*, *10*, 341–349.

Conen, F., Zerva, A., Arrouays, D., Jolivet, C., Jarvis, P. G., Grace, J., & Mencuccini, M. (2005). The carbon balance of forest soils: detectability of changes in soil carbon stocks in temperate and Boreal forests. In H. Griffiths & P. G. Jarvis (Eds.), *The carbon balance of forest biomes* (pp. 252–268). Abingdon: Taylor & Francis.

Conforti, M., Lucà, F., Scarciglia, F., Matteucci, G., & Buttafuoco, G. (2016). Soil carbon stock in relation to soil properties and landscape position in a forest ecosystem of southern Italy (Calabria region). *Catena*, *144*, 23–33. https://doi.org/10.1016/j.catena.2016.04.023

Cremer, M., Kern, N. V., & Prietzel, J. (2016). Soil organic carbon and nitrogen stocks under pure and mixed stands of European beech, Douglas fir and Norway spruce. *Forest Ecology and Management*, *367*, 30–40. https://doi.org/10.1016/j.foreco.2016.02.020

de Wit, H. A., Eldhuset, T. D., & Mulder, J. (2010). Dissolved Al reduces Mg uptake in Norway spruce forest: Results from a long-term field manipulation experiment in Norway. *Forest Ecology and Management*, *259*, 2072–2082. https://doi.org/10.1016/j.foreco.2010.02.018

Dieleman, W. I. J., Venter, M., Ramachandra, A., Krockenberger, A. K., & Bird, M. I. (2013). Soil carbon stocks vary predictably with altitude in tropical forests: Implications for soil carbon storage. *Geoderma*, *204–205*, 59–67. https://doi.org/10.1016/j.geoderma.2013.04.005

Doetterl, S., Stevens, A., Six, J., Merckx, R., Van Oost, K., Casanova Pinto, M., … Boeckx, P. (2015). Soil carbon storage controlled by interactions between geochemistry and climate. *Nature Geoscience*, *8*, 780–783.

Du, B., Kang, H., Pumpanen, J., Zhu, P., Yin, S., Zou, Q., … Liu, C. (2014). Soil organic carbon stock and chemical composition along an altitude gradient in the Lushan Mountain, subtropical China. *Ecological Research*, *29*, 433–439.

Duan, L., Yu, Q., Zhang, Q., Wang, Z., Pan, Y., Larssen, T., … Mulder, J. (2016). Acid deposition in Asia: Emissions, deposition, and ecosystem effects. *Atmospheric Environment*, *146*, 55–69.

FAO. (2006). *Guidelines for soil description* (4th ed.). Rome: Food and Agriculture Organization of the United Nations.

Frouz, J. (2018). Effects of soil macro- and mesofauna on litter decomposition and soil organic matter stabilization. *Geoderma*, *332*, 161–172. https://doi.org/10.1016/j.geoderma.2017.08.039

Garcia-Pausas, J., Casals, P., Camarero, L., Huguet, C., Sebastià, M. T., Thompson, R., & Romanyà, J. (2007). Soil organic carbon storage in mountain grasslands of the Pyrenees: Effects of climate and topography. *Biogeochemistry*, *82*, 279–289.

Grand, S., & Lavkulich, L. M. (2011). Depth distribution and predictors of soil organic carbon in Podzols of a forested watershed in Southwestern Canada. *Soil Science*, *176*, 164–174.

Gurmesa, G. A., Schmidt, I. K., Gundersen, P., & Vesterdal, L. (2013). Soil carbon accumulation and nitrogen retention traits of four tree species grown in common gardens. *Forest Ecology and Management*, *309*, 47–57. https://doi.org/10.1016/j.foreco.2013.02.015

Hansen, K., Vesterdal, L., Schmidt, I. K., Gundersen, P., Sevel, L., Bastrup-Birk, A., … Bille-Hansen, J. (2009). Litterfall and nutrient return in five tree species in a common garden experiment. *Forest Ecology and Management*, *257*, 2133–2144.

Harrison, R. B., Footen, P. W., & Strahm, B. D. (2011). Deep soil horizons: Contribution and importance to soil carbon pools and in assessing whole-ecosystem response to management and global change. *Forest Science*, *57*, 67–76.

Hassink, J. (1997). A model of the physical protection of organic matter in soils the capacity of soils to preserve organic C and N by their association with clay and silt particles. *Plant and Soil*, *191*, 77–87. https://www.researchgate.net/publication/40154117

Hobbie, S. E. (2008). Nitrogen effects on decomposition: A five-year experiment in eight temperate sites. *Ecology*, *89*, 2633–2644.

Hofmeister, J., Oulehle, F., Krám, P., & Hruška, J. (2008). Loss of nutrients due to litter raking compared to the effect of acidic deposition in two spruce stands, Czech Republic. *Biogeochemistry*, *88*, 139–151.

Homann, P. S., Bormann, B. T., & Boyle, J. R. (2001). Detecting treatment differences in soil carbon and nitrogen resulting from forest manipulations. *Soil Science Society of America Journal*, *65*, 463–469. https://doi.org/10.2136/sssaj2001.652463x

Hruška, J., Moldan, F., & Krám, P. (2002). Recovery from acidification in central Europe - Observed and predicted changes of soil and streamwater chemistry in the Lysina catchment, Czech Republic. *Environmental Pollution*, *120*, 261–274.

Huntington, T. G., Ryan, D. F., & Hamburg, S. P. (1988). Estimating soil nitrogen and carbon pools in a northern hardwood forest ecosystem. *Soil Science Society of America Journal*, *52*, 1162–1167.

Innangi, M., d'Alessandro, F., & Fioretto, A. (2015). Modeling distribution of mediterranean beech forests and soil carbon stock under climate change scenarios. *Climate Research*, *66*, 25–36. http://www.int-res.com/abstracts/cr/v66/n1/p25-36/

IPCC. (2003). *Good Practice Guidance for Land Use, Land-Use Change and Forestry*. Institute for Global Environmental Strategies (IGES), Kamiyamaguchi, Hayama.

ISO 11277. (2009). Soil quality—Determination of particle size distribution in mineral soil material—Method by sieving and sedimentation. https://www.iso.org/standard/69496.html

IUSS Working Group WRB. (2015). *World reference base for soil resources 2014. International soil classification system for naming soils and creating legends for soil maps*. Rome: Food and Agriculture Organization of the United Nations.

Jandl, R., Rodeghiero, M., Martinez, C., Cotrufo, M. F., Bampa, F., van Wesemael, B., ... Miglietta, F. (2014). Current status, uncertainty and future needs in soil organic carbon monitoring. *Science of the Total Environment*, *468–469*, 376–383. https://doi.org/10.1016/j.scitotenv.2013.08.026

Janssens, I. A., Dieleman, W., Luyssaert, S., Subke, J. A., Reichstein, M., Ceulemans, R., ... Law, B. E. (2010). Reduction of forest soil respiration in response to nitrogen deposition. *Nature Geoscience*, *3*, 315–322.

Janssens, I. A., Freibauer, A., Schlamadinger, B., Ceulemans, R., Ciais, P., Dolman, A. J., & Heimann, M. (2005). The carbon budget of terrestrial ecosystems at country-scale—A European case study. *Biogeosciences*, *1*, 15–26.

Jobbágy, E. G., & Jackson, R. B. (2000). The vertical distribution of soil organic carbon and its relation to climate and vegetation. *Ecological Applications*, *10*, 423–436. https://doi.org/10.1890/1051-0761(2000)010(0423:TVDOSO)2.0.CO;2

Jonard, M., Nicolas, M., Coomes, D. A., Caignet, I., Saenger, A., & Ponette, Q. (2017). Forest soils in France are sequestering substantial amounts of carbon. *Science of the Total Environment*, *574*, 616–628. https://doi.org/10.1016/j.scitotenv.2016.09.028

Jones, R. J. A., Hiederer, R., Rusco, E., & Montanarella, L. (2005). Estimating organic carbon in the soils of Europe for policy support. *European Journal of Soil Science*, *56*, 655–671.

Kleber, M., Mikutta, R., Torn, M. S., & Jahn, R. (2005). Poorly crystalline mineral phases protect organic matter in acid subsoil horizons. *European Journal of Soil Science*, *56*, 717–725.

Kopáček, J., & Veselý, J. (2005). Sulfur and nitrogen emissions in the Czech Republic and Slovakia from 1850 till 2000. *Atmospheric Environment*, *39*, 2179–2188.

Lal, R. (2005). Forest soils and carbon sequestration. *Forest Ecology and Management*, *220*, 242–258.

Landscape Atlas of the Czech Republic. 2009. Ministry of the Environment, Prague.

Lavelle, P., Chauvel, A. & Fragoso, C. (1995). Faunal activity in acid soils. In: Date, R. A., Grundon, N. J., Rayment, G. E., Probert, M. E. (eds.), *Plant-Soil Interactions at Low pH: Principles and Management*, (pp. 201–211). Dordrecht: Kluwer Academic Publishers.

Liptzin, D., & Seastedt, T. R. (2010). Regional and local patterns of soil nutrients at Rocky Mountain treelines. *Geoderma*, *160*, 208–217. https://doi.org/10.1016/j.geoderma.2010.09.022

Liski, J., Perruchoud, D., & Karjalainen, T. (2002). Increasing carbon stocks in the forest soils of western Europe. *Forest Ecology and Management*, *169*, 159–175.

Liu, L., & Greaver, T. L. (2010). A global perspective on belowground carbon dynamics under nitrogen enrichment. *Ecology Letters*, *13*, 819–828.

Lorenz, K., & Lal, R. (2010). *Carbon sequestration in forest ecosystems*. Dordrecht: Springer.

Lorenz, K., Lal, R., & Shipitalo, M. J. (2011). Stabilized soil organic carbon pools in subsoils under forest are potencial sinks for atmospheric CO_2. *Forest Science*, *57*, 19–25.

Lundström, U. S., Van Breemen, N., & Bain, D. (2000). The podzolization process. A review. *Geoderma*, *94*, 91–107.

Lützow, M. V., Kögel-Knabner, I., Ekschmitt, K., Matzner, E., Guggenberger, G., Marschner, B., & Flessa, H. (2006). Stabilization of organic matter in temperate soils: Mechanisms and their relevance under different soil conditions—A review. *European Journal of Soil Science*, *57*, 426–445.

Marková, I., Janouš, D., Pavelka, M., Macků, J., Havránková, K., Rejšek, K., & Marek, M. V. (2016). Potential changes in Czech forest soil carbon stocks under different climate change scenarios. *Journal of Forest Science*, *2016*, 537–544.

Martin, M. P., Wattenbach, M., Smith, P., Meersmans, J., Jolivet, C., Boulonne, L., & Arrouays, D. (2011). Spatial distribution of soil organic carbon stocks in France. *Biogeosciences*, *8*, 1053–1065.

Meier, I. C., & Leuschner, C. (2010). Variation of soil and biomass carbon pools in beech forests across a precipitation gradient. *Global Change Biology*, *16*, 1035–1045.

Moldan, F., Kjønaas, O. J., Stuanes, A. O., & Wright, R. F. (2006). Increased nitrogen in runoff and soil following 13 years of experimentally increased nitrogen deposition to a coniferous-forested catchment at Gårdsjön, Sweden. *Environmental Pollution*, *144*, 610–620.

Morais, T. G., Teixeira, R. F. M., & Domingos, T. (2019). Detailed global modelling of soil organic carbon in cropland, grassland and forest soils. *PLoS One*, *14*, 1–27.

Mou, P., Jones, R. H., Guo, D., & Lister, A. (2005). Regeneration strategies, disturbance and plant interactions as organizers of vegetation spatial patterns in a pine forest. *Landscape Ecology*, *20*, 971–987.

Mulder, J., De Wit, H. A., Boonen, H. W., & Bakken, L. R. (2001). Increased levels of aluminium in forest soils: effects on the stores of soil organis carbon. *Water, Air, and Soil Pollution*, *130*, 989–994.

Mylona, S. (1996). Sulphur dioxide emissions in Europe 1880-1991 and their effect on sulphur concentrations and depositions. *Tellus B*, *48*, 662–689.

Nabuurs, G., Thürig, E., Heidema, N., Armolaitis, K., Biber, P., Cienciala, E., ... Vallet, P. (2008). Hotspots of the European forests carbon cycle. *Forest Ecology and Management*, *256*, 194–200.

Navrátil, T., Kurz, D., Krám, P., Hofmeister, J., & Hruška, J. (2007). Acidification and recovery of soil at a heavily impacted forest catchment (Lysina, Czech Republic) - SAFE modeling and field results. *Ecological Modelling*, *205*, 464–474.

Norton, S. A., Kopáček, J. & Fernandez, I. J. (2014). Acid Rain-Acidification and Recovery. In: Holland, H. D., Turekian, K. K. (eds.): Treatise on Geochemistry: Second Edition. Elsevier, 379–414.

Olsson, P. A., Burleigh, S. H., & Van Aarle, I. M. (2005). The influence of external nitrogen on carbon allocation to Glomus intraradices in monoxenic arbuscular mycorrhiza. *New Phytologist*, *168*, 677–686.

Oulehle, F., Chuman, T., Hruška, J., Krám, P., McDowell, W. H., Myška, O., ... Tesař, M. (2017). Recovery from acidification alters concentrations and fluxes of solutes from Czech catchments. *Biogeochemistry*, *132*, 251–272.

Oulehle, F., Evans, Ch. D., Hofmeister, J., Krejci, R., Tahovska, K., Persson, T., ... Hruska, J. (2011). Major changes in forest carbon and nitrogen cycling caused by declining sulphur deposition. *Global Change Biology*, *17*(10), 3115–3129. http://dx.doi.org/10.1111/j.1365-2486.2011.02468.x.

Oulehle, F., Hofmeister, J., Cudlín, P., & Hruška, J. (2006). The effect of reduced atmospheric deposition on soil and soil solution chemistry at a site subjected to long-term acidification, Načetín, Czech Republic. *Science of the Total Environment*, *370*, 532–544.

Oulehle, F., & Hruška, J. (2005). Tree species (Picea abies and *Fagus sylvatica*) effects on soil water acidification and aluminium chemistry at sites subjected to long-term acidification in the Ore Mts., Czech Republic. *Journal of Inorganic Biochemistry*, *99*, 1822–1829.

Oulehle, F., Kopáček, J., Chuman, T., Černohous, V., Hůnová, I., Hruška, J., ... Evans, C. D. (2016). Predicting sulphur and nitrogen deposition using a simple statistical method. *Atmospheric Environment*, *140*, 456–468.

Oulehle, F., Mcdowell, W. H., Hruška, J., Aitkenhead-peterson, J. A., Kra, P., & Fottova, D. (2008). Long-term trends in stream nitrate concentrations and losses across watersheds undergoing recovery from acidification in the Czech Republic. *Ecosystems*, *11*, 410–425.

Oulehle, F., Růžek, M., Tahovská, K., Bárta, J., & Myška, O. (2016). Carbon and nitrogen pools and fluxes in adjacent mature Norway spruce and european beech forests. *Forests*, *7*, 1–17.

Oulehle, F., Tahovská, K., Chuman, T., Evans, C. D., Hruška, J., Růžek, M., & Bárta, J. (2018). Comparison of the impacts of acid and nitrogen additions on carbon fluxes in European conifer and broadleaf forests. *Environmental Pollution*, *238*, 884–893.

Persson, T., Lundkvist, H., Wirén, A., Hyvönen, R., & Wessén, B. (1989). Effects of acidification and liming on carbon and nitrogen mineralization and soil organisms in mor humus. *Water, Air, and Soil Pollution*, *45*, 77–96.

Rasmussen, C., Heckman, K., Wieder, W. R., Keiluweit, M., Lawrence, C. R., Berhe, A. A., ... Wagai, R. (2018). Beyond clay: towards an improved set of variables for predicting soil organic matter content. *Biogeochemistry*, *137*, 297–306.

Rumpel, C., & Kögel-Knabner, I. (2011). Deep soil organic matter-a key but poorly understood component of terrestrial C cycle. *Plant and Soil*, *338*, 143–158.

Ružek, M., Myška, O., Kučera, J., & Oulehle, F. (2019). Input-output budgets of nutrients in adjacent Norway spruce and European beech monocultures recovering from acidification. *Forests*, *10*(1), 1–22.

Salomé, C., Nunan, N., Pouteau, V., Lerch, T. Z., & Chenu, C. (2010). Carbon dynamics in topsoil and in subsoil may be controlled by different regulatory mechanisms. *Global Change Biology*, *16*, 416–426.

Šantrůčková, H., Tahovská, K., & Kopáček, J. (2009). Nitrogen transformations and pools in N-saturated mountain spruce forest soils. *Biology and Fertility of Soils*, *45*, 395–404.

Sauer, D., Sponagel, H., Sommer, M., Giani, L., Jahn, R., & Stahr, K. (2007). Podzol: Soil of the year 2007. A review on its genesis, occurrence, and functions. *Journal of Plant Nutrition and Soil Science*, *170*, 581–597.

Schmidt, M. W. I., Torn, M. S., Abiven, S., Dittmar, T., Guggenberger, G., Janssens, I. A., ... Trumbore, S. E. (2011). Persistence of soil organic matter as an ecosystem property. *Nature*, *478*, 49–56.

Schöning, I., Morgenroth, G., & Kögel-Knabner, I. (2005). O/N-alkyl and alkyl C are stabilised in fine particle size fractions of forest soils. *Biogeochemistry*, *73*, 475–497.

Schulp, C. J. E., Nabuurs, G. J., & Verburg, P. H. (2008). Future carbon sequestration in Europe-Effects of land use change. *Agriculture, Ecosystems and Environment*, *127*, 251–264.

Schulze, E.-D., Lange, O., & Oren, R. (1989). Processes Leading to Forest Decline: a Synthesis. In Schulze, E., Lange, O., Oren, R. (eds.), *Forest decline and air pollution*, (pp. 459–468). Berlin: Springer-Verlag.

Spielvogel, S., Prietzel, J., & Kögel-Knabner, I. (2008). Soil organic matter stabilization in acidic forest soils is preferential and soil type-specific. *European Journal of Soil Science*, *59*, 674–692.

Tan, Z., Lal, R., Smeck, N. E., Calhoun, F. G., Slater, B. K., Parkinson, B., & Gehring, R. M. (2004). Taxonomic and geographic distribution of soil organic carbon pools in Ohio. *Soil Science Society of America Journal*, *68*, 1896–1904.

Tashi, S., Singh, B., Keitel, C., & Adams, M. (2016). Soil carbon and nitrogen stocks in forests along an altitudinal gradient in the eastern Himalayas and a meta-analysis of global data. *Global Change Biology*, *22*, 2255–2268.

Taylor, A. R., Wang, J. R., & Chen, H. Y. H. (2007). Carbon storage in a chronosequence of red spruce (*Picea rubens*) forests in central Nova Scotia, Canada. *Canadian Journal of Forest Research*, *37*, 2260–2269. https://doi.org/10.1139/X07-080

Tolasz, R., Míková, T., Valeriánová, A., & Voženílek, V. (2007). *Climate Atlas of Czechia*. Prague: Czech Hydrometeorological Institute.

Tóth, G., Montanarella, L., Stolbovoy, V., Maté, F., Bódis, K., Jones, A., ... Van Liedekerke, M. (2008). *Soils of the European Union*. Luxembourg: European Commission.

Trum, F., Titeux, H., Ranger, J., & Delvaux, B. (2011). Influence of tree species on carbon and nitrogen transformation patterns in forest floor profiles. *Annals of Forest Science*, *68*, 837–847.

Vanmechelen, L., Groenemans, R., & Van Ranst, E. (1997). *Forest soil conditions in Europe*. Geneva: Springer.

Vávrová, E., Cudlín, O., Vavříček, D., & Cudlín, P. (2009). Ground vegetation dynamics in mountain spruce (*Picea abies* (L.) Karsten) forests recovering after air pollution stress impact. *Plant Ecology*, *205*, 305–321.

Vesterdal, L. (1999). Influence of soil type on mass loss and nutrient release from decomposing foliage litter of beech and Norway spruce. *Canadian Journal of Forest Research*, *29*, 95–105. https://doi.org/10.1139/x98-182#.XZNCqn_gphE

Vesterdal, L., Clarke, N., Sigurdsson, B. D., & Gundersen, P. (2013). Do tree species influence soil carbon stocks in temperate and boreal forests? *Forest Ecology and Management*, *309*, 4–18. https://doi.org/10.1016/j.foreco.2013.01.017

Vesterdal, L., Schmidt, I. K., Callesen, I., Nilsson, L. O., & Gundersen, P. (2008). Carbon and nitrogen in forest floor and mineral soil under six common European tree species. *Forest Ecology and Management*, *255*, 35–48.

Vet, R., Artz, R. S., Carou, S., Shaw, M., Ro, C. U., Aas, W., ... Reid, N. W. (2014). A global assessment of precipitation chemistry and deposition of sulfur, nitrogen, sea salt, base cations, organic acids, acidity and pH, and phosphorus. *Atmospheric Environment*, *93*, 3–100. https://doi.org/10.1016/j.atmosenv.2013.10.060

Viewegh, J., Kusbach, A., & Mikeska, M. (2003). Czech forest ecosystem classification. *Journal of Forest Science*, *49*, 85–93. http://agriculturejournals.cz/publicFiles/55710.pdf

Waldrop, M. P., Zak, D. R., & Sinsabaugh, R. L. (2004). Microbial community response to nitrogen deposition in northern forest ecosystems. *Soil Biology and Biochemistry*, *36*, 1443–1451.

Wang, Y., Li, Y., Ye, X., Chu, Y., & Wang, X. (2010). Profile storage of organic/inorganic carbon in soil: From forest to desert. *Science of the Total Environment*, *408*, 1925–1931. https://doi.org/10.1016/j.scitotenv.2010.01.015

Watson, R. T., Noble, I. R., Bolin, B., Ravindranath, N. H., Verardo, D. J., & Dokken, D. J. (2000). *Land use, land use change, and forestry—A special report of the intergovernmental panel on climate change*. Cambridge: IPCC.

Wiesmeier, M., Prietzel, J., Barthold, F., Spörlein, P., Geuß, U., Hangen, E., ... Kögel-Knabner, I. (2013). Storage and drivers of organic carbon in forest soils of southeast Germany (Bavaria) - Implications for carbon sequestration. *Forest Ecology and Management*, *295*, 162–172. https://doi.org/10.1016/j.foreco.2013.01.025

Yanai, R. D., Stehman, S. V., Arthur, M. A., Prescott, C. E., Friedland, A. J., Siccama, T. G., & Binkley, D. (2003). Detecting change in forest floor carbon. *Soil Science Society of America Journal*, *67*, 1583–1593. https://doi.org/10.2136/sssaj2003.1583

Software

Bartoń, K., 2013. MuMIn: Model selection and model averaging based on information criteria. R package. http://cran.r-project.org/web/packages/MuMIn/index.html.

Lefcheck, J. S. (2015). piecewiseSEM: Piecewise structural equation modeling in R for ecology, evolution, and systematics. *Methods in Ecology and Evolution*, *7*(5), 573–579. https://doi.org/10.1111/2041-210X.12512

Pinheiro, J., Bates, D., DebRoy, S., Sarkar, D., and R Core Team, 2017. nlme: Linear and nonlinear mixed effects models. R package version 3.1-131. https://CRAN.R-project.org/package=nlme.

R Development Core Team. (2013). *R: A language and environment for statistical computing*. Vienna: R Foundation for Statistical Computing. http://www.R-project.org

SUPPORTING INFORMATION

Additional supporting information may be found online in the Supporting Information section at the end of this article.

How to cite this article: Chuman T, Oulehle F, Zajícová K, Hruška J. The legacy of acidic deposition controls soil organic carbon pools in temperate forests across the Czech Republic. *Eur J Soil Sci*. 2021;72:1780–1801. https://doi.org/10.1111/ejss.13073

9.2. Publication II

Zajícová, K., Chuman, T., 2021. Spatial variability of forest floor and topsoil thicknesses and their relation to topography and forest stand characteristics in managed forests of Norway spruce and European beech. European Journal of Forest Research 140, 77–90. https://doi.org/10.1007/s10342-020-01316-1

European Journal of Forest Research (2021) 140:77–90
https://doi.org/10.1007/s10342-020-01316-1

ORIGINAL PAPER

Spatial variability of forest floor and topsoil thicknesses and their relation to topography and forest stand characteristics in managed forests of Norway spruce and European beech

Kateřina Zajícová[1,2] · **Tomáš Chuman**[1,3]

Received: 2 March 2020 / Revised: 14 August 2020 / Accepted: 5 September 2020 / Published online: 25 September 2020

Abstract
Soils play a significant role in climate regulation, especially due to soil organic carbon (SOC). The SOC pool is therefore modeled for various environments, and forest floor and topsoil thicknesses are important parameters for most of these models as they store most of the SOC. However, the forest floor and topsoil thicknesses show high spatial variability which is a result of multiple factors which are not agreed upon among scientists. Out of these factors, we choose topography parameters (elevation, slope, and topography wetness index) and forest stand characteristics (stand age, dominant tree species, and forest floor cover), and soil moisture, and we analyzed their relationship to the forest floor and topsoil thicknesses. The study was performed in a managed submontaneous forest in Central Europe dominated by *Picea abies* (L.) *Karsten* with small patches of *Fagus sylvatica* L. or other species. The thicknesses of the O horizons (Oi, Oe, Oa) and topsoil were measured at 221 sampling pits. Geographically weighted regression showed that the spatial variability of the overall forest floor plus topsoil thickness (OA) is responsible for 8% of its variability. The thickness of the OA is the most strongly controlled by forest floor cover explaining approximately 6% of its variability and soil moisture explaining 2–6% of the variability. The Oi + Oe horizon thickness is controlled only by forest floor cover explaining 10.7% of its variability, and the thickness of Oa + A horizon can be explained mainly by soil moisture in mineral horizon explaining 9% of the variability.

Keywords Soil organic carbon · Temperate climate · Geographically weighted regression · Cambisols · Podzols

Introduction

Soils provide important ecosystem services (Adhikari and Hartemink 2016) owing to their key functions, i.e., carbon storage, biomass production, water filtration and water storage, nutrients' supply, or provide habitat for numerous species and their activity (Adhikari and Hartemink 2016; Wiesmeier et al. 2019). The principal soil component controlling most of these soil functions is soil organic matter. It increases water retention capacity and hydraulic conductivity (Bens et al. 2007), it is a source of nutrients (Hansson et al. 2013), and thickness of the organic layer (forest floor) controls soil thermoregulation (Wang et al. 2014).

Nowadays, the soil organic carbon pools are modeled in all environments from tropical forests (e.g., Rossi et al. 2009), desserts and semi-desserts (e.g., Brahim et al. 2014), through subtropical vegetation (e.g., Conforti et al. 2016; Francaviglia et al. 2017), temperate forests (e.g., Ahmed et al. 2016; Cremer et al. 2016; Marty et al. 2015; Schöning et al. 2006) to boreal forests (e.g., Hansson et al. 2013; Kristensen et al. 2015; Marty et al. 2015; Strand et al. 2016). The thicknesses of the forest floor and topsoil are important parameters for these models (e.g., Kristensen et al. 2015; Muukkonen et al. 2009; Strand et al. 2016). However, due to very high spatial variability it is often not well represented in models, only as mean thickness.

High spatial variability of forest floor and topsoil thicknesses is a result of multiple factors. These factors include

Communicated by Agustín Merino.

✉ Kateřina Zajícová
katerina.zamazalova@natur.cuni.cz

[1] Department of Physical Geography and Geoecology, Faculty of Science, Charles University, Albertov 6, 128 43 Prague 2, Czech Republic

[2] Global Change Research Institute of the Czech Academy of Sciences, Bělidla 986/4a, 603 00 Brno, Czech Republic

[3] Czech Geological Survey, Klárov 3, 118 21 Prague 1, Czech Republic

parent material, topography, climate and soil moisture, vegetation, and bioturbation. At global to local scale, the forest floor and topsoil thicknesses, thus carbon pools in these soil horizons in most cases, increase with precipitation and decrease with temperature (Marty et al. 2015; Wiesmeier et al. 2019). At (sub)regional and local scale, elevation can be a good indicator instead of them (Wiesmeier et al. 2019). The forest floor thickness and its carbon pool were observed to increase with elevation e.g., by Labaz et al. (2014); Marty et al. (2015); Anschlag et al. (2017). In other studies, crucial role in soil organic matter accumulation has been attributed to soil moisture because it controls ecosystem net primary production, thus organic matter input on the one hand, on the other hand soil microbial activity and carbon loses via heterotrophic respiration (De Nicola et al. 2014; Strand et al. 2016; Wiesmeier et al. 2019). High moisture reduces the microbial activity due to reduced oxygen availability, and low moisture decreases the biomass production (Wiesmeier et al. 2019). Micro-climate and the soil moisture are influenced by topography creating conditions favoring water accumulation or drainage, thus controlling carbon accumulation (Laamrani et al. 2014a, b; De Nicola et al. 2014; Wiesmeier et al. 2019). Lower slopes and low or concave curvatures favor water accumulation, whereas steep slopes and convex curvatures lead to higher water discharge with additional erosion in most cases. Conforti et al. (2016) confirmed a close relationship between the topography and carbon pool in the topsoil (A horizon) but not in the forest floor.

Parent material characteristics are projected mainly to soil physical and chemical properties regulating water retention, biomass production, and its decomposition rate (Ponge et al. 2011; De Nicola et al. 2014; Wiesmeier et al. 2019). For example, Ponge et al. (2011) and Schöning et al. (2006) declared bedrock as the main factor controlling forest floor and topsoil characteristics; however, Wiesmeier et al. (2019) based on literature review concluded that the effect of parent material was rather low.

Vegetation controls forest floor and topsoil thicknesses, thus soil organic matter accumulation and its storage through differences in biomass production and its decomposability; the latter is considered as more important (Marty et al. 2015). According to numerous studies, carbon pools in the forest floor are higher under conifers due to their acid and recalcitrant litter (Marty et al. 2015; Cremer et al. 2016; Strand et al. 2016; Wiesmeier et al. 2019) but also due to their higher litter production (Hansson et al. 2013). The average forest floor thicknesses under spruce (*Picea abies* (L.) *Karsten* or *Picea mariana* (Mill.)) were observed to reach from 4.7 to 8.4 cm (Hansson et al. 2013; Labaz et al. 2014; Kristensen et al. 2015) or even 19–21 cm (Yu et al. 2002), and under pine (*Pinus sylvestris* L. or *Pinus banksiana* Lamb.) they were from 2 to 10.7 cm (Liski 1995; Smit 1999; Yu et al. 2002; Bens et al. 2006; Hansson et al. 2013). The average forest floor thicknesses under European beech (*Fagus sylvatica* L.) were recorded between 1 and 6.4 cm (Schöning et al. 2006; Labaz et al. 2014; Conforti et al. 2016) and under silver birch (*Betula pendula* Roth) 2.1 cm (Hansson et al. 2013). It is well known that the forest floor thickness and its carbon pool increase with stand age because of lower biomass productivity of younger trees (Yu et al. 2002; Peltoniemi et al. 2004; Pregitzer and Euskirchen 2004; Bens et al. 2006; Strand et al. 2016). Contemporaneously with tree growth, forest floor thickness and its carbon pool change, e.g., in managed forest it reaches its minimum 20 years after harvesting, and then, it increases till the age of 120 years when the litter production slows down (Peltoniemi et al. 2004; Pregitzer and Euskirchen 2004). Trap et al. (2013) also showed that the litter decomposability changes as well with tree aging, at least for *Fagus sylvatica* L. It decreases with tree age as lignin concentration increases in the litter (Trap et al. 2013).

Several studies, e.g., Šamonil et al. (2011), Brahim et al. (2014), Labaz et al. (2014) and Strand et al. (2016) analyzed the differences in forest floor carbon accumulation among soil types. Since the soil types are results of soil forming factors and processes which influence the forest floor carbon pool as discussed above, these studies proved significant differences among the soil types as well.

Recently, several studies showed a significant relation of the forest floor carbon pool and historical sulfur deposition due to elevated soil acidity and subsequent mobilization of Al^{3+} with toxic effect on plant roots (de Wit et al. 2010), which leads to accumulation of the organic carbon in the forest floor (Mulder et al. 2001), induces changes in soil biota (Persson et al. 1989), and increases fungal to bacterial ratio by decreasing the abundance of bacteria (Oulehle et al. 2018).

All of these factors act at global to local scale driving very high spatial variability of the forest floor thickness and its carbon stock. Spatial variability of the soil organic carbon pool was analyzed in several studies (e.g., Conforti et al. 2016; Heim et al. 2009; Marty et al. 2015; Muukkonen et al. 2009; Rossi et al. 2009; Schöning et al. 2006), but only few studies (Liski 1995; Bens et al. 2006; Šamonil et al. 2011; Valtera et al. 2013; Kristensen et al. 2015) focused on the forest floor and topsoil thicknesses; therefore, the controlling factors are still not well understood. For that reason, the aim of this study was to reveal spatial variability of the forest floor and topsoil thicknesses in a managed forest and their relation to environmental factors. We hypothesize that factors that drive soil organic carbon accumulation and storage affect also the forest floor and topsoil thicknesses. These factors include topography and forest stand characteristics: elevation, slope, topography wetness index (TWI), stand age, dominant tree species, forest floor cover, and soil moisture.

Materials and methods

Study site

The study was conducted in a long term monitored LIZ catchment (0.9 km^2) situated on the border of the Bohemian Forest (Šumava Mountains) in the southwest of Bohemia ("Annex 1"). The catchment is a part of the GEOMON network managed by the Czech Geological Survey (Oulehle et al. 2016). The LIZ catchment lies at 826–1071 m a. s. l. and has southeast to northeast exposition. The bedrock is formed by metamorphic rock (paragneiss) of low alkalinity (Chuman et al. 2014). It is covered by a managed forest dominated by Norway spruce (*Picea abies* (L.) *Karsten*) with patches of European beech (*Fagus sylvatica* L.) and patches of mixed stands of Norway spruce (*Picea abies* (L.) *Karsten*) with either European larch (*Larix decidua* Mill.) or Silver birch (*Betula pendula* Roth) or Scots pine (*Pinus sylvestris* L.). Mean annual temperature is 5.5 °C and mean annual precipitation 892 mm for 1994–2014 period (Oulehle et al. 2017).

Soils are dominated by Cambisols, mostly Haplic Cambisol (CMha), but Dystric (CMdy) and Gleyic Cambisol (CMgl) are also present throughout the catchment together with Entic Podzols (PZet) in the highest parts of the catchment and hydromorphic soil at sites with high water table (Gleysols; GL) or periodically wet depressions (Stagnosols; ST) ("Annex 2"). Soil texture shows rather low variability, and most of the soils are classified as sandy soils ("Annex 3").

The soil texture was analyzed by hydrometer method (ISO 11277 2009); textural classes were defined according to USDA particle sizes. The particle density was analyzed by pycnometer method (ISO 11508 2009). The bulk density was determined by weighting dried samples taken quantitatively within a 10 × 10 cm reference frame and subdivided onto the horizon complexes: Oi + Oe, Oa + A, and the underlying horizon (B or E) separately. The thickness of each horizon within the reference frame was measured.

Data collection

Thicknesses of the O horizons (Oi, Oe, Oa) and A ("topsoil") were measured at 300 sampling points (spoil pits) ("Annex 1") selected by a stratified random sampling. The stratified random sampling was based on forest soil edaphic categories (Viewegh 2003) ("Annex 4"), and forest stand ages ("Annex 5") delineated and regularly updated by the forest management inventories (Forest Management Institute—ÚHUL). There are three edaphic categories in the study catchments: oligotrophic, hydric, and stony slope. The oligotrophic edaphic category is characterized by unexposed relief, acid soil parent material, partly developed soils, and mostly Dystric Cambisols and Cambic Podzols with Mor-moder and Mor humus form (Viewegh 2003). It is the most common category of the forest in the Czech Republic. The hydric edaphic category—"moist to wet"—contains water-enriched soils on stagnic tall deluvia and steep slope bases, mostly Stagni-Dystric Cambisols, Gleyic Cambisols, and Cambic Gleysols with nitrophilous species (Viewegh 2003). The stony slope category is described by nutrient-poor, stony soils on slopes, and exposed relief, mostly undeveloped and eroded oligotrophic Skeletic Cambisols and their transition to Skeletic Leptosols (Viewegh 2003).

The number of samples per each unique combination of forest age and forest site complex was proportional to its area and varied from 2 to 86. Out of 300 randomly generated positions of soil pits, 79 fell onto hyperskeletic soils or block fields ("Annex 2") that correspond with the stony slope edaphic category. At such sites, any accurate measurement of the forest floor and topsoil thickness was not possible; thus, we measured soil horizon' thicknesses at 221 soil pits and the stony slope edaphic category was excluded from the analysis. In these pits, the organic litter horizon Oi was very often indistinguishable from the fragmented organic horizon Oe and the humified organic horizon Oa from the very thin organic mineral topsoil A. Therefore, the horizons Oi + Oe and Oa + A were considered as complexes and only the thicknesses of these two complexes were measured.

The predictors, used in this study for an explanation of spatial variability of Oi + Oe and Oa + A thicknesses, were topography and forest stand characteristics. The topography was described by elevation, slope, and topography wetness index (TWI). The forest stand characteristics were described by soil edaphic category, forest stand age, dominant tree species, forest floor cover, and measured soil moisture. The topography attributes (elevation, slope, curvature, TWI) were derived from DEM with 10 × 10 m resolution (CUZK 2006) in ArcGIS 10.2. TWI was calculated based on Sorensen et al. (2006). The forest stand characteristics were recorded in the field (dominant tree species, forest floor cover, soil moisture) or extracted from existing databases of the Forest management institute (ÚHÚL 2015), which record edaphic category (see "Annex 4") and forest stand age (see "Annex 5").

The dominant tree species were assessed within a 100 m^2 circular plot around each soil pit, and all species with cover of 20% and higher were recorded. The forest floor cover classified to needles, leaves, graminoids, moss, myrtilles, and spruce seedlings was assessed within a circular plot with 50 cm diameter around each soil pit. Each type was named according to the dominant forest floor cover, i.e., the

category covering more than 50% of the ground (e.g., sites with scattered spruce seedlings on a ground covered with needles were classified as needles, sites with dense cover of spruce seedlings were classified as spruce seedlings, etc.). We recorded all types of the forest floor cover which covered at least 20% of the circular plot. The soil moisture was measured using TDR probe Decagon GS3 during field sampling in both horizon complexes (Oi + Oe and Oa + A) and in the underlying mineral horizon.

Data analysis

The thicknesses of measured horizons Oi + Oe and Oa + A were tested for spatial autocorrelation using Moran's I and subsequently characterized in more detail by variogram analysis. Theoretical variograms using Gaussian model were created by means of ArcGIS (ESRI) Ordinary Kriging function for the horizon complexes of Oi + Oe, Oa + A and combined Oi + Oe + Oa + A (hereafter OA) using all samples. Then, we created theoretical variograms separately for the hydric edaphic category and the oligotrophic edaphic category. The average nearest neighbor determined in ArcGIS (around 40 m) was used as the lag size.

Since the data showed the spatial autocorrelation, we analyzed the data by means of geographically weighted regression (Fotheringham et al. 2002). We analyzed the relationship between the OA, Oi + Oe and Oa + A thicknesses and the forest stand characteristics (stand age category, forest floor cover, and dominant tree species), the topography parameters (elevation, slope, curvature, and TWI) and the soil moisture measured in the field.

The explanatory variables were tested for multicollinearity by means of Spearman correlation analysis (Table 1) and by means of Distance analyses in case of categorical explanatory variables (stand age category, forest floor cover, and dominant tree species). The distance analysis showed no similarity between the tested variables; however, the Spearman correlation analysis showed relatively strong correlation of the TWI and the slope, and of the TWI and the curvature, and further correlation among the moisture variables.

Thus, two statistical models were compiled for the geographically weighted regression: the first including the TWI and omitting the slope and the curvature, and the second including the slope and the curvature but omitting the TWI. Out of the highly correlated moisture variables, the moisture in the mineral horizon was chosen as the variable with the closest relation (Table 2) to horizon "complexes" thicknesses. Since the moisture determination in the mineral horizon had not been successfully performed at all locations because of too many rock fragments which made the measurement using the device (GS3 sensor) impossible, only 164 out of 221 samples were suitable for the geographically weighted regression (GWR).

As explained above, subsequent models were compiled:

1. Topography wetness index, forest floor cover, stand age, dominant tree species, elevation, moisture.
2. Slope, curvature, forest floor cover, dominant tree species, moisture, stand age, elevation.

The geographically weighted regression was performed in GWR 4.09 (Nakaya et al. 2009, update 2016). At first, a model with the local intercept alone was computed

Table 2 Spearman correlation coefficient between horizons' complexes' thicknesses and measured moistures

Horizon complex thickness	Moisture Oi + Oe	Moisture Oa + A	Moisture mineral
OA	−0.07	0.05	0.16*
Oi + Oe	−0.07	−0.15	0
Oa + A	−0.07	0.18*	0.22**

OA—forest floor plus topsoil thickness in total, Oi—organic litter horizon, Oe—fragmented organic horizon, Oa—humified organic horizon, A—topsoil

Table 1 Spearman correlation coefficient of explanatory variables

Variable	Slope	Moisture Oi + Oe	Moisture Oa + A	Moisture in mineral soil	Curvature	TWI	Elevation
Slope							
Moisture Oi + Oe							
Moisture Oa + A		0.45					
Moisture in mineral soil		0.30	0.60				
Curvature							
TWI	0.53	−0.16			−0.27		
Elevation							

Oi—organic litter horizon, Oe—fragmented organic horizon, Oa—humified organic horizon, A—topsoil; TWI—topography wetness index
Only correlations of a value over 0.15 are shown

in order to estimate the part of the data variability that could be explained by the spatial variability itself. Subsequently, the other explanatory variables were added one by one as independent variables to the model to observe their impact on the horizon "complexes" thicknesses. The bandwidth of the local computation was left to find by GWR 4.09 Golden search, but it was kept to stay similar for all computations belonging to the same model. For further computation details, see "Annex 6."

Results

The average total thickness of OA horizons is 15.5 cm in the Liz catchment. It consists of 4.7 cm thick less decomposed organic horizons Oi + Oe and 10.8-cm-thick horizons Oa + A. The organomineral A horizon is very thin and often indistinguishable. The data show the difference in horizons "complexes" thicknesses between edaphic categories (see Table 3 for detailed information about classes and numbers of cases). The Oi + Oe organic horizons are of a similar thickness at both edaphic categories, but the thickness of the Oa + A makes the difference. There seems to be also higher variability of the thickness of the studied horizons

Table 3 Horizons "complexes" thicknesses in different forest stand characteristics

	N	OA		Oi + Oe		Oa + A	
		Mean	SD	Mean	SD	Mean	SD
Oligotrophic stand	151	14.9	4.8	4.8	2.3	10.1	4.5
Hydric stand	70	17.0	8.4	4.4	2.1	12.7	8.1
Stand age							
Young (under 40 years)	35	15.2	6.0	4.3	2.3	11.0	5.8
Middle (61–100 years)	92	16.0	8.0	4.6	2	11.4	8.0
Old (over 100 years)	94	15.3	4.0	5.1	2.5	10.2	4.0
Soil type							
Haplic Cambisol	94	14.3	5.3	4.7	2.4	9.6	4.9
Dystric Cambisol	19	14.3	5.0	4.8	2.1	9.5	3.9
Gleyic Cambisol	26	17.2	9.6	4.0	1.3	13.3	9.5
Entic Podzol	62	17.0	5.4	5.2	2.3	11.8	5.4
Stagnosol	7	19.1	6.6	3.6	1.8	15.6	5.4
Gleysol	13	13.5	4.4	3.5	1.8	10.0	4.0
Dominant tree species							
Spruce	150	15.4	5.6	4.7	2.3	10.8	5.3
Beech	8	14.3	5.4	4.9	1.2	9.4	5.8
Spruce + beech	15	15.0	5.9	5.1	2.1	9.9	6.2
Spruce + beech + larch	13	15.1	5.2	5.4	2.4	9.7	3.4
Spruce + larch	21	14.4	4.5	3.9	1.6	10.3	3.7
Spruce + rowan + willow + birch	14	14.9	7.9	3.4	0.5	11.5	7.5
Forest floor cover							
Needles	50	15.0	8.4	3.8	2.0	11.1	8.1
Needles + moss	54	15.4	6.0	4.6	2.1	11.2	5.7
Moss	37	17.1	5.8	5.7	2.2	11.4	5.3
Gramineous plants	9	14.1	1.2	4.4	1.2	9.7	1.6
Gramineous plants + moss	12	13.9	2.2	4.4	1.8	9.5	2.8
Gramineous plants + needles	2	19.5	9.5	2.5	0.5	17.0	10.0
Leaves	14	15.3	5.7	5.7	1.9	9.7	5.3
Leaves + needles	20	14.0	3.9	5.3	3.0	8.7	3.2
Myrtilles	11	17.0	5.5	6.0	1.9	12.0	6.5
Spruce seedlings	12	16.0	5.1	4.5	2.3	12.0	4.5

OA—forest floor plus topsoil in total, Oi—organic litter horizon, Oe—fragmented organic horizon, Oa—humified organic horizon, A—topsoil; *N*—number of cases; SD——standard deviation

Table 4 Variability of the studied horizons' complexes based on variograms

Forest stands	Horizons' complex	Range (m)	Nugget to sill ratio (% of sill)
All	OA	253	78.1
	Oi + Oe	273	80.4
	Oa + A	292	70.4
Oligotrophic	OA	206	73.3
	Oi + Oe	268	71.4
	Oa + A	294	58.7
Hydric	OA	262	69.6
	Oi + Oe	–	–
	Oa + A	270	65.3

OA—forest floor plus topsoil in total, Oi—organic litter horizon, Oe—fragmented organic horizon, Oa—humified organic horizon, A—topsoil

"complexes" in hydric edaphic category due to the variability of the Oa + A horizons as well.

The spatial autocorrelation of the thicknesses is significant according to the Moran's I function. However, regarding the variogram ("Annex 7–14," Table 4), the spatial autocorrelation reaches rather low values. The ranges of variograms, i.e., the spatial autocorrelation threshold, for Oi + Oe, Oa + A, and OA, are 273 m, 292 m, and 253 m, respectively. The ratio of the nugget semivariance to the sill semivariance (Essington 2015) oscillates from 80.4% of sill for Oi + Oe, 70.4% of sill for Oa + A to 78.1% of sill for OA, showing slightly better spatial autocorrelation of lower horizons. The Oa + A layer is more spatially autocorrelated at stands in the oligotrophic edaphic category, the variogram range reaching 294 m and the nugget ratio 58.7% of sill, compared to 270 m and the nugget ratio of 65.3% of sill at the hydric stands. By contrast, the Oi + Oe horizons at stands of the hydric edaphic category are not autocorrelated at all, compared to the spatial autocorrelation ranging 268 m and the nugget ratio reaching 71.4% of sill at the oligotrophic stands. The spatial autocorrelation of the OA is stronger at the hydric stands (262 m range, nugget ratio 69.6% of sill) compared to the soils of the oligotrophic stands (range 206 m, nugget ratio 73.3% of sill). It follows that the nugget effect is large for all horizons showing high fine-scale variability.

The geographically weighted regression showed that the spatial variability of OA thickness is responsible for its overall variability from approximately 8% (Table 5a, b). In some models with many explanatory variables included, it is even less, around 4 (Table 5b). This could happen because some other variable (especially moisture) or their combination explained part of the data variability originally explained by the spatial variability. Among the attributes that could influence the OA (forest floor and topsoil) thickness studied in the area, the forest floor cover shows the biggest influence. It explains approximately 6% of the OA thickness variability in the LIZ catchment. The second most influential variables are those explicitly or implicitly expressing soil moisture: the moisture of the mineral horizon measured in the field and the slope or the TWI. These variables explain 2–6% of the variability; the variable "moisture" is the best in most models. It is surprising that the slope explains the data variability better than the TWI. The dominant tree species, the elevation, and the stand age have no or very low influence on the OA thickness. All the designed models explained 15–17% of the variability in the OA thickness.

As it was previously mentioned, the Oi + Oe horizon complex is spatially less autocorrelated, so that even Kernel bandwidth was calculated more tightly. However, in that tight bandwidth, 30% of the data variability can be explained by the spatial variability. From other attributes, only forest floor cover has a significant impact in the model (10.7%), but it explains only a part of the variability explained by the spatial variability as well; the model does not exceed higher R2 (Table 5c). By contrast, the variability of the thickness of the Oa + A can be explained, together with the spatial variability (10–15%), mostly by soil moisture in the mineral horizon (9%). The forest floor cover and the slope are also important (Table 5d). The model can explain 28.4% of the data variability.

Discussion

The difference in the thicknesses of the horizons' complexes between the stands of oligotrophic and hydric edaphic categories corresponds with the studies by Strand et al. (2016), Olsson et al. (2009) or Laamrani et al. (2014a), and it is the result of a lower rate of organic matter decomposition at wet sites. The higher variance of organic horizons thicknesses in the soils influenced by water was shown also by Šamonil et al. (2011). Lexer and Hönninger (1998) found a relation of the forest floor and topsoil thicknesses to the wetness of the stand as well, but they suggested that soil particle distribution is of main importance and that soil types can be used as an alternative of that. Labaz et al. (2014) observed decreasing average forest floor thickness in the order: Podzols (8.7 cm), Gleysols and Stagnosols, Dystric Cambisols, Eutric Cambisols, and Luvisols (4.5 cm). According to Šamonil et al. (2011), this sequence slightly differs being the highest for Gleysols (15.9 cm) and decreasing through Albic Podzols, Stagnosols, Entic Podzols, down to Haplic and Dystric Cambisols (6.2 cm). Total forest floor plus topsoil thickness according to Šamonil et al. (2011) decreases in order from Gleysols (27.6 cm), Stagnosols (16.6 cm), Albic Podzols (13.7 cm), Entic Podzols (12.9 cm), Haplic

Table 5 Geographically weighted regression, models' parameters

Variables	Last added variable	R2[a] (%)	Kernel[b] (m)	OLS[c] R2g (%)	R2–R2g (spatial variability %)	Variability explained by the last attribute (%)	Increase in explained variability (%)
(a) Model I OA thickness (N = 164)							
0	Intercept	7.5	311	0	7.5		
0 + 1	Wetness index	9.6	301	1.4	8.2	1.4	**2.2**
0 + 1+2	Forest floor cover	13.3	284	6.9	6.4	5.5	**3.7**
0 + 1+2 + 3	Moisture	15.1	350	11.9	3.2	5.0	**1.8**
0 + 1+2 + 3+4	Tree species	No raise					
0 + 1+2 + 3+5	Stand age	No raise					
0 + 1+2 + 3+6	Elevation	No raise					
(b) Model II OA thickness (N = 164)							
0	Intercept	7.5	311	0	7.5		
0 + 1	Slope	10.0	301	1.9	8.1	**1.9**	**2.6**
0 + 1+2	Curvature	No raise					
0 + 1+3	Forest floor cover	11.9	412	7.6	4.3	**5.7**	**1.9**
0 + 1+3 + 4	Tree species	No raise					
0 + 1+3 + 5	Moisture	17.1	293	13.2	3.9	**5.6**	**5.2**
0 + 1+3 + 5+6	Elevation	Model disruption					
0 + 1+2 + 4+7	Stand age	No raise					
(c) model I + II Oi + Oe thickness (N = 164)							
0	Intercept	30.0	102		30		
0 + 1	Wetness index	No raise	101				**Excluded from model**
0 + 2	Slope	No raise	101				
0 + 3	Curvature	No raise	103				
0 + 4	Forest floor cover	30.0	122	10.7	19.3	**10.7**	
0 + 4+5	Tree species	No raise	134	12.0	18.0	**1.3**	
0 + 4+6	Moisture	No raise	125	12.0	18.0	**1.3**	
0 + 4+7	Stand age	30.0	126	11.0	19.0	**0.3**	
0 + 4+8	Elevation	No raise	292				
(d) Model I + II Oa + A thickness (N = 164)							
0	Intercept	15.0	187		15.0		
0 + 1	Wetness index	No raise	212				**Excluded from model**
0 + 2	Slope	17.8	191	2.4	15.4	**2.4**	**2.8**
0 + 2+3	Curvature	no raise	194				
0 + 2+4	Forest floor cover	20.0	212	8.3	11.7	**5.9**	**2.2**
0 + 2+4 + 5	Tree species	22.0	211	9.4	12.6	**1.1**	**2.0**
0 + 2+4 + 5+6	Moisture	28.04	238	18.4	10.0	**9.0**	**6.4**
0 + 2+4 + 5+6 + 7	Stand age	No raise	240				
0 + 2+4 + 5+6 + 8	Elevation	No raise	242				

Oi—organic litter horizon, Oe—fragmented organic horizon, Oa—humified organic horizon, A—topsoil; *N*—number of cases

[a]R2…variability explained by the model

[b]Kernel…Kernel fixed distance bandwidth

[c]OLS R2g…R2 (=explained variability) by Ordinary least square method computed with global intercept instead of the local intercept (=non-spatial OLS)

Cambisol (12.3 cm) to Dystric Cambisol (11.2 cm): In our study, the sequence of the forest floor plus topsoil thickness is similar with an exception of Gleysols which are surprisingly at the end of the sequence (Table 3). However, in our results, the thicknesses are quite similar, with no marked differences. There are no significant differences in the texture of the soils as well ("Annex 3") which would result from the fact that the soils in the small LIZ catchment develop from similar parent rock in similar climatic conditions.

The spatial autocorrelation in the LIZ catchment reaches rather high thresholds and low values close to 300 m threshold distance (Table 4). Šamonil et al. (2011) found significantly lower threshold of spatial autocorrelation in a natural unmanaged forest. They detected the ranges of 50–100 m. Valtera et al. (2013) found even lower thresholds up to 20 m in a wild montanain forest. It is probable that managed forest is less heterogeneous than unmanaged. The species composition can play a role as well. Bens et al. (2006) showed significantly higher spatial autocorrelation in monospecies stands compared to mixed stands. On the other hand, Smit (1999) found no spatial autocorrelation at all of the forest floor thickness in a pine forest with a herb layer. However, the comparison of the studies is difficult due to different sampling protocols and sampling scales. For example, studies of Liski (1995), Bruckner et al. (1999) and Muukkonen et al. (2009) performed at microscale suggested that forest floor thickness is spatially dependent only up to 2 m but with the nugget ratio below 35% of sill. These authors observed increasing forest floor thickness with decreasing distance to trees. On the other hand, Smit (1999) found no relation between forest floor thickness and the distance to trees, but the study was performed at larger scale. This implies that sampling protocol is of crucial importance as noted also by Kristensen et al. (2015). The sampling protocol must be suitable for detecting variability at the desired scales. In our study, performed rather at mesoscale, the nugget effect and its ratio are large for all organic layers (Table 4) showing big microvariability of the studied forest floor and topsoil. The influence of the microtopography which was not investigated at the scale of our study could be of a big importance. The influence of, e.g., pit mounds to organic horizons thicknesses was observed by Šamonil et al. (2011).

According to the outputs of the geographically weighted regression, the spatial variability of the OA thickness is responsible for its overall variability from approximately 7.5%. However, the results generally correspond with those of Šamonil et al. (2011) who worked at similar scale and the values are probably common for forest soil at this scale. The results show slightly better spatial autocorrelation of lower (Oa + A) layer in our study. By contrast, Šamonil et al. (2011) observed higher spatial autocorrelation for organic horizons than topsoil. They refer to natural disturbances in the natural forest after which the forest floor restoration is faster than that of the topsoil and mineral horizon. Bens et al. (2006) observed lower variability for Oi horizon compared to the underlying organic horizons, similar to our study. They suggested that litter deposition is quite homogenous in space and that the decomposition is responsible for organic horizons' thickness variability. It is in line with our results which show that Oi + Oe and Oa + A thicknesses are driven by different stand characteristics. While the thicknesses of Oi + Oe horizons are influenced by forest floor cover, associated with litter deposition, and its decomposability influencing the first phases of organic matter decomposition, the thicknesses of Oa + A horizons depend mainly on soil moisture which slowers organic matter decomposition.

The forest floor cover explains around 6% of overall data variability and almost 11% for Oi + Oe separately. Anschlag et al. (2017) observed an increased organic horizon thickness under moss and heather compared to forbs, and they argued by different litter decomposability. Similarly, Bens et al. (2006) observed a lower forest floor thickness under vegetation composed from gramineous species (*Calamagrostis epigeios, Avenella flexuosa, Rubus idaeus, and Pleurozium schreberi)* compared to the forest floor at a stand with uncovered pine litter. In the LIZ catchment, the lowest forest floor and topsoil thickness (OA) seem to be under graminoids as well (Table 3). The areas without ground vegetation are covered by spruce needles or beech leaves which are more recalcitrant; thus, the OA thickness is rather increased at these sites and the results correspond with the study by Bens et al. (2006). Bastianelli et al. (2017) found a significant difference in thicknesses of all soil horizons between two forest stands with different ground vegetation: moss cover in a forest with dense tree canopies and lichens cover in more open forest stands. All horizons were thicker under the moss. Bastianelli et al. (2017) suggested that the moss due to its higher water capacity forms a water-saturated environment which lowers decomposition rates. The same phenomenon was observed by Yu et al. (2002) comparing a spruce forest with moss cover, an aspen forest with forbs, and a pine forest with lichens. However, in their study, there was some difference in soil characteristics at the sites: the soil was with higher sand content at the pine site enhancing the drainage (Yu et al. 2002). It corresponds with findings of Lexer and Hönninger (1998) mentioned above. In the LIZ catchment, the ground vegetation varied significantly at the hydric stands and at the oligotrophic stands. There are moss species and graminoid species at both stand types, but the exact species were not determined. Moreover, some moss species (e.g., *Leucobryum glaucum*) occurring at the oligotrophic stands would have low water capacity. Therefore, the moss cover shows only slightly increased forest floor and topsoil thicknesses in the LIZ catchment (Table 3).

Forest floor cover is tightly related to tree species at a stand. Density of tree canopy is an important factor (Valtera

et al. 2013; Anschlag et al. 2017; Bastianelli et al. 2017), but the role of tree litter recalcitrance is at the first place. Bens et al. (2006) reported significantly higher average forest floor thickness for a forest stand with pins (age 84) that reached 7.9 cm compared to a beech stand (age 91) with a 3.6 cm thick forest floor. Similarly, Labaz et al. (2014) found the litter layer three times thinner at a pure beech stand than that at a spruce stand, and Rothe et al. (2002) observed an average thickness of the forest floor at beech stands from 0.5 to 3 cm, whereas at spruce stands it was from 4 to 6.5 cm. Cremer et al. (2016) observed a decreasing forest floor in sequence: spruce, douglas fir, and beech. However, according to our results, the role of tree species composition in forest floor and topsoil thicknesses is negligible (0–1% of explained data variability) and the differences between the stands are very small. Forest floor cover which partially includes the tree species composition characterizes better conditions of a stand.

The stand age showed no influence to forest floor and topsoil thicknesses in our study. It could result from the distribution of the young stages which are situated mainly at the hydric sites and the effects of the increased moisture and the decreased litter of young trees are then contradictory.

Conclusion

In a managed submontaneous forest in Central Europe, the forest floor and topsoil thicknesses were found to be spatially autocorrelated up to 300 m but with the ratio of the nugget semivariance to the sill semivariance not getting below 58.7%. By means of geographically weighted regression, 17.1% of the forest floor plus topsoil thickness variability was explained. According to the model, 7.5% of the explained variability is attributable to spatial autocorrelation; the other factors are soil moisture, forest floor cover, and slope.

Acknowledgements This research was supported by the institutional resources of the Ministry of Education, Youth and Sports of the Czech Republic for the support of science and research, Project No. SVV260438, and by Global Change Research Institute of the Czech Academy of Sciences. We thank M. Tesar for enabling us to carry out the field work at the LIZ catchment operated by the Institute of Hydrodynamics, The Czech Academy of Sciences.

Funding This research was supported by the institutional resources of the Ministry of Education, Youth and Sports of the Czech Republic for the support of science and research, Project No. SVV260438, and by Global Change Research Institute of the Czech Academy of Sciences.

Data availability The datasets generated and analyzed during the current study are available from the corresponding author on reasonable request.

Code availability Not applicable.

Compliance with ethical standards

Conflict of interest The authors declare that they have no conflict of interest.

Annex

Annex 1: Location of the study catchment and the position of the sampling points

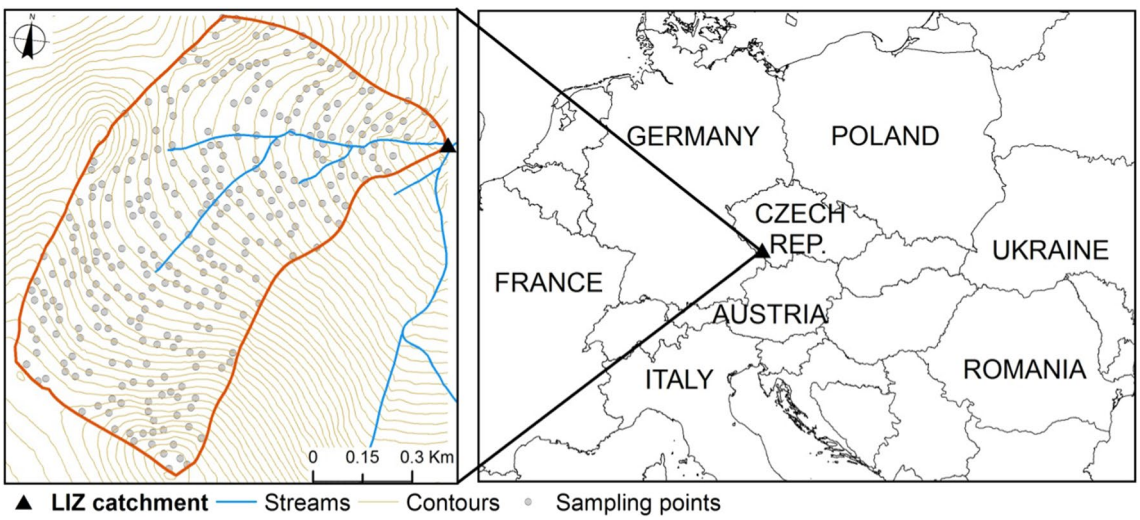

Annex 2: Soil type distribution in LIZ catchment

Map of soil types based on 30 randomly distributed sampling cores down to 70 cm and refined by 300 sampling pits down to 25 cm.

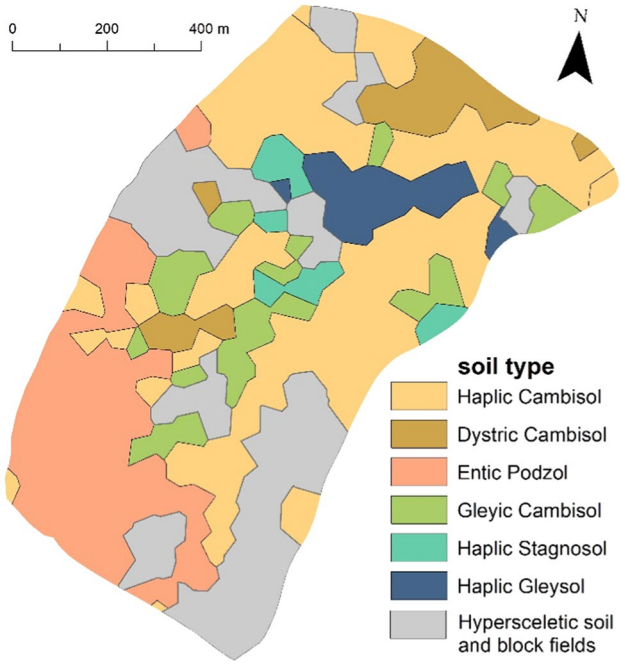

Annex 3: Soil density and particle size distribution

Soil type	Horizon complex	Number of samples	Bulk density (g/cm^3)	Particle density (g/cm^3)	Sand (%)	Silt (%)	Clay (%)	Textural class
	Oi + Oe	3	0.12	–	–	–	–	
CMha	Oa + A	3	0.63	2.48	57	37	5	Sandy loam
	Mineral	3	1.22	2.51	53	40	8	Sandy loam
	Oi + Oe	3	0.14	–	–	–	–	
CMdy	Oa + A	3	0.46	2.03	57	36	7	Sandy loam
	Mineral	3	1.17	2.45	56	37	7	Sandy loam
	Oi + Oe	3	0.09	–	–	–	–	
PZet	Oa + A	3	0.62	2.17	56	38	9	Sandy loam
	Mineral	3	1.10	2.49	64	30	6	Sandy loam
	Oi + Oe	3	0.10	–	–	–	–	
CMgl	Oa + A	3	0.43	2.3	56	40	3	Sandy loam
	Mineral	3	1.81	2.5	53	40	8	Sandy loam
	Oi + Oe	2	0.14	–	–	–	–	
ST	Oa + A	2	0.11	1.52	49	33	18	Loam
	Mineral	2	1.02	2.5	59	33	8	Sandy loam
	Oi + Oe	2	0.04	–	–	–	–	
GL	Oa + A	2	0.50	2.45	53	38	9	Sandy loam
	Mineral	2	2.13	2.61	70	22	8	Sandy loam

CMha—Haplic Cambisol, CMdy—Dystric Cambisol, CMgl—Gleyic Cambisol, PZet—Entic Podzol, GL—Gleysol, ST—Stagnosol

Annex 4: Soil edaphic categories in LIZ catchment

Retrieved from maps produced by ÚHUL at scale 1:10,000 and based on the forest site classification described by Viewegh (2003).

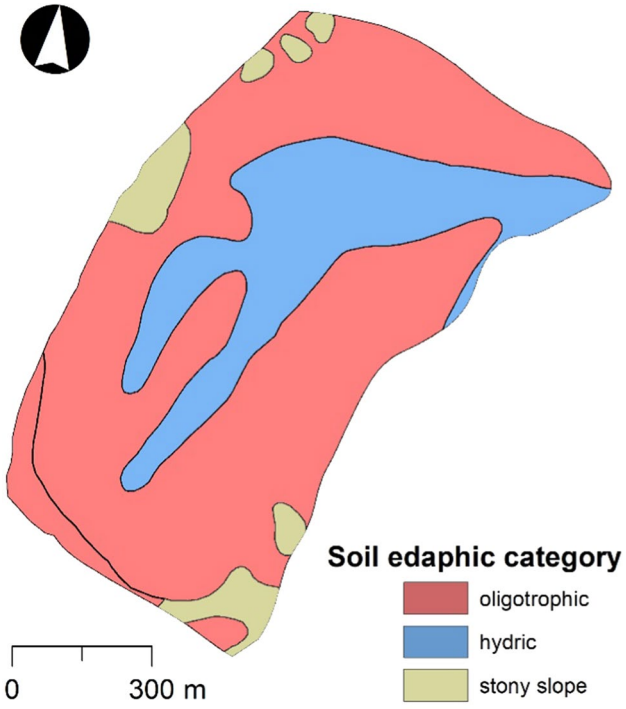

Annex 5: Stand age in LIZ catchment

Retrieved from maps produced by ÚHUL at scale 1:10,000.

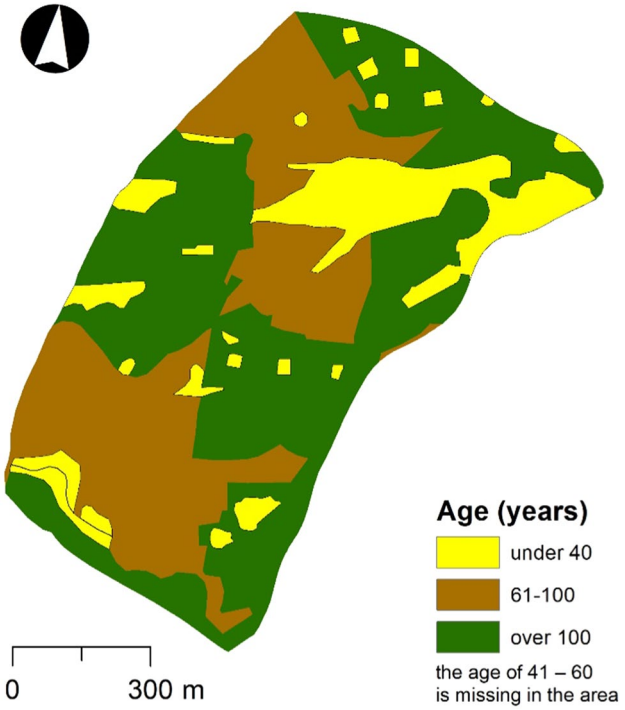

Annex 6 Geographically weighted regression computation details

In GWR 4.09, the fixed distance of Gaussian Kernel was left to find out by Golden selection search with the criterion of minimum AICc (AIC with a correction for small sample sizes). The categories of the categorical explanatory variables (forest floor cover, dominant tree species and forest stand age) were recoded as dummy variables. From the dummy variables representing the same categorical explanatory variable one was always omitted from the analysis due to multicollinearity (see Fotheringham et al. 2002). However, all of the dummy variables representing a particular categorical explanatory variable were analyzed and interpreted as one phenomenon.

The data were supposed spatially variable. On the other hand, no justification was found for the spatial variability of explanatory variables. For instance, slope or dominant tree species should influence the forest floor and topsoil thicknesses in the same way over the whole area. Furthermore, this assumption was verified by a geographical variability test embodied in GWR 4.09. No significant geographical variability was found for most explanatory variables with an exception of the forest floor cover. However, the data of explanatory variables was assumed to be geographically invariable as a whole. The explanatory variables were then classified to those with local influence (Intercept) and those with global influence (all the others) (see Fotheringham et al. 2002).

Local variables are computed locally from neighbor values within the bandwidth and weighted by their distance. As a result, there is not an exact estimation of their value in the model, the estimation could be slightly different at every location (Fotheringham et al. 2002). Locally computed intercept works similarly as an interpolation in this case, and substitutes a role of an autoregressive parameter which deals with the spatial autocorrelation. The spatial independency of the model residuum was verified by Moran's I. The advantage of using the local intercept instead of the model without intercept but employing an autoregressive parameter is at first that it can be computed by Ordinary least squares method compared to the latter model which should be performed by Maximum likelihood computation and the second advantage is the interpretation which is more intuitive for the models with the intercept. The use of the local intercept and the autoregressive parameter at the same model is not possible due to their multicollinearity and a model combining a global intercept with an autoregressive parameter was less flexible.

The two above mentioned models which were run separately for Oi + Oe, Oa + A, and OA horizons can be written as follows:

$$\begin{aligned}\mathrm{FLTH}_i = {} & \alpha_0(u_i, v_i) + \alpha_1\mathrm{WETIN} + \alpha_2\mathrm{COV} \\ & + \alpha_3\mathrm{AGE} + \alpha_4\mathrm{TREE} + \alpha_5\mathrm{ELEV} \\ & + \alpha_6\mathrm{MOIST} + \varepsilon_i\end{aligned}$$

$$\begin{aligned}\mathrm{FLTH}_i = {} & \alpha_0(u_i, v_i) + \alpha_1\mathrm{SLOPE} + \alpha_2\mathrm{CURV} \\ & + \alpha_3\mathrm{TREE} + \alpha_5\mathrm{MOIST} \\ & + \alpha_6\mathrm{AGE} + \alpha_7\mathrm{ELEV} + \varepsilon_i\end{aligned}$$

where FLTH_i = the thickness of a modeled horizon complex at location i, COV = forest floor cover, TREE = dominant tree species; AGE = forest stand age, ELEV = elevation, WETIN = wetness index, MOIST = moisture in the mineral soil measured in the field, SLOPE = slope, CURV = relief curvature, α_1–α_7 are model estimates, α_0 is intercept estimate computed locally.

Annex 7: OA thickness variability

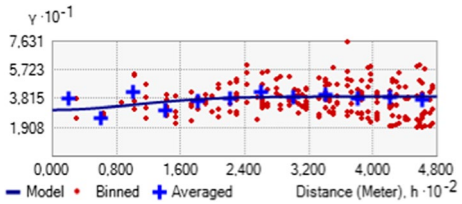

Annex 8: Variability of the thickness of Oi + Oe horizons' complex

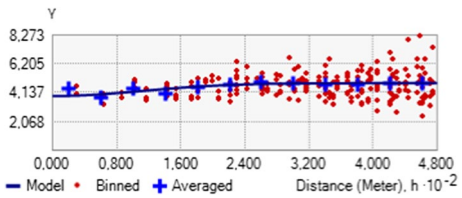

Annex 9: Variability of the thickness of Oa + A horizon's complex

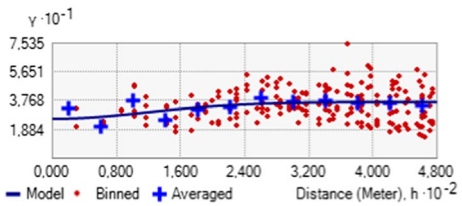

Annex 10: OA thickness variability at stands of oligotrophic edaphic category

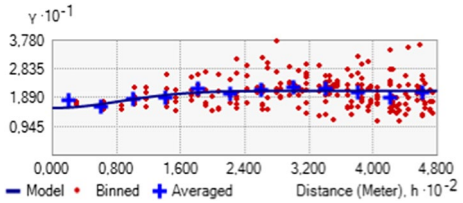

Annex 11: The variability of the thickness of Oi + Oe horizon's complex at stands of oligotrophic edaphic category

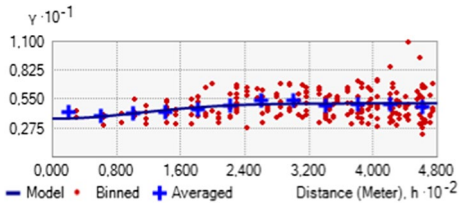

Annex 12: The variability of the thickness of Oa + A horizon's complex at stands of oligotrophic edaphic category

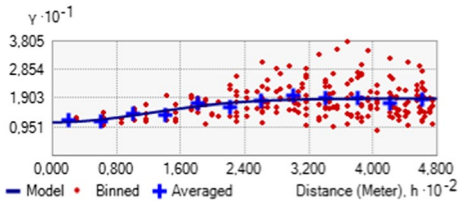

Annex 13: OA thickness variability at stands of hydric edaphic category

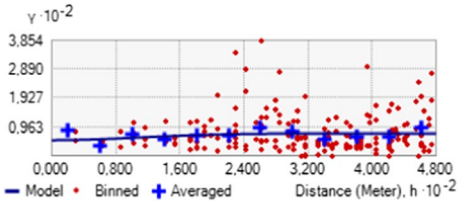

Annex 14: The variability of the thickness of Oa + A horizon's complex at stands of hydric edaphic category

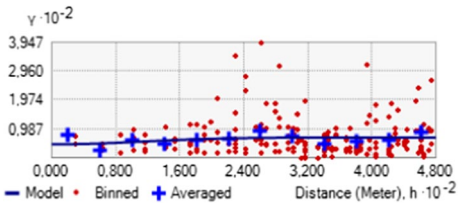

Annex 7–14: Oi—organic litter horizon, Oe—fragmented organic horizon, Oa—humified organic horizon, A—topsoil, OA—forest floor plus topsoil in total

References

Adhikari K, Hartemink AE (2016) Linking soils to ecosystem services—a global review. Geoderma 262:101–111. https://doi.org/10.1016/j.geoderma.2015.08.009

Ahmed IU, Smith AR, Jones DL, Godbold DL (2016) Tree species identity influences the vertical distribution of labile and recalcitrant carbon in a temperate deciduous forest soil. For Ecol Manag 359:352–360. https://doi.org/10.1016/j.foreco.2015.07.018

Anschlag K, Tatti D, Hellwig N et al (2017) Vegetation-based bioindication of humus forms in coniferous mountain forests. J Mt Sci 14:662–673. https://doi.org/10.1007/s11629-016-4290-y

Bastianelli C, Ali AA, Beguin J et al (2017) Boreal coniferous forest density leads to significant variations in soil physical and geochemical properties. Biogeosciences 14:3445–3459. https://doi.org/10.5194/bg-14-3445-2017

Bens O, Buczko U, Sieber S, Hüttl RF (2006) Spatial variability of O layer thickness and humus forms under different pine beech-forest transformation stages in NE Germany. J Plant Nutr Soil Sci 169:5–15. https://doi.org/10.1002/jpln.200521734

Bens O, Wahl NA, Fischer H, Hüttl RF (2007) Water infiltration and hydraulic conductivity in sandy cambisols: impacts of forest transformation on soil hydrological properties. Eur J For Res 126:101–109. https://doi.org/10.1007/s10342-006-0133-7

Brahim N, Ibrahim H, Hatira A (2014) Tunisian soil organic carbon stock—spatial and vertical variation. Procedia Eng 69:1549–1555. https://doi.org/10.1016/j.proeng.2014.03.154

Bruckner A, Kandeler E, Kampichler C (1999) Plot-scale spatial patterns of soil water content, pH, substrate-induced respiration and N mineralization in a temperate coniferous forest. Geoderma 93:207–223. https://doi.org/10.1016/S0016-7061(99)00059-2

Chuman T, Gürtlerová P, Hruška J, Adamová M (2014) Geochemical reactivity of rocks of the Czech Republic. J Maps 10:341–349. https://doi.org/10.1080/17445647.2013.867418

Conforti M, Lucà F, Scarciglia F et al (2016) Soil carbon stock in relation to soil properties and landscape position in a forest ecosystem of southern Italy (Calabria region). CATENA 144:23–33. https://doi.org/10.1016/j.catena.2016.04.023

Cremer M, Kern NV, Prietzel J (2016) Soil organic carbon and nitrogen stocks under pure and mixed stands of European beech, Douglas fir and Norway spruce. For Ecol Manag 367:30–40. https://doi.org/10.1016/j.foreco.2016.02.020

CUZK (2006) ZABAGED: database of geographic data of the Czech republic. https://geoportal.cuzk.cz

De Nicola C, Zanella A, Testi A et al (2014) Humus forms in a Mediterranean area (Castelporziano Reserve, Rome, Italy): classification, functioning and organic carbon storage. Geoderma 235–236:90–99. https://doi.org/10.1016/j.geoderma.2014.06.033

de Wit HA, Eldhuset TD, Mulder J (2010) Dissolved Al reduces Mg uptake in Norway spruce forest: results from a long-term field manipulation experiment in Norway. For Ecol Manag 259:2072–2082. https://doi.org/10.1016/j.foreco.2010.02.018

Essington ME (2015) Soil and water chemistry: an integrative approach, 2nd edn. CRC Press, Boca Raton

Fotheringham AS, Brudson C, Charlton M (2002) Geographically weighted regression: the analysis of spatially varying relationships. Wiley, Chichester

Francaviglia R, Renzi G, Doro L et al (2017) Soil sampling approaches in Mediterranean agro-ecosystems. Influence on soil organic carbon stocks. CATENA 158:113–120. https://doi.org/10.1016/j.catena.2017.06.014

Hansson K, Fröberg M, Helmisaari H et al (2013) Carbon and nitrogen pools and fluxes above and below ground in spruce, pine and birch stands in southern Sweden. For Ecol Manag 309:28–35. https://doi.org/10.1016/j.foreco.2013.05.029

Heim A, Wehrli L, Eugster W, Schmidt MWI (2009) Effects of sampling design on the probability to detect soil carbon stock changes at the Swiss CarboEurope site Lägeren. Geoderma 149:347–354. https://doi.org/10.1016/j.geoderma.2008.12.018

ISO 11277 (2009) Soil quality—determination of particle size distribution in mineral soil material—method by sieving and sedimentation

Kristensen T, Ohlson M, Bolstad P, Nagy Z (2015) Spatial variability of organic layer thickness and carbon stocks in mature boreal forest stands—implications and suggestions for sampling designs. Environ Monit Assess. https://doi.org/10.1007/s10661-015-4741-x

Laamrani A, Valeria O, Bergeron Y et al (2014a) Effects of topography and thickness of organic layer on productivity of black spruce boreal forests of the Canadian Clay Belt region. For Ecol Manag 330:144–157. https://doi.org/10.1016/j.foreco.2014.07.013

Laamrani A, Valeria O, Fenton N et al (2014b) The role of mineral soil topography on the spatial distribution of organic layer thickness in a paludified boreal landscape. Geoderma 221–222:70–81. https://doi.org/10.1016/j.geoderma.2014.01.003

Labaz B, Galka B, Bogacz A et al (2014) Factors influencing humus forms and forest litter properties in the mid-mountains under temperate climate of southwestern Poland. Geoderma 230–231:265–273. https://doi.org/10.1016/j.geoderma.2014.04.021

Lexer MJ, Hönninger K (1998) Estimating physical soil parameters for sample plots of large-scale forest inventories. For Ecol Manag 111:231–247. https://doi.org/10.1016/S0378-1127(98)00335-1

Liski J (1995) Variation in soil organic carbon and thickness of soil horizons within a boreal forest stand—effect of trees and implications for sampling. Silva Fenn 29:255–266

Marty C, Houle D, Gagnon C (2015) Variation in stocks and distribution of organic C in soils across 21 eastern Canadian temperate and boreal forests. For Ecol Manag 345:29–38. https://doi.org/10.1016/j.foreco.2015.02.024

Mulder J, De Wit HA, Boonen HW, Bakken LR (2001) Increased levels of aluminium in forest soils: effects on the stores of soil organic carbon. Water Air Soil Pollut 130:989–994

Muukkonen P, Häkkinen M, Mäkipää R (2009) Spatial variation in soil carbon in the organic layer of managed boreal forest soil-implications for sampling design. Environ Monit Assess 158:67–76. https://doi.org/10.1007/s10661-008-0565-2

Nakaya T, Charlton M, Brunsdon C et al (2009) GWR 4.09 software. https://gwr4.software.informer.com/

Olsson MT, Erlandsson M, Lundin L et al (2009) Organic carbon stocks in Swedish podzol soils in relation to soil hydrology and other site characteristics. Silva Fenn 43:209–222

Oulehle F, Kopáček J, Chuman T et al (2016) Predicting sulphur and nitrogen deposition using a simple statistical method. Atmos Environ. https://doi.org/10.1016/j.atmosenv.2016.06.028

Oulehle F, Chuman T, Hruška J et al (2017) Recovery from acidification alters concentrations and fluxes of solutes from Czech catchments. Biogeochemistry 132:251–272. https://doi.org/10.1007/s10533-017-0298-9

Oulehle F, Tahovská K, Chuman T et al (2018) Comparison of the impacts of acid and nitrogen additions on carbon fluxes in European conifer and broadleaf forests. Environ Pollut 238:884–893. https://doi.org/10.1016/j.envpol.2018.03.081

Peltoniemi M, Mäkipää R, Liski J, Tamminen P (2004) Changes in soil carbon with stand age—an evaluation of a modelling method with empirical data. Glob Change Biol 10:2078–2091. https://doi.org/10.1111/j.1365-2486.2004.00881.x

Persson T, Lundkvist H, Wirén A et al (1989) Effects of acidification and liming on carbon and nitrogen mineralization and soil organisms in mor humus. Water Air Soil Pollut 45:77–96

Ponge JF, Jabiol B, Gegout JC (2011) Geology and climate conditions affect more humus forms than forest canopies at large scale in temperate forests. Geoderma 162:187–195

Pregitzer KS, Euskirchen ES (2004) Carbon cycling and storage in world forests: biome patterns related to forest age. Glob Change Biol 10:2052–2077. https://doi.org/10.1111/j.1365-2486.2004.00866.x

Rossi J, Govaerts A, De Vos B et al (2009) Spatial structures of soil organic carbon in tropical forests-a case study of Southeastern Tanzania. CATENA 77:19–27. https://doi.org/10.1016/j.catena.2008.12.003

Rothe A, Kreutzer K, Kuchenhoff H (2002) Influence of tree species composition on soil and soil solution properties in two mixed spruce-beech stands with contrasting history in Southern Germany. Plant Soil 240:47–56. https://doi.org/10.1023/A:1015822620431

Šamonil P, Valtera M, Bek S et al (2011) Soil variability through spatial scales in a permanently disturbed natural spruce-fir-beech forest. Eur J For Res 130:1075–1091. https://doi.org/10.1007/s10342-011-0496-2

Schöning I, Totsche KU, Kögel-Knabner I (2006) Small scale spatial variability of organic carbon stocks in litter and solum of a forested Luvisol. Geoderma 136:631–642. https://doi.org/10.1016/j.geoderma.2006.04.023

Smit A (1999) The impact of grazing on spatial variability of humus profile properties in a grass-encroached Scots pine ecosystem. CATENA 36:85–98. https://doi.org/10.1016/S0341-8162(99)00003-X

Sorensen R, Zinko U, Seibert J (2006) On the calculation of the topographic wetness index: evaluation of different methods based on field observations. Hydrol Hydrol Earth Syst Sci Earth Syst Sci 10:101–112

Strand LT, Callesen I, Dalsgaard L, de Wit HA (2016) Carbon and nitrogen stocks in Norwegian forest soils—the importance of soil formation, climate, and vegetation type for organic matter accumulation. Can J For Res 1473:1–15. https://doi.org/10.1139/cjfr-2015-0467

Trap J, Hättenschwiler S, Gattin I, Aubert M (2013) Forest ageing: an unexpected driver of beech leaf litter quality variability in European forests with strong consequences on soil processes. For Ecol Manag 302:338–345. https://doi.org/10.1016/j.foreco.2013.03.011

ÚHÚL (2015) Forest Management Institute. In: For. Inf. www.uhul.cz/mapy-a-data/

Valtera M, Šamonil P, Boublík K (2013) Soil variability in naturally disturbed Norway spruce forests in the Carpathians: Bridging spatial scales. For Ecol Manag 310:134–146. https://doi.org/10.1016/j.foreco.2013.08.004

Viewegh J (2003) Klasifikace lesních rostlinných společenstev (se zaměřením na Typologický systém ÚHÚL). Česká zemědělská univerzita v Praze, Praha

Wang G, Mao T, Chang J, Du J (2014) Impacts of surface soil organic content on the soil thermal dynamics of alpine meadows in permafrost regions: data from fi eld observations. Geoderma 232–234:414–425. https://doi.org/10.1016/j.geoderma.2014.05.016

Wiesmeier M, Urbanski L, Hobley E et al (2019) Soil organic carbon storage as a key function of soils—a review of drivers and indicators at various scales. Geoderma 333:149–162. https://doi.org/10.1016/j.geoderma.2018.07.026

Yu Z, Apps MJ, Bhatti JS (2002) Implications of floristic and environmental variation for carbon cycle dynamics in boreal forest ecosystems of central Canada. J Veg Sci 13:327–340. https://doi.org/10.1111/j.1654-1103.2002.tb02057.x

9.3. Publication III

Zajícová, K., Chuman, T., 2019. Application of ground penetrating radar methods in soil studies: A review. Geoderma 343, 116–129. https://doi.org/10.1016/j.geoderma.2019.02.024

Geoderma 343 (2019) 116–129

Contents lists available at ScienceDirect

Geoderma

journal homepage: www.elsevier.com/locate/geoderma

Application of ground penetrating radar methods in soil studies: A review

Katerina Zajícová[a,*], Tomas Chuman[a,b]

[a] Charles University in Prague, Faculty of Science, Department of Physical Geography and Geoecology, Albertov 6, 12843 Praha 2, Czech Republic
[b] Czech Geological Survey, Geologická 6, 15200 Praha 5, Czech Republic

ARTICLE INFO

Handling Editor: Morgan Cristine L.S.

Keywords:
Electromagnetic methods
Geophysical methods
Humus
Soil moisture
Soil stratigraphy

ABSTRACT

Applications of ground penetrating radar (GPR) in soil surveys promise cost and time benefits together with the possibility of repeating surveys at the same locations due to the method's non-destructiveness to the ground surface. After its successful application to earth sciences surveying of the deep subsurface, GPR was used in soil surveys; however, its application in soil surveys has been difficult. This paper aims to provide an overview of the application of GPR in soil surveys. This paper focuses on methods to estimate the soil water content by various approaches, such as determining the electromagnetic signal velocity in a soil by analyses of reflections, ground wave or guided wave approaches, and the full-waveform inversion method; to characterize soil and peat stratigraphy, with an emphasis on organic horizons; and to detect tree roots. GPRs have been relatively successfully applied in a wide spectrum of surveys, but under favourable conditions. More complex techniques using numerical modelling that have emerged in recent years might have the potential to be more successful.

1. Introduction

Geophysical methods are appreciated for their cost and time effectiveness and their ability to be repeated at exact locations because they are non-destructive to the ground surface. For these reasons, they have become popular in belowground surveys in various disciplines of earth science. Although most of these methods were primarily developed for deep below ground surveying, several of them, especially electromagnetic methods, can also be used for shallow depths, such as in soils. Of the geophysical methods available, ground penetrating radar (GPR) and electromagnetic induction (EMI) have been the most widely applied in soil surveys. These two methods differ in the physical properties they measure. While GPR measures the soil dielectric permittivity, EMI detects changes in soil electrical conductivity. Applications of the electromagnetic induction method were reviewed recently by Doolittle and Brevik (2014) and will not be further discussed in this paper. A review of a broad spectrum of GPR applications to agriculture soils was provided by Liu et al. (2016). However, an evaluation of the different GPR measurement approaches and data treatments employed in soil surveys for agricultural, forestry, or environmental purposes and of the strengths and weaknesses of these methods are lacking. Therefore, in this article, we review > 100 articles published on WoS and SCOPUS in the period 1995–2018 that use GPR for soil surveying.

Among the reviewed studies, applications related to soil water content are by far the most frequent (Table 1). The next most frequent application was for soil and peatland stratigraphy. Non-pedological applications focus predominantly on tree roots.

Because the intent of this paper is mainly to show different GPR approaches, their principles and to review their strengths and weaknesses in various soil science applications, it begins with an introduction to the general principles of the GPR method and describes the electromagnetic properties of soils that strongly influence the results of GPR soil surveys. Yet the paper's focus is not in technical details, but in the potential of GPR methods for use in soil surveys by the soil science community.

1.1. General principles of the GPR method

Ground penetrating radar emits electromagnetic waves via an antenna-transmitter and receives them by an antenna-receiver. In general, there are two main types of GPR units and antennas: ground-coupled shielded antennas, which are in direct contact with or up to several centimetres above the studied surface during data acquisition, and air-coupled horn antennas, which are designed to acquire data from a distance of a few tens of centimetres to > 1 m above the surface. GPR units also can be divided into those with a separable antenna-transmitter and antenna-receiver and those in which the antennas are tied together at an unchangeable distance called a “fixed” or “common-offset.”

Traditional surveys employ reflections of electromagnetic waves

* Corresponding author.
E-mail addresses: katerina.zamazalova@natur.cuni.cz (K. Zajícová), tomas.chuman@natur.cuni.cz (T. Chuman).

https://doi.org/10.1016/j.geoderma.2019.02.024
Received 1 March 2018; Received in revised form 21 January 2019; Accepted 13 February 2019
Available online 25 February 2019

Table 1
A summary the soil studies that employed GPR methods, organised by their specific application.

Application	Method	Studies
Soil water content	Velocity analysis from the two-way travel time of a wave reflected by a known reflector	Ercoli et al., 2018; van Overmeeren et al., 1997
	Velocity analysis by "Common-midpoint"	Greaves et al., 1996; Koyama et al., 2017; Lu et al., 2017; Steelman and Endres, 2012; van Overmeeren et al., 1997
	Ground wave velocity	Ardekani, 2013; Galagedara et al., 2005a, 2005b, 2003; Grote et al., 2003; Huisman et al., 2001; Lu et al., 2017; Pallavi et al., 2010; van Overmeeren et al., 1997
	Guided wave velocity and scattering	Arcone et al., 2003; Mangel et al., 2015; Rege and Godio, 2012; Strobbia and Cassiani, 2007; van der Kruk et al., 2010, 2006
	Reflection coefficient	al Hagrey and Müller, 2000; Ardekani, 2013; Reppert et al., 2000
	Early-time signal analysis	Algeo et al., 2016; Benedetto, 2010; Comite et al., 2016, 2014; Di Matteo et al., 2013; Ferrara et al., 2013; Pettinelli et al., 2014, 2007
	Full-wave inversion	Ardekani et al., 2014a; Ardekani, 2013; Lambot et al., 2008, 2006, 2004, Minet et al., 2012, 2011; Mourmeaux et al., 2014; Tran et al., 2015; Weihermüller et al., 2007
	Other wave-form inversion modelling approaches	Busch et al., 2014; Lavoué et al., 2014; Oden et al., 2008
Soil salinity	Reflection coefficient	al Hagrey and Müller, 2000
Soil texture	Early-time signal analysis	Benedetto and Tosti, 2013; Meadows et al., 2006; Tosti et al., 2013
	Wave-form inversion modelling approaches	Busch et al., 2014
Soil profile stratigraphy	Reflection Imaging	André et al., 2012; Nováková et al., 2013; Simeoni et al., 2009; Zhang et al., 2014
	Wave-form inversion modelling approaches	Buchner et al., 2012
Organic horizons thicknesses estimation	Reflection Imaging	Li et al., 2015; Winkelbauer et al., 2011
	Full-wave inversion	André et al., 2016, 2015, 2014
Peatlands stratigraphy	Reflection Imaging	Comas et al., 2017, 2015; Fyfe et al., 2014; Karuss and Berzins, 2015; Kettridge et al., 2012, 2008; Laamrani et al., 2013; Parry et al., 2014; Parsekian et al., 2012a; Parsekian et al., 2012b; Plado et al., 2011; Proulx-McInnis et al., 2013; Rosa et al., 2009; Sass et al., 2010; Slater and Reeve, 2002; Walter et al., 2016
Biogenic gases in peatlands	Reflection Imaging	Comas et al., 2008, 2005; William and Comas, 2016
	Signal velocity analysis	Chen and Slater, 2015; Parsekian et al., 2012a; Strack and Mierau, 2010
	Signal frequency spectra analysis	Terry and Slater, 2017
Roots and root system	Reflection Imaging	Borden et al., 2016; Freeland, 2015; Guo et al., 2013b; Hirano et al., 2009; Li et al., 2016; Q. Liu et al., 2018; Raz-Yaseef et al., 2013; Rodríguez-Robles et al., 2017; Tanikawa et al., 2013; Tardío et al., 2016; Wu et al., 2014; Yeung et al., 2016
Root diameters and biomass	Indexes extracted from signal strength or waveform	Barton and Montagu, 2004; Borden et al., 2014; Cui et al., 2011; Hirano et al., 2009; Q. Liu et al., 2018; X. Liu et al., 2018; Rodríguez-Robles et al., 2017; Simms et al., 2017; Stover et al., 2016; Zhu et al., 2014

from boundaries between environments of different electromagnetic properties (Annan, 2009). Other approaches, designed for borehole GPR, were briefly presented elsewhere (e.g., Slob et al., 2010). The borehole methods miss one of the main advantages of the GPR survey method, the non-destructiveness to the ground surface. Thus, this paper does not focus on the borehole methods. GPR has been more broadly applied in soil surveys using antennas with frequencies that exceed 500 MHz, which enable higher resolution results and more transient boundaries to be distinguished. The resolution depends on the antenna frequency, i.e., on the electromagnetic wave length. It is assumed to be approximately one-fourth the electromagnetic wave length and higher in less permeable media (Bristow and Jol, 2003). The layer boundaries should be detectable by electromagnetic wave reflection if $W/\lambda \leq 0.3$ (van Dam et al., 2003) (Eq. (1)), where W is the boundary width and λ is the electromagnetic wave length.

A common output of a GPR measurement consists of the two-way travel times and the magnitudes of the received reflected electromagnetic waves (Bristow and Jol, 2003). These outputs are most frequently displayed in 2D radargrams (Fig. 1) and are edited using image processing algorithms, such as those implementing frequency filters. To create an image corresponding to the subsurface at a realistic scale, the electromagnetic wave spreading velocities or subsurface electromagnetic properties must be known. Numerical modelling and simulations have enhanced the development of GPR applications in soil surveys in recent years because they enable better expressions of theoretical electromagnetic signal response and, inversely, gain interpretations of GPR outputs. The data treatment has therefore transitioned from image processing to more objective numerical methods. Most numerical modelling approaches use data obtained using multi-offset antenna settings, commonly with antenna-transmitters and antenna-receivers separated at diverse distances (e. g., Sena et al., 2008). The implementation of broadband antennas that transmit over wide frequency bands enables further development at this stage (e.g., Lambot et al., 2004; Lavoué et al., 2014). An additional advantage of using multi-offset data and inverse modelling is the simultaneous determination of all (sub)surface properties without the need to know at least some of them in advance.

The full-wave inversion of broad-band frequencies introduced by Lambot et al. (2004) and Lambot et al. (2006), tested for very wide spectrum of soil survey types, is one of the most advanced approaches of GPR signal numerical modelling. In its original form, it uses an off-ground GPR with an air-coupled antenna. This approach considers only surface reflections because the effect of the subsurface is not important. The radar – antenna – subsurface system is modelled using the linear system transfer functions of 3D Maxwell's equations. By a Green's function inversion, the air-subsurface function is computed, and the electromagnetic properties of the (sub)surface—dielectric permittivity, permeability, and electrical conductivity—are determined (Lambot et al., 2004). The latter two properties are often neglected due to their low influence. For on-ground GPR systems in which the subsurface also affects the measurement, the subsurface was added in the model by Lambot and André (2014).

The full-wave inversion method has been applied to broad spectrum of soil surveys: soil description (Mourmeaux et al., 2014), soil moisture estimation (Ardekani, 2013; Lambot et al., 2008; Minet et al., 2012, 2011), organic matter thickness and its description (André et al., 2014; André et al., 2016, 2015; Jonard et al., 2014) and the description of ground vegetation, which enables the vegetation layer to be added to the measuring model (Ardekani et al., 2014b). Other numerical modelling methods are rather scarce or focus on specific applications and will be discussed later in broader detail.

In addition to 2D GPR imaging, 3D image models are sometimes

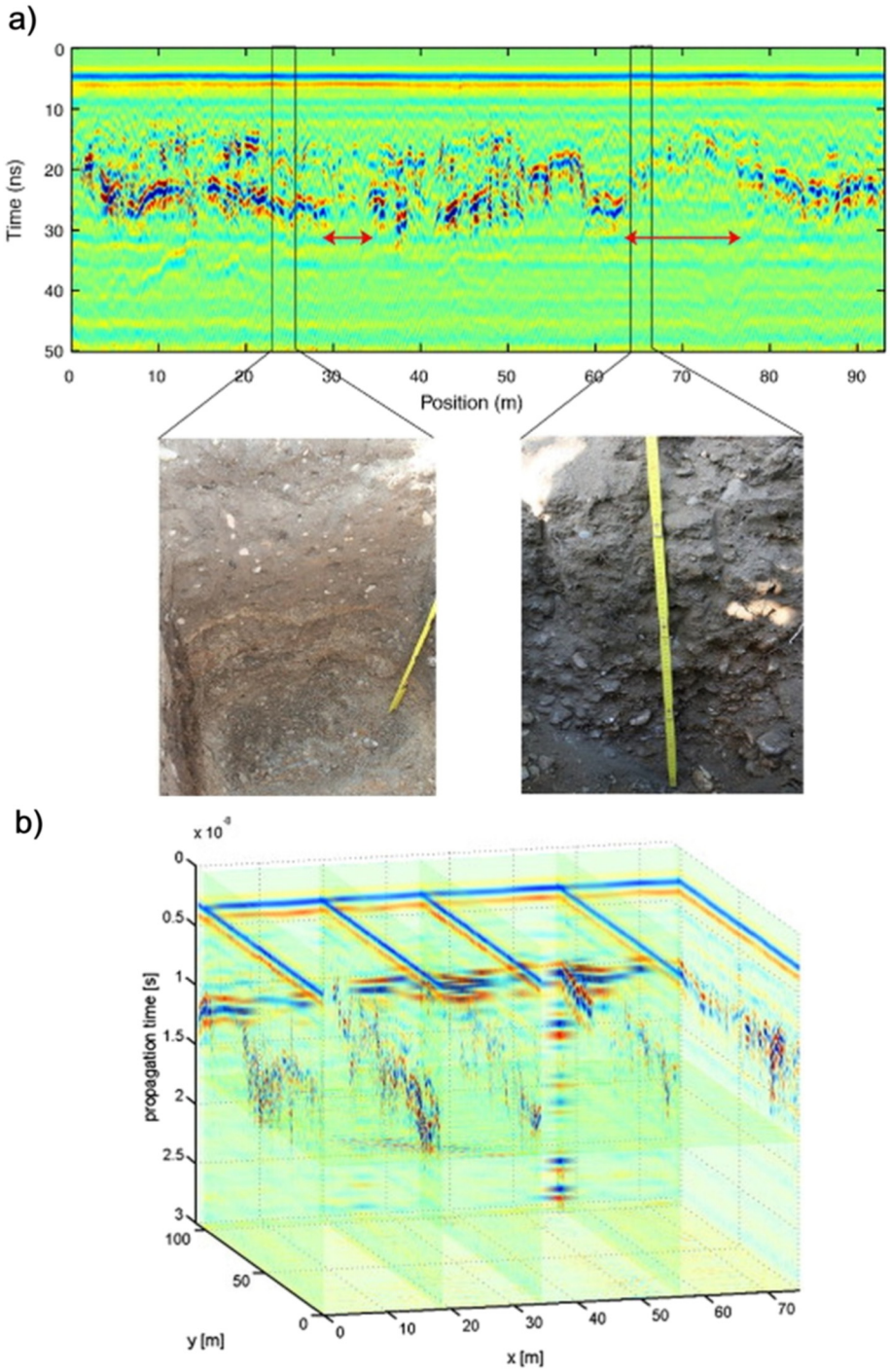

Fig. 1. a) Example of a 2D radargram along a transect verified by soil profiles. The reflections in the zone between 20 and 30 ns show a boundary between layers with differing electromagnetic properties. The depth of the boundary is determined from the electromagnetic waves velocity.
b) Example of a 3D radargram (block model) showing reflections on a boundary interpolated to a xy space.
From André et al., 2012.

employed to provide more detailed interpretations of the profile stratigraphy, including determinations of thicknesses and volume calculations. The data are collected along closely spaced parallel lines or on a grid and then converted into a 3D block model (Bristow and Jol, 2003). A disadvantage of these models is the more demanding data acquisition and treatment required. Three dimensional surveys are rarely applied in soil science with the exception of tree root detection. Apart from this application, the most frequent visualizations using 3D models are surveys of soil wedges, relict polygonal patterns and other cryogenic structures, which can be much easily distinguished in 3D (e.g., Doolittle and Nelson, 2009; Watanabe et al., 2013). A soil profile was visualized in 3D by André et al. (2012) (Fig. 1).

1.2. Electromagnetic waves velocity

The velocity of electromagnetic waves emitted by antenna-transmitter, entering the soil and coming back after a reflection, is defined according to Reppert et al. (2000) as:

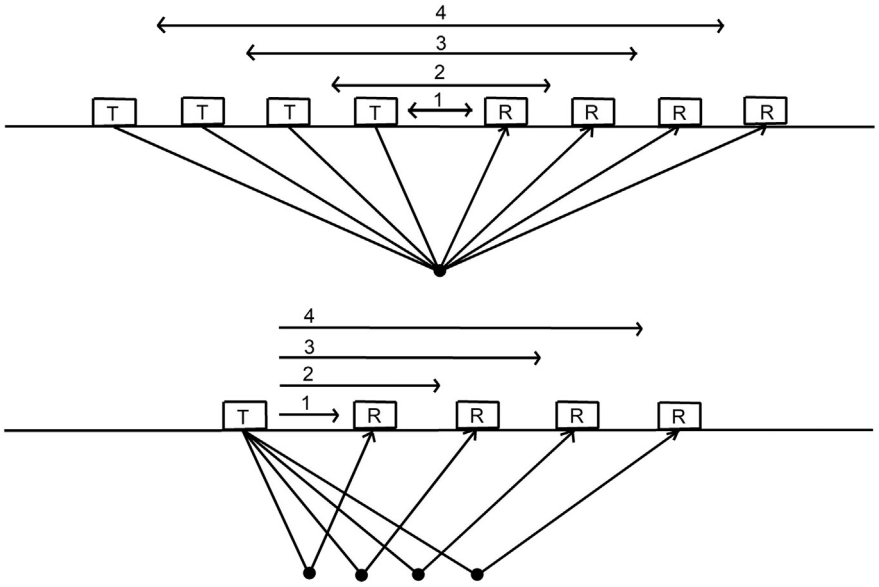

Fig. 2. Conceptual scheme showing the differences between the Common midpoint (CMP) method (on top) and the Wide-Angle-Reflection-and-Refraction (WARR) method (on bottom). While the CMP changes the position of both the transmitter and receiver in each step and the point of reflection is the same, in the WARR method, the position of the transmitter is constant and only the position of the receiver is changed. Thus, the point of reflection changes as well. (T - transmitter; R – receiver). Modified according to Bristow and Jol (2003); Galagedara et al. (2003); Huisman et al. (2003).

$$v = \frac{1}{\left(\frac{\varepsilon\mu}{2}\right)^{\frac{1}{2}}\left(\sqrt{1+\frac{\sigma^2}{\omega^2\varepsilon^2}}+1\right)^{\frac{1}{2}}} \quad (2)$$

where v is the electromagnetic wave velocity; ε is the dielectric permittivity; μ is the magnetic permeability, σ is the electric conductivity and ω is the angular frequency. Since the magnetic permeability of most rocks is close to 1, then if the frequency of the electromagnetic signal exceeds 100 MHz or the electrical conductivity of the environment is low (below 100 mS/m), the Eq. (1) can be simplified to $v = 1/\sqrt{\mu\varepsilon}$ (Eq. (3)) (al Hagrey and Müller, 2000; Reppert et al., 2000).

Several methods are used to determine the electromagnetic wave velocity. The most common approaches using multi-offset measurements, e.g., "Wide-Angle-Reflection-and-Refraction" (WARR) and "Common midpoint" (CMP) or its enhancement using Brewster angles, which allow the velocity below the deepest reflector to be determined (Reppert et al., 2000), were adopted from refraction seismology. Thus, they require a GPR unit with separated transmitter and receiver antennas, which are then used to undertake measurements at diverse distances (Fig. 2) to derive the function of electromagnetic signal travel time in relation to the antenna separation distance. This function is then used to determine the GPR signal velocity along the centre point (i.e., the midpoint) (Greaves et al., 1996). However, the standard errors in such determined depths are as large as 10–20 cm (Bristow and Jol, 2003), and therefore these methods are not recommendable for most soil surveys.

A simple approach works with the two-way travel time of the wave reflected from a reflector at a known depth. The reflector can be either a natural object or an artefact introduced at a known depth. This approach is more accurate and it appears simple, but realization in the field can be difficult because it requires the object to be buried without disturbing the surrounding ground or excavating the natural object (Ercoli et al., 2018; Goodman et al., 2009; van Overmeeren et al., 1997). The ground water table can also be used as the reflecting object but it is not fixed as it fluctuates with time (van Overmeeren et al., 1997).

By contrast, the velocity determination from a GPR output radargram has been considered a reliable method, but too demanding for many studies. This method is performed by matching the shape of hyperbolas originating in a reflection (e.g. Elkarmoty et al., 2017; Goodman et al., 2009; Olhoeft, 2000). A wider hyperbola indicates a higher velocity of the reflected wave; however, the size and orientation of the detected object also plays a role. The algorithm of hyperbola picking is still being improved, for example, by including an automatic mode as tested by, e.g., Mertens et al. (2016).

Measuring the dielectric permittivity of the soil and computing the velocity according to the formulas (Eq. (2)) or its simplified form (Eq. (3)) have been found to be reasonable methods even for soil surveys that require high accuracy (e.g., van Dam et al., 2003, 2002; van Dam and Schlager, 2000). The dielectric permittivity of the soil should be measured in the field because its properties can be changed during extraction and transport (Goodman et al., 2009; Jonard et al., 2014). Commonly, devices using the time-domain reflectivity (TDR) principle are employed for this purpose and a GPR survey is then combined with the resulting measurements (e.g., Ardekani et al., 2014a; Benedetto, 2010; van Dam et al., 2003, 2002; van Dam and Schlager, 2000). The TDR method also uses electromagnetic waves, but its frequency range is broader. The device commonly is comprised of probes, along which the velocity of electromagnetic waves is measured (Robinson et al., 2008). Commonly, an average signal velocity is used for the radargram interpretation; however, soils are highly heterogeneous and the velocity often changes. Therefore, it would be more accurate to divide the radargram into homogenous parts, which would be interpreted separately using a specific velocity (Elkarmoty et al., 2017). This task is so laborious that an average signal velocity was used in almost all studies.

1.3. Electromagnetic properties of soils

Because ground penetrating radar depends on the principle of the penetration of electromagnetic waves in a medium, the output of a GPR measurement reflects the electromagnetic properties of a medium and indicates boundaries that have considerable changes in properties on either side. In more detail, the reflectivity on a boundary is defined as $RC = (\sqrt{\varepsilon_{r2}} - \sqrt{\varepsilon_{r1}})/(\sqrt{\varepsilon_{r2}} + \sqrt{\varepsilon_{r1}})$ (Eq. (4)) (al Hagrey and Müller, 2000; Huisman et al., 2003; van Dam et al., 2003), where RC is the reflectivity and $\varepsilon_{r2,1}$ is the relative dielectric permittivity of medium 2 and 1.

In general, the electromagnetic properties of substances/materials are summarized by their electromagnetic impedance, which consists of the dielectric permittivity and the magnetic permeability. The magnetic permeability is considered only in materials that contain ferromagnetic minerals (magnetite and haematite). In these materials, a higher permeability reduces the electromagnetic signal penetration. In other substances, its influence is negligible (Cassidy, 2009). The dielectric permittivity of a material is the dominant property that controls the spread of electromagnetic waves and is usually expressed relative to the

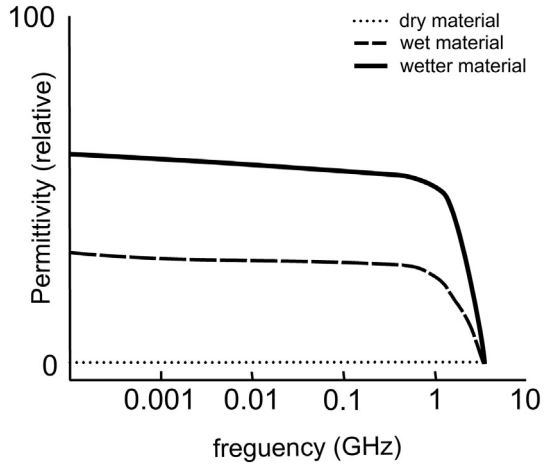

Fig. 3. Illustration of permittivity-frequency dependence. Outlined according to Cassidy (2009); Lauer et al. (2010).

dielectric permittivity of a vacuum.

The relative dielectric permittivity of rocks varies significantly, from 3 to 8, depending on the rock type (e.g., igneous, sedimentary) and mineral composition (Cassidy, 2009). The relative permittivity of air is close to that of a vacuum, i.e., 1, and the highest permittivity of substances commonly found during a ground survey is that of water, which reaches 78–88 for temperatures of 25 °C–0 °C (Cassidy, 2009). The relative dielectric permittivity of water abruptly changes after freezing; therefore, ice is characterized by values between 3 and 4 (Cassidy, 2009).

Because soil consists of different phases (solid, liquid and gaseous), the dielectric permittivity of a soil is determined by the characteristics and proportions of each of these phases. Salat and Junge (2010) showed a linear correlation between the dielectric permittivity and the dry mass density of a soil, indicating that the permittivity of dry soils depends strongly on their porosity and compaction. Because soil compaction decreases the porosity and thus the proportion of gas, the dielectric permittivity increases (Salat and Junge, 2010). Layers compacted by agricultural machines have been detected using GPR outputs, for example by André et al. (2012) for a vineyard. Because dielectric permittivity varies significantly with mineral composition (Cassidy, 2009), the higher content of specific minerals, e.g., calcite vs. quartz, the higher its value (Salat and Junge, 2010). On the other hand, the soil dielectric permittivity decreases as the soil organic matter content increases due to the resulting decrease in the soil's bulk density (Jonard et al., 2014; Lauer et al., 2010). The dielectric permittivity of dry undecomposed biomass was found to be close to 1 and it increases as biomass decomposition increases (André et al., 2015; Ardekani et al., 2014b; Jonard et al., 2014). Higher temperatures reduce the permittivity by enhancing the polarization (Cassidy, 2009; Doolittle and Butnor, 2009).

However, because the substance commonly found in the ground with the highest permittivity is water, it is obvious that the water content has a dominant influence on the dielectric permittivity of materials (Annan, 2009). Therefore, there are many models of the relationship between the water content and the material's dielectric permittivity, including Archie's law (Archie, 1942), the complex refractive index method (Birchak et al., 1974), the Topp model (Topp et al., 1980), and the Bruggeman-Hanai-*Sen* (*BHS*) effective medium *model* (Sen et al., 1981). All of these models are the most valid for the material they were intended for, which generally, is sand, because for fine-grained materials, other factors, such as the structure or pore distribution, play a role, and these factors need to be included in models as well (van Dam et al., 2003). Thus, Conyers (2012) found that adding the same amount of water to dried samples of similar permittivity caused their permittivity to differ. Geophysical electromagnetic methods such as GPR detect dielectric permittivity, but soil characteristics such as moisture, porosity or bulk density have to be determined according to these previously mentioned models.

Saarenketo (1998) noticed that the permittivity of soil water differs among capillary, adsorption (hygroscopic) or free (gravitational) water types. For free water, the permittivity reaches 78–88, whereas for hygroscopic water, the permittivity can be below 4 (Saarenketo, 1998). The permittivity of capillary water is somewhere between these values. This effect is caused by particles with large specific surface areas (clays or humus) which have a higher potential to fix water molecules; therefore, the water molecules are not able to react to the electromagnetic fields and decrease the soil dielectric permittivity (Lauer et al., 2010). The soil water content-permittivity changes significantly as the proportion of soil water types changes (Saarenketo, 1998). Similarly, the dielectric permittivity is influenced by the soil Cation Exchange Capacity (CEC) and it increases as the CEC increases (with increasing cation concentration, the hydrated cations disrupt the structure the water molecules arrangement around the soil particles) (Saarenketo, 1998).

In addition to the properties of a material, the dielectric permittivity depends on the electromagnetic signal frequency (Cassidy, 2009), but only for materials that contain water (Fig. 3). The dielectric permittivity of a dried material is frequency independent, dependence on the electromagnetic signal frequency increases as water content increases. The dielectric permittivity of the material decreases non-linearly as the frequency increases; however, importantly, this is only true for frequencies over 1 GHz, as a result of the dipolar polarization process (Cassidy, 2009; Huisman et al., 2001; Lauer et al., 2010; Salat and Junge, 2010).

Another physical property that influences the GPR measurements is the soil electrical conductivity. This property reduces the depth of penetration of GPR measurements because it attenuates the emitted electromagnetic signal. The electrical conductivity is driven primarily by water content and salinity, and secondly by clay content, especially the dominant clay mineral types (Arcone et al., 2008; al Hagrey and Müller, 2000; Doolittle and Butnor, 2009; Saarenketo, 1998). For example, montmorillonite causes an increase in permittivity as frequency decreases, but an increase in kaolinite results in a much smaller increase in permittivity. Illite is characterized by values between these types (Arcone et al., 2008). High electromagnetic signal attenuations in clayey soils have been noted in many studies. For example, in soils with a 35% and above clay content, the penetration depth of the GPR measurements do not reach > 0.5 m (Doolittle and Butnor, 2009). For this reason, clayey soils are often not recommended for GPR surveys, but for many soil science applications, the reduced penetration depth suffices. Generally, grain size does not play a major role because the dominant factor influencing clay electrical conductivity is soil cation exchange capacity (Arcone et al., 2008; Lauer et al., 2010; Mourmeaux et al., 2014; Saarenketo, 1998).

2. GPR applications in soil surveys

2.1. Soil water content

Soil moisture estimation is the most frequent application of GPR in soil surveys as water content influences electromagnetic signal propagation. Several approaches have been suggested for this purpose, all of which measure soil dielectric permittivity. To define soil moisture, these methods use the water content models that are based on the dielectric permittivity relationship mentioned above. Reviews of soil moisture determination using GPR have been provided by Huisman et al. (2003), Slater and Comas (2009) and recently by Klotzsche et al. (2018), who updated the review by Huisman et al. (2003) by presenting the latest principles of soil moisture estimation using GPR. In this paper we present the key principles, the progress achieved by every approach

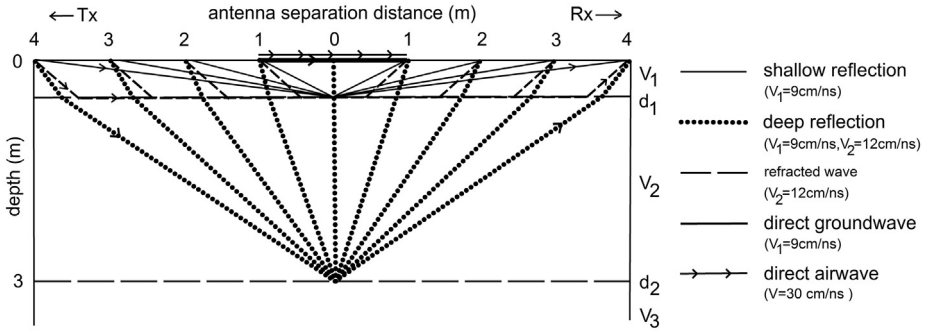

Fig. 4. CMP approach using reflectors ($d_{1,2,3}$) at different depths to estimate the soil water content in a vertical profile; $V_{1,2,3}$ - signal velocities. Modified from van Overmeeren et al., 1997.

and their applications.

2.1.1. Approaches based on signal velocity analysis

Traditional approaches are most often based on the electromagnetic signal reflectivity from a distinct soil layer. Soil dielectric permittivity is then calculated from the electromagnetic wave velocity determined using antenna-reflection travel time and layer depth. The reflection boundary is often the groundwater table. For example, this approach has been successfully applied by van Overmeeren et al. (1997) when mapping the soil moisture of podzols. However, this method requires a material penetrable by electromagnetic waves and a reflecting boundary at a known depth. If the known reflecting boundary is missing, the CMP method can be used to determine the electromagnetic signal velocity and to estimate the soil water content. If there are several reflectors, the soil water content in a vertical profile can be estimated (Fig. 4); currently, the approaches based on this principle allow the estimation of soil water content for each layer detected by GPR (Greaves et al., 1996; Koyama et al., 2017; Lu et al., 2017; Steelman and Endres, 2012; van Overmeeren et al., 1997).

2.1.1.1. Ground wave approach. The ground wave velocity (Huisman et al., 2001; van Overmeeren et al., 1997) from a direct wave spreading from a transmitter to a separated receiver through the upper centimetres of soil can be employed to determine the soil water content. The ground wave can be recognized, for instance, using the CMP measurement (Fig. 5) or using the Wide Angle Reflection and Refraction (WARR) measurement. The electromagnetic signal velocity in the soil is calculated from the ground wave travel time and the antenna separation distances (Grote et al., 2003; Huisman et al., 2001; van Overmeeren et al., 1997). This approach was adapted from seismology and the approximation for GPR was defined by van Overmeeren et al. (1997) as

$$z = \frac{1}{2}\left(\frac{vS}{f}\right)^{\frac{1}{2}},$$

where z is the depth of influence of the ground wave; v is the electromagnetic wave velocity in the soil; S is the separation distance between the transmitting and receiving antennas; and f is the frequency of the GPR signal. The ground wave is the first to arrive at the receiver after the air wave, which spreads directly from the transmitter to the receiver through the air.

The multi-offset survey approach is costly and time-consuming. Furthermore, the spatial resolution is low because a single parameter value results from multiple measurements with an increasing distance of antennas (Grote et al., 2003). For this reason, the common-offset approach was suggested instead (Galagedara et al., 2003; Grote et al., 2003). The travel time of the ground wave is calculated relative to the arrival time of the air wave. However, under dry conditions, it is difficult to differentiate the ground and air waves (Ardekani, 2013; Grote et al., 2003).

The ground wave penetration and therefore the sampling depths of GPR ground waves depend on antenna frequency. This depth was suggested to be 10 cm by Huisman et al. (2001) and Lu et al. (2017) who used 225–450 MHz antenna frequencies; Grote et al. (2003) suggested the depth was 17–25 cm, using 450 MHz and 900 MHz antennas. According to numerical modelling conducted by Galagedara et al.

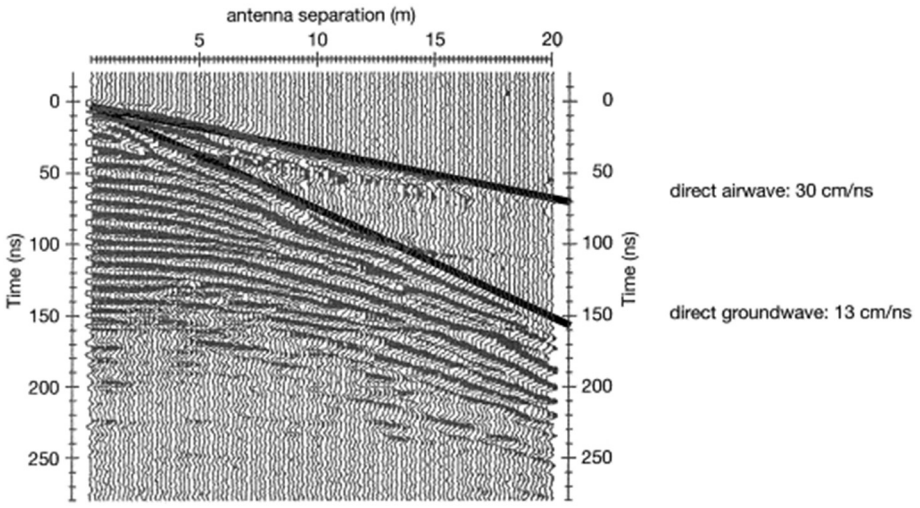

Fig. 5. Air-wave and ground wave delineated by a CMP measurement. From van Overmeeren et al. (1997).

(2005b), the penetration depth is 0.85 m for 100 MHz, 0.38 m for 200 MHz, 0.26 m for 450 MHz and 0.13 m for 900 MHz in dry soils. In wet soils, the depths decrease (Galagedara et al., 2005b; Lu et al., 2017). The penetration depth is also influenced by the antenna separation distance. The depth increases as the antenna distance increases (Galagedara et al., 2005a; Grote et al., 2003).

Based on the publications reviewed above, the ground wave approach could be considered relatively reliable. This approach has been applied, for example, to monitor seasonal variations in soil water content (Pallavi et al., 2010). However, the method is problematic under specific conditions, e.g., if there are very contrasting environments within the soil profile and if the thickness of the soil is less than the wavelength of the GPR signal, as well as if there is a strongly reflecting layer, with a higher signal velocity, underneath the soil profile or underneath the surveyed soil profile. These cases occur when there is a shallow soil over a low-porosity bedrock or when the studied upper part of the soil profile is wet and lies over dry sand or gravel. In other cases, these conditions occur when a permafrost layer is present at depth, or precipitation forms a wet infiltration front in relatively homogenous soils (Strobbia and Cassiani, 2007; van der Kruk et al., 2010, 2006; Lu et al., 2017). Under such conditions, the ground waves are hardly identifiable due to the generation of guided waves and the critically refracted electromagnetic waves (Fig. 6) (Arcone et al., 2003; van der Kruk et al., 2006). In these cases, the low-velocity layer catches part of the GPR signal and acts as a waveguide. The captured signals are the electromagnetic waves that achieve the lower boundary of the low-velocity layer with angles exceeding the Snell critical angle, and in consequence, these waves are entirely reflected (Fig. 6). Subsequently, they reach the upper boundary of this layer at the same angle and are entirely reflected again. As a final result, they spread horizontally in the low-velocity layer (Fig. 6) (Strobbia and Cassiani, 2007; van der Kruk et al., 2006).

The guided waves have a dispersive character. As the dispersion characteristics are determined by the dielectric permittivity, the thickness of the waveguide layer and the permittivity of the underlying layer (van der Kruk et al., 2006), the guided wave dispersion characteristics can be used for soil moisture estimation under specific conditions in significantly differentiated soil profiles. To accomplish this, van der Kruk et al. (2006) introduced a scheme analogous to the analysis of dispersed Rayleigh waves recorded on multi-channel seismic data. The original single-layer approach was later extended to multiple layers and applied to a soil wetted by precipitation in its upper layer (van der Kruk et al., 2010) as well as to a layered sandy soil in another field experiment (Rege and Godio, 2012). Another multi-layer GPR waveguide model was suggested by Strobbia and Cassiani (2007) to solve the underestimation of soil thickness caused by the dominant influence of the lowest velocity layer. In this model, the soil water content of the wettest layer is measured quite precisely (the uncertainty is within a few percent), but the moisture of the adjacent layers might be erroneous (Strobbia and Cassiani, 2007). Instead of a multi-layer model, Mangel et al. (2015) suggested using a piece-wise linear function model, which better represents the gradational nature of the water distribution in the waveguide. However, this approach has not yet been tested in the field.

2.1.2. Approaches based on reflection amplitude analysis

The reflection coefficient method determines the electromagnetic properties of a medium by analysing the amplitude of an electromagnetic wave reflected from a distinct layer (al Hagrey and Müller, 2000; Reppert et al., 2000) according to the Eq. (4). The soil surface can also be used as the reflection layer for the amplitude analysis, and this approach is the most common. The relative permittivity of the air is used as a permittivity of one of the mediums and the permittivity of the soil is defined from the reflection amplitude (al Hagrey and Müller, 2000; Huisman et al., 2003) according to Eq. (6),

$$\varepsilon_r = \left(\frac{1 + \frac{A_r}{A_m}}{1 - \frac{A_r}{A_m}} \right)^2$$

where ε_r is the relative permittivity of soil; A_r is the amplitude of the detected reflection and A_m is the amplitude of a perfect reflector, commonly a metal plate.

The surface reflection coefficient method was tested and found to be relatively accurate (RMSE = 0.04 cm^3/cm^3) by, for example, Ardekani (2013), who demonstrated relatively good results for soil surface moisture (0–10 cm uppermost layer) in sandy soil using 900 MHz antennas in a laboratory setting (RMSE = 0.006 cm^3/cm^3); however, the method was less reliable for silty soil (RMSE = 0.04 cm^3/cm^3) measured in the field.

2.1.3. Early Time Signal analysis

To circumvent the problem of separating the ground and air waves, which can occur using common-offset antennas (e.g., Ardekani, 2013; Grote et al., 2003), Early Time Signal analysis was suggested by Pettinelli et al. (2007) and Pettinelli et al. (2014). Early Time Signal analysis is based on analysing the envelope amplitude of the radar traces in several time windows. This analysis works on the early-time part of a GPR signal that contains air and ground wave wavelets. Pettinelli et al. (2007) showed that the waveforms differ in terms of amplitude and time-stretching and that the variations are related to the soil electrical parameters, i.e., dielectric permittivity and conductivity; for example, higher amplitudes and shorter wavelengths correspond to lower soil permittivity values (Fig. 7). The approach mainly examines the relationships between the waveform attributes and the soil electromagnetic properties measured by TDR, but a mathematical model using Green functions and comprising the principles of the ground wave and the reflection coefficient approaches was also added by Di Matteo et al. (2013). In addition, they suggest using the first positive half cycle of the early-time radar signal to minimize the effect of the shallow reflectors or local heterogeneities and to prevent interference between the reflected and direct waves. In addition, they show that the early-time signal is influenced by the soil dielectric permittivity variations much more significantly than by soil conductivity. The soil electrical conductivity affects the peak value of the GPR waveform, but it does not significantly influence the correlation between the early-time amplitudes and the dielectric permittivity. Ferrara et al. (2013) applied this method to measure soil water content in the field and found good agreement between the ground wave approach and a multi-offset CMP approach. Algeo et al. (2016) tested the approach to monitor changes in

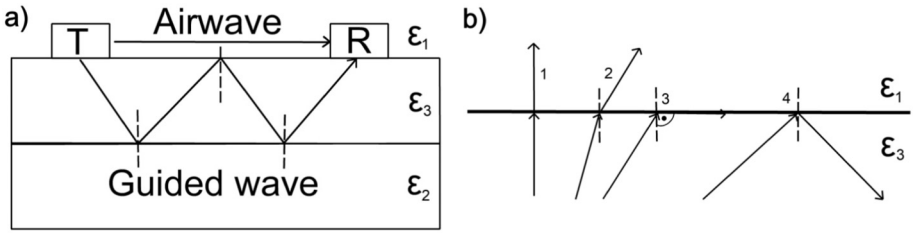

Fig. 6. a) Scheme for a guided wave; T - transmitter; R – receiver; $\varepsilon_{1,2,3}$-dielectric permittivity of medium; $\varepsilon_1 < \varepsilon_2 < \varepsilon_3$.
b) Electromagnetic wave refraction and reflection on an interface.
1 - direct wave; 2 - refracted wave; 3 - snell critical angle; 4 - reflected wave, $\varepsilon_{1,3}$-dielectric permittivity of medium; $\varepsilon_1 < \varepsilon_3$.
Modified according to van der Kruk et al. (2006); Strobbia and Cassiani (2007) (a) and outlined according to Lekner (2016) (b).

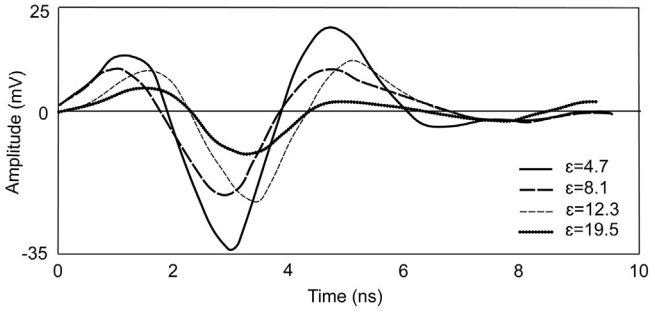

Fig. 7. Influence of soil permittivity on the amplitude of the early-time signal, showing a decrease in the reflection amplitude as the dielectric permittivity of a material increases.
ε - relative soil dielectric permittivity.
Modified from Pettinelli et al. (2007).

the soil water content after irrigation in a clay-rich soil in which the ground-wave method fails. The mathematical model has continued to be improved, and better parameters, such as the distance between the transmitter and the receiver or the antenna position above the surface, have been explored (e.g., Comite et al., 2016, 2014).

Benedetto (2010) related the theories and principles to an early-time signal analysis based on Fresnel theory and Rayleigh scattering, in which the frequency spectrum dependence on soil moisture is analysed. The frequency spectrum is extracted employing the fast Fourier transform and shows a shift in the peak towards lower frequencies as soil water content increases.

2.1.4. Full-waveform inversion

Lambot et al. (2004) proposed a new method based on numerical modelling of signal response operating in the frequency domain and inverting the full waveform of the radar signal. They replaced the multi-offset antenna approach using a broad frequency spectrum employing wideband frequency antennas. The method originally works only with surface reflections and they used an off-ground GPR device with air-coupled antenna located above the ground to accentuate the surface reflection and suppress the deeper reflections. The height of the antenna position above the ground determines the influence of deeper layers (Ardekani et al., 2014a).

The method was tested to determine the moisture in the soil surface layer (ca 10 cm) by Weihermüller et al. (2007) and Ardekani (2013) using 0.8–1.8 GHz and 0.2–2 GHz wideband antennas in silty soils but without satisfactory results, which could have been caused by the higher electrical conductivity that very often characterizes loamy and clayey soils that is generally neglected in the approach. Lambot et al. (2008) showed that this method performs well (good agreement with volumetric and TDR measurements) in sandy soils, except for those with soil moistures close to water saturation, which is also explained by higher electrical conductivity. The electrical conductivity depends, in addition to clay content and salinity, on the water content (Mourmeaux et al., 2014). Similar findings were presented by Minet et al. (2012) for silty loam soil when using an off-ground antenna at 1.1 m height and a frequency spectrum of only 200–800 MHz. At higher frequencies the measurement is also influenced by soil roughness (Minet et al., 2011). According to Rayleigh's criterion a surface is considered to be rough if the protuberances heights are over $\lambda/8$ (Lambot et al., 2006). Tran et al. (2015) tested the full-wave inversion approach using an on-ground GPR system proposed by Lambot and André (2014) to estimate soil moisture in the field and reported satisfactory results (RMSE = 0.05 cm^3/cm^3). The full-waveform inversion scheme in its on-ground version was also adapted to the ground wave approach and subsequently tested in silt loam soil using a 200 MHz antenna and the WARR method (Busch et al., 2014). The ground wave method was improved to measure the soil electrical conductivity in addition to the dielectric permittivity and Busch et al. (2014) suggested applying the method to determine the soil texture.

2.2. Soil stratigraphy

Based on the known factors controlling the successful employment of the GPR method, several authors used GPR to study soil stratigraphy (e.g. André et al., 2012; Nováková et al., 2013; Simeoni et al., 2009; van Dam et al., 2003; van Dam and Schlager, 2000). The research was based on the prerequisite that soil horizons differ in the properties that control the soil water content, e.g., soil texture or soil organic matter content, which should be able to be distinguished by GPR. Van Dam and Schlager (2000), who detected horizons of fossil soils buried in aeolian sediments, suggested that texture differences can possibly be detected when volumetric water content exceeds 0.055.

2.2.1. Soil profile survey

Complex soil stratigraphy surveys have been performed since the late 1970s to the early 1990s with 100–500 MHz antennas, especially in the USA, or later, for example, in Australia (Simeoni et al., 2009), and a good overview of these surveys was provided by Doolittle and Butnor (2009). The surveys were based on visualizations of signal reflections. Generally, sandy soils with contrasting horizons were considered to be favourable for GPR soil surveys. The depths of argillic, spodic, and placic horizons; cemented, indurated or frozen horizons; and R or C horizons in coarse-textured soils were detected with a horizon depth measurement error between 2 and 40%. However, surveys of fine-textured soils were often unsuccessful because the higher electrical conductivity of clays reduced the penetration of the electromagnetic signal, and therefore, the signal response was disguised and inferred by strong reflections near the soil surface (e.g., Doolittle and Collins, 1998; Meadows et al., 2006; Stroh et al., 2001). For finer-textured soils, the Bg horizon in gleyic Cambisols and the R horizon in a haplic Cambisol were identified by Nováková et al. (2013) in Central Europe using a 250 MHz antenna. Similarly, Zhang et al. (2014) detected the Bw-BC horizon boundary and the R horizon upper boundary in ochric Cambisol and lithic Cambisol in Pennsylvania in reflections using a 400 MHz antenna.

Furthermore, Zhang et al. (2014) observed profiles under different moisture conditions. The horizons were more distinct under wet conditions if one of the horizons was wetter than the other or if a water-restricted lower horizon caused the water to accumulate at the boundary. However, the clear reflections representing horizon boundaries under wet conditions were disrupted by tree roots, which formed a preferential path for water infiltration. André et al. (2012) showed the stratigraphy in a gravelly sandy soil and in Planosols and Stagnosols in a vineyard using 2D and 3D visualizations of electromagnetic signal reflections. An anthropogenic compacted layer was especially apparent in this location.

A different approach to studying soil stratigraphy was suggested by Buchner et al. (2012). The approach is based on a signal inversion. The signal response was first numerically modelled, simulating probable scenarios, and then the parameters such as soil water content and the layers' geometry (shape, thickness) were inversely estimated by minimizing the squared differences in the travel times and amplitudes of reflections between the acquired and modelled data. The method thus requires clear reflections that can be processed. Numerical modelling approaches usually need multi-offset antenna settings data or multi-frequency data. However, Buchner et al. (2012) used data acquired by a common-offset antenna in multiple positions and demonstrated that the subsurface stratigraphy can be determined with an accuracy of 5 cm using this approach, and the water content of the layers can be simultaneously estimated with a 2% deviation.

2.2.2. Organic horizon thicknesses

For several years, the GPR method has been tested to determine

organic horizon thicknesses for carbon stock estimation and environmental modelling. A GPR survey to assess the thickness of an organo-mineral horizon over limestone bedrock based on radargram image processing was performed by Li et al. (2015) in a karst area. Li et al. (2015) used a 500 MHz antenna and achieved a maximum measurement error of only 3.8%; they proposed measuring the horizon thickness under the driest conditions possible to reduce radar signal attenuation. Similarly, Winkelbauer et al. (2011) used an 800 MHz antenna and a conventional 2D visualization of the electromagnetic signal response in the altimontane zone in the Bavarian Alps to distinguish organic horizons from mineral horizons and to distinguish individual organic horizons. The authors were able to distinguish the organic horizon-mineral subsoil boundary with an average 15% measurement error in its depth but found that the individual organic horizons (Oi, Oe, Oa) and Ah could not be separated. Winkelbauer et al. (2011) argued that this resulted from the insufficient thicknesses of the individual organic horizons relative to the antenna resolution, as well as insignificant differences in the dielectric permittivity. The dielectric permittivity of organic horizons was studied by André et al. (2014) and André et al. (2015). In the laboratory they determined the following relative dielectric permittivity of nearly dry (1.4% moisture) organic and organo-mineral horizons as follows: horizon Oi (almost undecomposed organic matter) $\varepsilon = 1.19$, horizon Oe (slightly decomposed organic matter) $\varepsilon = 3.95$, and Ah (organo-mineral horizon) $\varepsilon = 10.3$. In the field under more natural conditions of higher moisture (volumetric water content 4.4% for Oi and 13.5–22.8% for Oe), they detected values of $\varepsilon = 2.9$ for Oi and $\varepsilon = 6.3$ for Oe (André et al., 2016). However, Winkelbauer et al. (2011) considered soil organic horizon dielectric permittivity to be 40–60 in a natural state with common soil moisture contents, suggesting that the soil moisture conditions during GPR measurements are of enormous importance, as proven, for example, by Zhang et al. (2014) and van Dam et al. (2002). The latter study suggested that more measurements under different moisture conditions can be compared to distinguish and characterize individual horizons. Van Dam et al. (2002) observed a higher time variability of the electromagnetic signal response in buried soil horizons with higher organic matter contents compared to that for an aeolian sandy material, which is consistent with the findings of Conyers (2012), who was unable to detect a dry wooden object with a GPR, but could detect the object when wetted. However, the boundaries of soil layers with different water contents do not have to be identical with those of diagnostic organic horizons boundaries (Winkelbauer et al., 2011).

2.2.2.1. Full-waveform inversion. Apart from several previously mentioned studies, there is an overall lack of studies that determine the thicknesses of organic horizons using image processing approaches. Recently, an organic horizons survey was performed using the full-wave inversion method suggested by Lambot et al. (2004). André et al. (2014) carried out a controlled experiment on a beech forest floor to design various thicknesses of artificial Oi and Oe horizons. Using a 0.8–4 GHz wide-band off-ground antenna, they modelled the thickness of organic horizons with an accuracy of 1 cm, which represented a 6% relative measurement error in the Oi horizon thickness and an 11% relative error in the Oe horizon thickness (André et al., 2014; André et al., 2015). Application under natural conditions confirmed most of their findings. However, the separation of Oi and Oe horizons was difficult due to a small difference in dielectric permittivity (André et al., 2016). The authors suggest performing the measurement after a rainy period, when the less decomposed litter in the upper layer should be drier compared to the slightly decomposed organic matter below. Furthermore, they suggest estimating carbon storage in litter biomass according to the soil organic matter bulk density determined from GPR measurements using a correlation between the dielectric permittivity and the bulk density. In addition, forest litter, especially leaf litter, causes strong signal scattering, resulting in reduced clarity and higher attenuation in the lower layers (André et al., 2015; Tanikawa et al., 2016).

2.2.3. Survey of peatlands

The ability of soil organic matter to bind to water has been widely used in GPR surveys of peats for several decades to estimate the depths of peat bogs or, less successfully, to determine horizons that differ by various levels of decomposition (e.g., Kettridge et al., 2008; Plado et al., 2011; Sass et al., 2010). Surveys of peats are often complicated because fieldwork in peats is difficult and sometimes has to be performed when the peatland is frozen. The interpretation of results is made even more difficult when there is snow cover (e.g., Plado et al., 2011; Proulx-McInnis et al., 2013). Most studies have focused on high latitude peatlands, and only a reduced number of studies have focused on wetlands in warmer climates (e.g., Comas et al., 2015; William and Comas, 2016).

The water content of a peat can reach 95% but depends on the decomposition rate and plant species composition. As a result, the dielectric permittivity of peats reaches 50–70. By contrast, the maximum volumetric soil water content in mineral subsoils is commonly 30–40%, creating a difference that makes the peat-mineral subsoil boundary easily detectable (Slater and Reeve, 2002). However, the peat layer stratigraphy remains a subject that requires additional research. In peat strata, less decomposed peats are characterized by lower bulk densities and higher porosities, and therefore, in a fully saturated peatland, a less decomposed peat should have a higher moisture content and, consequently, increased dielectric permittivity compared to that of a more decomposed layer (Plado et al., 2011). However, peatlands are not always fully saturated; for example, Plado et al. (2011) detected a higher electromagnetic signal intensity in a less decomposed peat layer but no distinct boundary. Reflections correlating with peat horizons boundaries were detected by Kettridge et al. (2008) and Kettridge et al. (2012), for example. However, they also observed reflections where no horizon boundaries were present. Karuss and Berzins (2015) suggest that only peat moisture content changes of at least 3% can cause reflections of GPR signals. Because reflections that did not correlate with moisture changes were also detected by these authors, they argue that all reflections cannot result from water content differences. However, Laamrani et al. (2013) determined the thickness of a fibric horizon, and Walter et al. (2016) identified the boundary between two types of peat (Carex peat and brown-moss peat), which were characterized by different bulk densities and organic matter contents due to the existence of different plant species.

Basic image processing is used to visualize peat – mineral soil boundaries. Under favourable conditions, GPR signals can penetrate up to 10 m in a peat profile and provide stratigraphy data with an average accuracy of 0.25 m (Proulx-McInnis et al., 2013). The electromagnetic wave propagation velocity is often determined via calibration using manual probe data (Rosa et al., 2009) or the CMP method (Kettridge et al., 2008; Sass et al., 2010; Comas et al., 2017), but rarely by reflection hyperbola analysis (Strack and Mierau, 2010). However, there are uncertainties in the accuracies of both manual probe data and the CMP method and hence in GPR measurements, as summarized by Parry et al. (2014). Manual probes can hit artefacts in peat or penetrate to underlying sediments, and the inaccuracy of the CMP method is caused by the different dielectric permittivity values present in peat strata. Most studies conclude that GPR measurements can aid peat surveys, but they cannot be employed as an independent method and should be combined with another geophysical method or manual probing (Proulx-McInnis et al., 2013).

In view of the high signal attenuation rates in environments of high dielectric permittivity and the significant depths of peats, 100–200 MHz antennas and, more rarely, higher frequency antennas of up to 400 MHz are commonly employed in surveys (Doolittle and Butnor, 2009; Proulx-McInnis et al., 2013; Slater and Reeve, 2002; Völkel et al., 2001). Similarly, as for dryland soils, GPR surveys are more successful

in peats with sandy subsoils and are even more successful in acidic peats lacking clays and exchangeable cations. The electrical conductivity of clays can cause electromagnetic signal attenuation and can be accentuated by a high cation content (Doolittle and Butnor, 2009; Laamrani et al., 2013; Völkel et al., 2001).

2.2.3.1. Biogenic gases in peatlands. Studies have shown the potential use of GPR to investigate biogenic gasses in peatlands, which can be identified as areas from which electromagnetic waves scatter (e.g., Comas et al., 2005) or in which the electromagnetic wave velocity changes (Strack and Mierau, 2010) and to monitor the seasonal dynamics of biogenic gasses (Comas et al., 2008). An approach to monitoring the release of gasses using the two-way travel time of the electromagnetic signal reflected from the peat-subsoil boundary to estimate the ratio of the solid, liquid and gas phases was also suggested (Chen and Slater, 2015; Parsekian et al., 2012a). However, this method requires the known dielectric permittivity for each phase and the peat porosity (Chen and Slater, 2015). In addition, the size of the gas bubbles can be estimated from the spectral analysis of received GPR signal, as bubbles smaller than the wavelength cause scattering attenuation (Terry and Slater, 2017).

2.3. Other applications in pedology

2.3.1. Soil salinity and soil texture

Soil salinity and clay content can be estimated by the same principles as underlying estimates of the soil moisture content. Soil salinity is, in fact, determined by the salt content in pore water, which increases as electrical conductivity increases. Thus, soil salinity can be estimated using reflection coefficients and a reflection amplitude analysis. The reflection amplitude is influenced by the electrical conductivity and increases with salinity as well as the reflection coefficient (al Hagrey and Müller, 2000). The different reflectivity of a soil with higher salinity was observed during field measurements by Rejšek et al. (2015). In addition, the authors used 3D modelling to estimate the depth of salt percolation.

GPR was also used to estimate the clay content. Meadows et al. (2006) used an early-time signal amplitude analysis in desert pavements to estimate clay content based on the signal attenuation caused by the electrical conductivity of clay. This approach was refined by Benedetto and Tosti (2013) and Tosti et al. (2013). The reflection frequency spectra were extracted using the Fourier transform. There is a significant shift in the frequency peak towards lower frequencies with an increased clay content (Fig. 8), as observed in a numerical study and in an experiment performed under laboratory conditions (Benedetto and Tosti, 2013).

2.3.2. Detection of tree roots

Studies have also shown the potential use of GPR to investigate tree root biomass and tree roots architecture. These studies are mainly conducted by forest ecologists and tree physiologists. The implementation of root detection could improve surveys of soil stratigraphy, where signal reflections by roots cause the soil horizons to be less distinct. A below ground tree root system and its parameters, such as the diameters of individual roots and root biomass, can be explored using electromagnetic signal reflections analysis. Various techniques and findings were briefly reviewed by Doolittle and Butnor (2009) and in more detail by Guo et al. (2013a). The roots are identified by imaging the radargram. The standard image processing techniques and filtering mentioned in the previous sections are commonly supplemented by a migration algorithm that is used to clarify roots' positions and parameters. Tree roots are commonly represented by hyperbolic reflections on radargrams, and the migration used to facilitate their interpretation tends to distort them. The locations of roots are then relatively evident, but estimating their size, shape and volume is more complicated (Doolittle and Butnor, 2009; Guo et al., 2013a). Cui et al. (2011) concluded that an antenna operating at a frequency of 450 MHz can detect larger roots (over 2 cm in diameter), and by contrast, 1.5 GHz antennas can detect roots that have diameters of 0.5 cm, but the feasible depth of a measurement is only approximately 30 cm. Thinner roots are commonly not detectable even using 2 GHz antennas (Cui et al., 2011). However, X. Liu et al. (2018) were able to detect fine roots of crops using a 1.6 GHz antenna in agricultural land. Some studies state a rapid change in detection accuracy between roots of < 1 cm in diameter and those with diameters exceeding 1 cm (Borden et al., 2016; Hirano et al., 2009). In general, the detectability of a root decreases as its diameter decreases and its depth increases. Root surveys are hard or even impossible to perform in highly water-saturated or clayey soils, similar to other GPR soil survey applications. In addition, identification of roots is difficult in soils with many coarse fragments and in rough forest terrains with herbaceous vegetation or fallen trees, which deteriorate the antenna's contact with the surface (Doolittle and Butnor, 2009). Plant litter also attenuates the signal (Tanikawa et al., 2016; Rodríguez-Robles et al., 2017). Therefore, most studies have been carried out under controlled experimental conditions in which sandy soils and favourable root orientations are used. The authors of these studies admit that under field conditions in soils with many heterogeneities, the results would not be the same (Guo et al., 2013a).

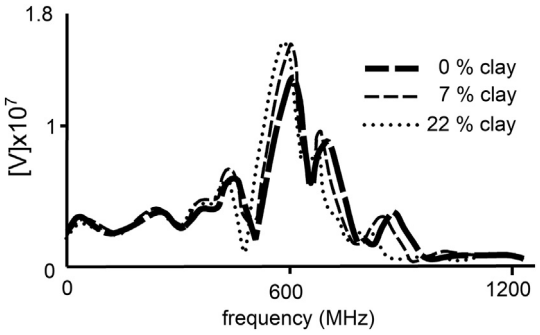

Fig. 8. Picture showing a shift in the frequency peak, with an increased clay content, towards lower frequencies.
Modified from Benedetto and Tosti, 2013.

2.3.2.1. Root system. Root systems are more evident when using 3D image visualization, and surveys require detailed measurements on small grids (Doolittle and Butnor, 2009). In the field, root distributions have been reconstructed, for example, by Raz-Yaseef et al. (2013) in a silt-loam textured soil in a Californian savannah with scattered trees; by Freeland (2015) in an orange grove in Florida; by Borden et al. (2016), who described the root system architecture of several tree species in a sandy-loam textured Luvisol; by Tardío et al. (2016), who detected coarse structural roots and finer root clusters using a 250 MHz antenna on a hill slope; and by Rodríguez-Robles et al. (2017) in a deciduous forest employing GPR on simple transects instead of a 3D grid.

An automatic method to join root points in neighbouring transects and to interpolate the 3D root system architecture using spline curve smoothing was suggested and tested on a natural site by Wu et al. (2014), and an algorithm for recognizing roots from reflection hyperbolas was developed by Li et al. (2016) using a randomized Hough transform, with an accuracy of approximately 80%. The method encounters problems in when roots are oriented parallel to the GPR measurements, when the distance between individual roots is too small, or when there are soil heterogeneities that disturb reflection hyperbolas and create clutter noise.

In general, the root orientation and distances between individual roots significantly influence GPR measurements. Many studies have found it difficult to detect roots oriented parallel to the measurements, and it was shown by Tanikawa et al. (2013) that roots oriented at angles between 45 and 135 degrees to the measurement direction were the

best detected. If the distance between individual roots is too small, the roots cannot be distinguished each from one another. For instance, it is suggested that their distances should exceed 20 cm in the case of a 900 MHz antenna (Hirano et al., 2009) or, more generally, for any antenna 4.5 times the root diameter (Yeung et al., 2016). However, Zhu et al. (2014) argue that clusters of fine roots are often indistinguishable from clutter noise on radargrams because they are represented by similar areas with a high signal reflection amplitude. Furthermore, if the finer roots overly a coarse root, even the coarse root can hardly be detected. In addition, the influence of the water content of roots cannot be neglected since the detectability depends on the contrast in the dielectric permittivity of the root and surrounding soil (Guo et al., 2013b). Roots with less than a 20% water content cannot be detected by GPR according to Hirano et al. (2009). The dielectric permittivity of roots can increase from 4.5 for dry roots to over 22 in water saturated roots (al Hagrey, 2007) and is a function of the root biomass density and the water content. An empirical study of this relationship was performed by Guo et al. (2013b).

2.3.2.2. Root biomass. The estimation of root diameter and biomass is based on various indexes extracted from GPR data. A brief review of most of these indexes was provided by Guo et al. (2013a). The relationship of various indexes to root parameters was determined using statistical regression. There are indexes based on the reflection strength (e.g., pixels within threshold ranges), which are extracted from GPR outputs after migration or application of Hilbert transformation algorithms, and indexes based on the reflection waveform (e.g., amplitudes of reflected waves, high amplitude areas, time intervals between two zero crossings) that is directly extracted from ordinarily processed waveforms (Guo et al., 2013a; Rodríguez-Robles et al., 2017; Simms et al., 2017). The disadvantage of reflection strength indexes is that they are strongly influenced by signal attenuation and by the depth of the measured object, which introduces confusion into the model (Barton and Montagu, 2004). The waveform parameters, especially the time interval between zero two crossings suggested by Barton and Montagu (2004) and improved by Cui et al. (2011), are independent of the signal attenuation. The relationship between the reflection amplitude and the root diameter was explained by Hirano et al. (2009) in a controlled experiment. The estimation of a root diameter, based on the time interval between zero-crossings, was successfully tested by Rodríguez-Robles et al. (2017) in the field with < 15% error in root diameter. Simms et al. (2017) and X. Liu et al. (2018) estimated the root diameter based on the signal strength. X. Liu et al. (2018) employed this approach to crops roots and, surprisingly, observed better agreement between GPR measurements and core samples under wet conditions and in clayey soils than in dry sandy soils. Most of the indexes were tested by Zhu et al. (2014) at a natural study site, and they suggested a new index – the magnitude width extracted from waveforms. This new index reasonably characterizes the root diameter, but is affected by the orientation of roots to the GPR measurements - the angle of which is often unknown. However, Cui et al. (2011) and Q. Liu et al. (2018) suggested a method to detect the root orientation from the shape of the reflection hyperbola. Only one index method - pixels within threshold range - is also applicable in 3D GPR models (Zhu et al., 2014).

Root biomass can be determined from the GPR-estimated root volume in combination with the root bulk density determined from core samples (e.g., Cui et al., 2011; Raz-Yaseef et al., 2013) or directly through a GPR index-biomass relationship (e.g., Borden et al., 2014; Stover et al., 2016). However, both approaches often neglect the biomass of roots finer than 0.5 cm in diameter, which are hardly detectable by GPR.

3. Conclusions

Under some conditions, a ground penetrating radar can successfully aid soil surveys, provide a significant amount of data and allow soil surfaces to remain undisturbed for future surveying. However, the measurement and data treatment approaches and antenna frequencies used in surveys must be chosen with respect to the exact survey purpose and field conditions. Traditional approaches are based on image processing of electromagnetic signals reflected at the boundaries of layers with different electromagnetic properties. These approaches are technically relatively simple in terms of field measurements and data treatments. However, the data processing and interpretations can be quite subjective. These approaches have been applied relatively successfully for a wide spectrum of tasks, but generally only under favourable conditions, which usually include sandy soils with a low CEC; low numbers of other objects, such as stones or dead wood, in the soils; and the absence of rough surfaces and hard overgrowing vegetation. Under favourable conditions, GPRs can assist with estimates of soil moisture, detecting soil stratigraphy in significantly layered soils, distinguishing organic and mineral horizons in peats, and detecting tree root systems. Some specific approaches are more demanding in terms of the data treatment required, but there have been some successes, even under less ideal conditions, e.g., the ground wave approach or the wave guide approach to soil moisture estimation. More complex techniques using numerical modelling devised during recent years might have more potential for success. However, there is still much work to be done in this field. To date, the full-waveform inversion method (Lambot et al., 2006, 2004) enables the detection of the widest spectrum of soil parameters. This method has been successfully applied to estimate soil moisture and detect and characterize soil organic horizons. However, this method requires rather favourable conditions to deliver successful results.

Declarations of interest

None.

Acknowledgements

This research was supported by the institutional resources of the Ministry of Education, Youth and Sports of the Czech Republic for the support of science and research. Project No. SVV260438.

References

al Hagrey, S.A., 2007. Geophysical imaging of root-zone, trunk, and moisture heterogeneity. J. Exp. Bot. 58, 839–854. https://doi.org/10.1093/jxb/erl237.
al Hagrey, S.A., Müller, C., 2000. GPR study of pore water content and salinity in sand. Geophys. Prospect. 48, 63–85. https://doi.org/10.1046/j.1365-2478.2000.00180.x.
Algeo, J., Van Dam, R.L., Slater, L., 2016. Early-time GPR: a method to monitor spatial variations in soil water content during irrigation in clay soils. Vadose Zone J. 15, 0. https://doi.org/10.2136/vzj2016.03.0026.
André, F., van Leeuwen, C., Saussez, S., Van Durmen, R., Bogaert, P., Moghadas, D., de Rességuier, L., Delvaux, B., Vereecken, H., Lambot, S., 2012. High-resolution imaging of a vineyard in south of France using ground-penetrating radar, electromagnetic induction and electrical resistivity tomography. J. Appl. Geophys. 78, 113–122. https://doi.org/10.1016/j.jappgeo.2011.08.002.
André, F., Jonard, M., Lambot, S., 2014. Full-wave inversion of ground-penetrating radar data for forest litter characterization. In: Proc. 15th Int. Conf. Grounds Penetrating Radar, 2014. GPR 2014, pp. 196–201.
André, F., Jonard, M., Lambot, S., 2015. Non-invasive Forest litter characterization using full-wave inversion of microwave radar data. IEEE Trans. Geosci. Remote Sens. 53, 828–840.
André, F., Jonard, F., Jonard, M., Lambot, S., 2016. In situ characterization of forest litter using ground-penetrating radar. J. Geophys. Res. Biogeosci. 121, 879–894. https://doi.org/10.1002/2015JG002952.Received.
Annan, A.P., 2009. Ground Penetrating Radar Principles, Procedure & Applications. Gr. Penetrating Radar Theory Appl. Ground Pen. ivhttps://doi.org/10.1016/B978-0-444-53348-7.00016-8.
Archie, G.E., 1942. The electrical resistivity log as an aid in determining some reservoir characteristics. Trans. AIME 145, 54–62.
Arcone, S., Peapples, P.R., Liu, L., 2003. Propagation of a ground-penetrating radar (GPR) pulse in a thin-surface waveguide. Geophysics 68, 1922–1933. https://doi.org/10.1190/1.1635046.
Arcone, S., Grant, S., Boitnott, G., Bostick, B., 2008. Complex permittivity and clay mineralogy of grain-size fractions in a wet silt soil. Geophysics 73, J1–J13. https://doi.

org/10.1190/1.2990634.
Ardekani, M.R., 2013. Off- and on-ground GPR techniques for field-scale soil moisture mapping. Geoderma 200–201, 55–66. https://doi.org/10.1016/j.geoderma.2013.02.010.
Ardekani, M.R., Neyt, X., Benedetto, D., Slob, E., Wesemael, B., Bogaert, P., Craye, C., Lambot, S., 2014a. Soil moisture variability effect on GPR data. In: 15th International Conference on Grounds Penetrating Radar, 2014a. 2014. GPR, pp. 214–217.
Ardekani, M.R., Nottebaeret, M., Jacques, D., 2014b. GPR data inversion for vegetation layer. In: Proc. 15th Int. Conf. Grounds Penetrating Radar, 2014. 2014. GPR, pp. 170–175.
Barton, C.V.M., Montagu, K.D., 2004. Detection of tree roots and determination of root diameters by ground penetrating radar under optimal conditions. Tree Physiol. 24, 1323–1331. https://doi.org/10.1093/treephys/24.12.1323.
Benedetto, A., 2010. Water content evaluation in unsaturated soil using GPR signal analysis in the frequency domain. J. Appl. Geophys. 71, 26–35. https://doi.org/10.1016/j.jappgeo.2010.03.001.
Benedetto, F., Tosti, F., 2013. GPR spectral analysis for clay content evaluation by the frequency shift method. J. Appl. Geophys. 97, 89–96. https://doi.org/10.1016/j.jappgeo.2013.03.012.
Birchak, J.R., Gardner, C.G., Hipp, J.E., Victor, J.M., 1974. High dielectric constant microwave probes for sensing soil moisture. Proc. IEEE 62, 93–102.
Borden, K.A., Isaac, M.E., Thevathasan, N.V., Gordon, A.M., Thomas, S.C., 2014. Estimating coarse root biomass with ground penetrating radar in a tree-based intercropping system. Agrofor. Syst. 88, 657–669. https://doi.org/10.1007/s10457-014-9722-5.
Borden, K.A., Thomas, S.C., Isaac, M.E., 2016. Interspecific variation of tree root architecture in a temperate agroforestry system characterized using ground-penetrating radar. Plant Soil 1–12. https://doi.org/10.1007/s11104-016-3015-x.
Bristow, C.S., Jol, H.M., 2003. Ground penetrating radar in sediments. Geol. Soc. Spec. Publ.(211).
Buchner, J.S., Wollschläger, U., Roth, K., 2012. Inverting surface GPR data using FDTD simulation and automatic detection of reflections to estimate subsurface water content and geometry. Geophysics 77, H45–H55. https://doi.org/10.1190/geo2011-0467.1.
Busch, S., van der Kruk, J., Vereecken, H., 2014. Improved characterization of fine texture soils using onground GPS full-waveform inversion. Trans. Geosci. Remote Sens. 52, 3947–3958.
Cassidy, N.J., 2009. Electrical and magnetic properties of rocks, soils and fluids. In: Jol, H.M. (Ed.), Ground Penetrating Radar Theory and Applications, pp. 41–72. https://doi.org/10.1016/B978-0-444-53348-7.00010-7.
Chen, X., Slater, L., 2015. Gas bubble transport and emissions for shallow peat from a northern peatland: the role of pressure changes and peat structure. Water Resour. Res. 51, 151–168. https://doi.org/10.1002/2014WR016268.
Comas, X., Slater, L., Reeve, A., 2005. Geophysical and hydrological evaluation of two bog complexes in a northern peatland: implications for the distribution of biogenic gases at the basin scale. Glob. Biogeochem. Cycles 19, 1–10. https://doi.org/10.1029/2005GB002582.
Comas, X., Slater, L., Reeve, A., 2008. Seasonal geophysical monitoring of biogenic gases in a northern peatland: implications for temporal and spatial variability in free phase gas production rates. J. Geophys. Res. Biogeosci. 113, 1–12. https://doi.org/10.1029/2007JG000575.
Comas, X., Terry, N., Slater, L., Warren, M., Kolka, R., Kristiyono, A., Sudiana, N., Nurjaman, D., Darusman, T., 2015. Imaging tropical peatlands in Indonesia using ground-penetrating radar (GPR) and electrical resistivity imaging (ERI): implications for carbon stock estimates and peat soil characterization. Biogeosciences 12, 2995–3007. https://doi.org/10.5194/bg-12-2995-2015.
Comas, X., Terry, N., Hribljan, J.A., Lilleskov, E.A., Suarez, E., Chimner, R.A., Kolka, R.K., 2017. Estimating belowground carbon stocks in peatlands of the Ecuadorian páramo using ground-penetrating radar (GPR). J. Geophys. Res. Biogeosci. 122, 370–386. https://doi.org/10.1002/2016JG003550.
Comite, D., Galli, A., Ferrara, C., Lauro, S.E., Mattei, E., Vannaroni, G., Pettinelli, E., 2014. Numerical and experimental surveys on the GPR early-time signal features for the evaluation of shallow-soil permittivity. In: Proc. 15th Int. Conf. Grounds Penetrating Radar, 2014. 2014. GPR, pp. 131–134.
Comite, D., Galli, A., Lauro, S.E., Mattei, E., Pettinelli, E., 2016. Analysis of GPR early-time signal features for the evaluation of soil permittivity through numerical and experimental surveys. IEEE J. Sel. Top. Appl. Earth Obs. Remote Sens. 9, 178–187. https://doi.org/10.1109/JSTARS.2015.2466174.
Conyers, L.B., 2012. Interpreting Ground-Penetrating Radar for Archaeology. Left Coast Press, Walnut Creek.
Cui, X.H., Chen, J., Shen, J.S., Cao, X., Chen, X.H., Zhu, X.L., 2011. Modeling tree root diameter and biomass by ground-penetrating radar. Sci. China Earth Sci. 54, 711–719. https://doi.org/10.1007/s11430-010-4103-z.
Di Matteo, A., Pettinelli, E., Slob, E., 2013. Early-time GPR signal attributes to estimate soil dielectric permittivity: a theoretical study. IEEE Trans. Geosci. Remote Sens. 51, 1643–1654. https://doi.org/10.1109/TGRS.2012.2206817.
Doolittle, J.A., Brevik, E.C., 2014. The use of electromagnetic induction techniques in soils studies. Geoderma 223–225, 33–45.
Doolittle, J., Butnor, J., 2009. Soils, peatlands, and biomonitoring. In: Jol, H.M. (Ed.), Ground Penetrating Radar Theory and Applications, pp. 179–202. https://doi.org/10.1016/B978-0-444-53348-7.00006-5.
Doolittle, J.A., Collins, M.E., 1998. A comparison of EM induction and GPR methods in areas of karst. Geoderma 85, 83–102. https://doi.org/10.1016/S0016-7061(98)00012-3.
Doolittle, J., Nelson, F., 2009. Characterising relict cryogenic macrostructures in mid-latitude areas of the USA with three-dimensional ground-penetrating radar. Permafr. Periglac. Process. 20, 257–268. https://doi.org/10.1002/ppp.
Elkarmoty, M., Colla, C., Gabrielli, E., Papeschi, P., Bonduà, S., Bruno, R., 2017. In-situ GPR test for three-dimensional mapping of the dielectric constant in a rock mass. J. Appl. Geophys. 146, 1–15. https://doi.org/10.1016/j.jappgeo.2017.08.010.
Ercoli, M., Di Matteo, L., Pauselli, C., Mancinelli, P., Frapiccini, S., Talegalli, L., Cannata, A., 2018. Integrated GPR and laboratory water content measures of sandy soils: from laboratory to field scale. Constr. Build. Mater. 159, 734–744. https://doi.org/10.1016/j.conbuildmat.2017.11.082.
Ferrara, C., Barone, P.M., Steelman, C.M., Pettinelli, E., Endres, A.L., 2013. Monitoring shallow soil water content under natural field conditions using the early-time GPR signal technique. Vadose Zone J. 12. https://doi.org/10.2136/vzj2012.0202.
Freeland, R.S., 2015. Imaging the lateral roots of the orange tree using three-dimensional GPR. J. Environ. Eng. Geophys. 20, 235–244. https://doi.org/10.2113/jeeg20.3.235.
Fyfe, R.M., Coombe, R., Davies, H., Parry, L., 2014. The importance of sub-peat carbon storage as shown by data from Dartmoor, UK. Soil Use Manag. 30, 23–31. https://doi.org/10.1111/sum.12091.
Galagedara, L.W., Parkin, G.W., Redman, J.D., 2003. An analysis of the ground-penetrating radar direct ground wave method for soil water content measurement. Hydrol. Process. 17, 3615–3628. https://doi.org/10.1002/hyp.1351.
Galagedara, L.W., Parkin, G.W., Redman, J.D., Von Bertoldi, P., Endres, A.L., 2005a. Field studies of the GPR ground wave method for estimating soil water content during irrigation and drainage. J. Hydrol. 301, 182–197. https://doi.org/10.1016/j.jhydrol.2004.06.031.
Galagedara, L.W., Redman, J.D., Parkin, G.W., Annan, A.P., Endres, A.L., 2005b. Numerical modeling of GPR to determine the direct ground wave sampling depth. Vadose Zone J. 4, 1096. https://doi.org/10.2136/vzj2004.0143.
Goodman, D., Piro, S., Nishimura, Y., Schneider, K., Hongo, H., Higashi, N., Steinberg, J., Damiata, B., 2009. GPR archaeometry. In: Ground Penetrating Radar Theory and Applications, https://doi.org/10.1016/B978-0-444-53348-7.00015-6.
Greaves, R.J., Lesmes, D.P., Lee, J.M., Toksoz, M.N., 1996. Velocity variations and water content estimated from multi-offset, ground-penetrating radar. Geophysics 61, 683–695.
Grote, K., Hubbard, S., Rubin, Y., 2003. Field-scale estimation of volumetric water content using ground-penetrating radar ground wave techniques. Water Resour. Res. 39, 1–14. https://doi.org/10.1029/2003WR002045.
Guo, L., Chen, J., Cui, X., Fan, B., Lin, H., 2013a. Application of ground penetrating radar for coarse root detection and quantification: a review. Plant Soil 362, 1–23. https://doi.org/10.1007/s11104-012-1455-5.
Guo, L., Lin, H., Fan, B., Cui, X., Chen, J., 2013b. Impact of root water content on root biomass estimation using ground penetrating radar: evidence from forward simulations and field controlled experiments. Plant Soil 371, 503–520. https://doi.org/10.1007/s11104-013-1710-4.
Hirano, Y., Dannoura, M., Aono, K., Igarashi, T., Ishii, M., Yamase, K., Makita, N., Kanazawa, Y., 2009. Limiting factors in the detection of tree roots using ground-penetrating radar. Plant Soil 319, 15–24. https://doi.org/10.1007/s11104-008-9845-4.
Huisman, J.A., Sperl, C., Bouten, W., Verstraten, J.M., 2001. Soil water content measurements at different scales: accuracy of time domain reflectometry and ground-penetrating radar. J. Hydrol. 245, 48–58. https://doi.org/10.1016/S0022-1694(01)00336-5.
Huisman, J.A., Hubbard, S.S., Redman, J.D., Annan, A.P., 2003. Measuring soil water content with ground penetrating radar a review. Vadose Zone J. 2, 476–491. https://doi.org/10.2113/2.4.476.
Jonard, F., Demontoux, F., Bircher, S., Razafindratsimat, S., Schwank, M., Weillermuller, L., Lambot, S., Wigneron, J.-P., Kerr, Y., Vereecken, H., 2014. Electromagnetic characterization of organic-rich soils at the microwave L-band with ground-penetrating radar, radiometry and laboratory measurements. In: Proc. 15th Int. Conf. Grounds Penetrating Radar, pp. 202–207.
Karuss, J., Berzins, D., 2015. Ground-penetrating radar study of the Cena Bog, Latvia: linkage of reflections with peat moisture content. Bull. Geol. Soc. Finl. 87, 87–98.
Kettridge, N., Comas, X., Baird, A., Slater, L., Strack, M., Thompson, D., Jol, H., Binley, A., 2008. Ecohydrologically important subsurface structures in peatlands revealed by ground-penetrating radar and complex conductivity surveys. J. Geophys. Res. Biogeosci. 113, 1–15. https://doi.org/10.1029/2008JG000787.
Kettridge, N., Binley, A., Comas, X., Cassidy, N.J., Baird, A.J., Harris, A., Van Der Kruk, J., Strack, M., Milner, A.M., Waddington, J.M., 2012. Do peatland microforms move through time? Examining the developmental history of a patterned peatland using ground-penetrating radar. J. Geophys. Res. Biogeosci. 117, 1–11. https://doi.org/10.1029/2011JG001876.
Klotzsche, A., Jonard, F., Looms, M.C., van der Kruk, J., Huisman, J.A., 2018. Measuring soil water content with ground penetrating radar: a decade of progress. Vadose Zone J. 17, 0. https://doi.org/10.2136/vzj2018.03.0052.
Koyama, C.N., Liu, H., Takahashi, K., Shimada, M., Watanabe, M., Khuut, T., Sato, M., 2017. In-situ measurement of soil permittivity at various depths for the calibration and validation of low-frequency SAR soil moisture models by using GPR. Remote Sens. 9, 1–14. https://doi.org/10.3390/rs9060580.
Laamrani, A., Valeria, O., Cheng, L., Bergeron, Y., Camerlynck, C., 2013. The use of ground penetrating radar for remote sensing the organic layer - mineral soil interface in paludified boreal forests. Can. J. Remote. Sens. 39, 74–88.
Lambot, S., André, F., 2014. Full-wave modeling of near-field radar data for planar layered media reconstruction. Trans. Geosci. Remote Sens. 52, 2295–2303.
Lambot, S., Slob, E.C., van den Bosch, I., Antoine, M., Gregoire, M., Vanclooster, M., 2004. Modeling of GPR signal and inversion for identifying the subsurface dielectric properties frequency dependence and effect of soil roughness. In: Proc. Tenth Int. Conf. Grounds Penetrating Radar, 2004. 2004. GPR, pp. 79–82. https://doi.org/10.1109/ICGPR.2004.179918.

Lambot, S., Antoine, M., Vanclooster, M., Slob, E.C., 2006. Effect of soil roughness on the inversion of off-ground monostatic GPR signal for noninvasive quantification of soil properties. Water Resour. Res. 42, 1–10. https://doi.org/10.1029/2005WR004416.
Lambot, S., Slob, E., Chavarro, D., Lubczynski, M., Vereecken, H., 2008. Measuring soil surface water content in irrigated areas of southern Tunisia using full-waveform inversion of proximal GPR data. NEAR Surf. Geophys. 6, 403–410.
Lauer, K., Albrecht, C., Salat, C., Felix-Henningsen, P., 2010. Complex effective relative permittivity of soil samples from the taunus region (Germany). J. Earth Sci. 21, 961–967. https://doi.org/10.1007/s12583-010-0149-2.
Lavoué, F., Brossier, R., Métivier, L., Garambois, S., Virieux, J., 2014. Two-dimensional permittivity and conductivity imaging by full waveform inversion of multioffset GPR data: a frequency-domain quasi-Newton approach. Geophys. J. Int. 197, 248–268. https://doi.org/10.1093/gji/ggt528.
Lekner, J., 2016. Theory of Reflection: Reflection and Transmission of Electromagnetic, Particle and Acoustic Waves, 2nd ed. Springer International Publishinghttps://doi.org/10.1007/978-3-319-23627-8.
Li, L., Xia, Y., Liu, S., Zhang, W., Chen, X., Zheng, H., Qiu, H., He, X., Su, Y., 2015. Modified method for estimating organic carbon density in discontinuous karst soil using ground-penetrating radar and geostatistics. J. Mt. Sci. 12, 1229–1240. https://doi.org/10.1007/s11629-015-3431-z.
Li, W., Cui, X., Guo, L., Chen, J., Chen, X., Cao, X., 2016. Tree root automatic recognition in Ground penetrating radar profiles based on randomized Hough transform. Remote Sens. 8. https://doi.org/10.3390/rs8050430.
Liu, X., Dong, X., Leskovar, D.I., 2016. Ground penetrating radar for underground sensing in agriculture: a review. Int. Agrophys. 30, 533–543. https://doi.org/10.1515/intag-2016-0010.
Liu, Q., Cui, X., Liu, X., Chen, J., Chen, X., Cao, X., 2018. Detection of root orientation using ground-penetrating radar. IEEE Trans. Geosci. Remote Sens. 56, 93–104.
Liu, X., Dong, X., Xue, Q., Leskovar, D.I., Jifon, J., Butnor, J.R., Marek, T., 2018. Ground penetrating radar (GPR) detects fine roots of agricultural crops in the field. Plant Soil 423, 517–531.
Lu, Y., Song, W., Lu, J., Wang, X., Tan, Y., 2017. An examination of soil moisture estimation using ground penetrating radar in dessert steppe. Water (Switzerland) 521, 1–11. https://doi.org/10.3390/w9070521.
Mangel, A.R., Moysey, S.M.J., van der Kruk, J., 2015. Resolving precipitation induced water content profiles by inversion of dispersive GPR data: a numerical study. J. Hydrol. 525, 496–505. https://doi.org/10.1016/j.jhydrol.2015.04.011.
Meadows, D.G., Young, M.H., McDonald, E.V., 2006. Estimating the fine soil fraction of desert pavements using ground penetrating radar. Vadose Zone J. 5, 720–730. https://doi.org/10.2136/vzj2005.0095.
Mertens, L., Persico, R., Matera, L., Lambot, S., 2016. Automated detection of reflection hyperbolas in complex GPR images with no a priori knowledge on the medium. IEEE Trans. Geosci. Remote Sens. 54, 580–596. https://doi.org/10.1109/TGRS.2015.2462727.
Minet, J., Wahyudi, A., Bogaert, P., Vanclooster, M., Lambot, S., 2011. Mapping shallow soil moisture profiles at the field scale using full-waveform inversion of ground penetrating radar data. Geoderma 161, 225–237. https://doi.org/10.1016/j.geoderma.2010.12.023.
Minet, J., Bogaert, P., Vanclooster, M., Lambot, S., 2012. Validation of ground penetrating radar full-waveform inversion for field scale soil moisture mapping. J. Hydrol. 424–425, 112–123. https://doi.org/10.1016/j.jhydrol.2011.12.034.
Mourmeaux, N., Tran, A.P., Lambot, S., 2014. Soil permittivity and conductivity characterization by full-wave inversion of near-field GPR data. Proc. In: 15th Int. Conf. Grounds Penetrating Radar, 2014. 2014. GPR, pp. 497–502.
Nováková, E., Karous, M., Zajíček, A., Karousová, M., 2013. Evaluation of ground penetrating radar and vertical electrical sounding methods to determine soil horizons and bedrock at the locality Dehtáře. Soil Water Res. 8, 105–112.
Oden, C.P., Olhoeft, G.R., Wright, D.L., Powers, M.H., 2008. Measuring the electrical properties of soil using a calibrated ground-coupled GPR system. Vadose Zone J. 7, 171–183. https://doi.org/10.2136/vzj2006.0128.
Olhoeft, G.R., 2000. Maximizing the information return from ground penetrating radar. J. Appl. Geophys. 43, 175–187. https://doi.org/10.1016/S0926-9851(99)00057-9.
Pallavi, B., Saito, H., Kato, M., 2010. Application of GPR ground wave for mapping of spatiotemporal variations in the surface moisture content at a natural field site. In: 19th World Congr. Soil Sci. Soil Solut. a Chang. World, pp. 13–16.
Parry, L.E., West, L.J., Holden, J., Chapman, P.J., 2014. Evaluating approaches for estimating peat depth. J. Geophys. Res. Biogeosci. 119, 567–576. https://doi.org/10.1002/2013JG002411.
Parsekian, A.D., Slater, L., Giménez, D., 2012a. Application of ground-penetrating radar to measure near-saturation soil water content in peat soils. Water Resour. Res. 48, 1–9. https://doi.org/10.1029/2011WR011303.
Parsekian, A.D., Slater, L., Ntarlagiannis, D., Nolan, J., Sebesteyen, S.D., Kolka, R.K., Hanson, P.J., 2012b. Uncertainty in peat volume and soil carbon estimated using ground-penetrating radar and probing. Soil Sci. Soc. Am. J. 76, 1911–1918. https://doi.org/10.2136/sssaj2012.0040.
Pettinelli, E., Vannaroni, G., Di Pasquo, B., Mattei, E., Di Matteo, A., De Santis, A., Annan, A.P., 2007. Correlation between near-surface electromagnetic soil parameters and early-time GPR signals: an experimental study. Geophysics 72, 28–31. https://doi.org/10.1190/1.2435171.
Pettinelli, E., Di Matteo, A., Beaubien, S.E., Mattei, E., Lauro, S.E., Galli, A., Vannaroni, G., 2014. A controlled experiment to investigate the correlation between early-time signal attributes of ground-coupled radar and soil dielectric properties. J. Appl. Geophys. 101, 68–76. https://doi.org/10.1016/j.jappgeo.2013.11.012.
Plado, J., Sibul, I., Mustasaar, M., Jõeleht, A., 2011. Ground-penetrating radar study of the Rahivere peat bog, eastern Estonia. Est. J. Earth Sci. 60, 31. https://doi.org/10.3176/earth.2011.1.03.
Proulx-McInnis, S., St-Hilaire, A., Rousseau, A.N., Jutras, S., 2013. A review of ground-penetrating radar studies related to peatland stratigraphy with a case study on the determination of peat thickness in a northern boreal fen in Quebec, Canada. Prog. Phys. Geogr. 37, 767–786. https://doi.org/10.1177/0309133313501106.
Raz-Yaseef, N., Koteen, L., Baldocchi, D.D., 2013. Coarse root distribution of a semi-arid oak savanna estimated with ground penetrating radar. J. Geophys. Res. Biogeosci. 118, 135–147. https://doi.org/10.1029/2012JG002160.
Rege, R.B., Godio, A., 2012. Multimodal inversion of guided waves in georadar data. J. Appl. Geophys. 81, 68–75.
Rejšek, K., Hruška, J., Kuba, L., Tichá, R., Drobný, D., Formánek, P., Vranová, V., 2015. A methodological contribution to use of Ground-Penetrating Radar (GPR) as a tool for monitoring contamination of urbansoils with road salt. Urban Ecosyst. 18, 169–188. https://doi.org/10.1007/s11252-014-0391-y.
Reppert, P.M., Morgan, F.D., Toksoz, M.N., 2000. Reflection coefficients. J. Appl. Geophys. 43, 189–197.
Robinson, D.A., Campbell, C.S., Hopmans, J.W., Hornbuckle, B.K., Jones, S.B., Knight, R., Ogden, F., Selker, J., Wendroth, O., 2008. Soil moisture measurement for ecological and hydrological watershed-scale observatories: a review. Vadose Zone J. 7, 358. https://doi.org/10.2136/vzj2007.0143.
Rodríguez-Robles, U., Arredondo, T., Huber-Sannwald, E., Ramos-Leal, J.A., Yépez, E.A., 2017. Technical note: application of geophysical tools for tree root studies in forest ecosystems in complex soils. Biogeosciences 14, 5343–5357. https://doi.org/10.5194/bg-14-5343-2017.
Rosa, E., Larocque, M., Pellerin, S., Gagné, S., Fournier, B., 2009. Determining the number of manual measurements required to improve peat thickness estimations by ground penetrating radar. Earth Surf. Process. Landf. 34, 377–383. https://doi.org/10.1002/esp.
Saarenketo, T., 1998. Electrical properties of water in clay and silty soils. J. Appl. Geophys. 40, 73–88. https://doi.org/10.1016/S0926-9851(98)00017-2.
Salat, C., Junge, A., 2010. Dielectric permittivity of fine-grained fractions of soil samples from eastern Spain at 200 MHz. Geophysics 75, J1–J9. https://doi.org/10.1190/1.3294859.
Sass, O., Friedmann, A., Haselwanter, G., Wetzel, K.F., 2010. Investigating thickness and internal structure of alpine mires using conventional and geophysical techniques. Catena 80, 195–203. https://doi.org/10.1016/j.catena.2009.11.006.
Sen, P.N., Scala, C., Cohen, M.H., 1981. A self-similar model for sedimentary rocks with application to the dielectric constant of fused glass beads. Geophysics 46, 781–795.
Sena, A.R., Sen, M.K., Stoffa, P.L., 2008. Modelling of ground penetrating radar data in stratified media using the reflectivity technique. J. Geophys. Eng. 5, 129–146. https://doi.org/10.1088/1742-2132/5/2/001.
Simeoni, M., Galloway, P., O'Neil, A., Gilkes, R., 2009. A procedure for mapping the depth to the texture contrast horizon of duplex soils in south-western Australia using ground penetrating radar, GPS and kriging. Aust. J. Soil Res. 47, 613–621. https://doi.org/10.1071/SR08241.
Simms, J.E., McKay, S.K., McComas, R.W., Fischenich, J.C., 2017. In situ root volume estimation using ground penetrating radar. J. Environ. Eng. Geophys. 22, 209–221.
Slater, L., Comas, X., 2009. The contribution of ground penetrating radar to water resource research. In: Ground Penetrating Radar Theory and Applications, First ed. Elsevier. https://doi.org/10.1016/B978-0-444-53348-7.00010-7.
Slater, L.D., Reeve, A., 2002. Investigating peatland stratigraphy and hydrogeology using integrated electrical geophysics. Geophysics 67, 365. https://doi.org/10.1190/1.1468597.
Slob, E., Sato, M., Olhoeft, G., 2010. Surface and borehole ground-penetrating-radar developments. Geophysics 75, A103–A120.
Steelman, C.M., Endres, A.L., 2012. Assessing vertical soil moisture dynamics using multi-frequency GPR common-midpoint soundings. J. Hydrol. 436–437, 51–66. https://doi.org/10.1016/j.jhydrol.2012.02.041.
Stover, D.B., Day, F.P., Butnor, J.R., Drake, B.G., Ecology, S., May, N., Stover, D.B., Day, F.P., Butnor, J.R., Drake, B.G., 2016. Effect of elevated CO_2 on Coarse-Root Biomass in Florida scrub Detected by Ground- Penetrating Radar. 88. Wiley, pp. 1328–1334. Stable URL: http://www.jstor.org/stable/27651231.
Strack, M., Mierau, T., 2010. Evaluating spatial variability of free-phase gas in peat using ground-penetrating radar and direct measurement. J. Geophys. Res. 115, 1–11. https://doi.org/10.1029/2009JG001045.
Strobbia, C., Cassiani, G., 2007. Multilayer ground-penetrating radar guided waves in shallow soil layers for estimating soil water content. Geophysics 72, J17. https://doi.org/10.1190/1.2716374.
Stroh, J.C., Archer, S., Doolittle, J.A., Wilding, L., 2001. Detection of edaphic discontinuities with ground-penetrating radar and electromagnetic induction. Landsc. Ecol. 16, 377–390. https://doi.org/10.1023/A:1017556712316.
Tanikawa, T., Hirano, Y., Dannoura, M., 2013. Root Orientation Can Affect Detection Accuracy of Ground-Penetrating Radar. 317–327https://doi.org/10.1007/s11104-013-1798-6.
Tanikawa, T., Ikeno, H., Dannoura, M., Yamase, K., Aono, K., Hirano, Y., 2016. Leaf litter thickness, but not plant species, can affect root detection by ground penetrating radar. Plant Soil 408, 271–283. https://doi.org/10.1007/s11104-016-2931-0.
Tardío, G., González-Ollauri, A., Mickovski, S.B., 2016. A non-invasive preferential root distribution analysis methodology from a slope stability approach. Ecol. Eng. 97, 46–57. https://doi.org/10.1016/j.ecoleng.2016.08.005.
Terry, N., Slater, L., 2017. Water resources research. Water Resour. Res. 53, 2755–2769. https://doi.org/10.1002/2016WR020339.Received.
Topp, G.C., Davis, J.L., Annan, A.P., 1980. Electromagnetic determination of soil water content: measurements in coaxial transmission lines. Water Resour. Res. 16, 574–582.
Tosti, F., Patriarca, C., Slob, E., Benedetto, A., Lambot, S., 2013. Clay content evaluation in soils through GPR signal processing. J. Appl. Geophys. 97, 69–80. https://doi.org/

10.1016/j.jappgeo.2013.04.006.
Tran, A.P., Bogaert, P., Wiaux, F., Vanclooster, M., Lambot, S., 2015. High-resolution space-time quantification of soil moisture along a hillslope using joint analysis of ground penetrating radar and frequency domain reflectometry data. J. Hydrol. 523, 252–261. https://doi.org/10.1016/j.jhydrol.2015.01.065.
van Dam, R.L., Schlager, W., 2000. Identifying causes of ground-penetrating radar reflections using time-domain reflectometry and sedimentological analyses. Sedimentology 47, 435–449. https://doi.org/10.1046/j.1365-3091.2000.00304.x.
van Dam, R.L., van den Berg, E.H., van Heteren, S., Kasse, C., Kenter, J.A.M., Groen, K., 2002. Influence of organic matter in soils on radar-wave reflection: sedimentological implications. J. Sediment. Res. 72, 341–352. https://doi.org/10.1306/092401720341.
van Dam, R.L., van den Berg, E.H., Schaap, M.G., Broekema, L.H., Schlager, W., 2003. Radar reflections from sedimentary structures in the vadose zone. In: Ground Penetrating Radar in Sediments, pp. 257–273.
van der Kruk, J., Streich, R., Green, A.G., 2006. Properties of surface waveguides derived from separate and joint inversion of dispersive TE and TM GPR data. Geophysics 71, K19. https://doi.org/10.1190/1.3467444.
van der Kruk, J., Jacob, R.W., Vereecken, H., 2010. Properties of precipitation-induced multilayer surface waveguides derived from inversion of dispersive TE and TM GPR data. Geophysics 75, WA263. https://doi.org/10.1190/1.3467444.
van Overmeeren, R., Sariowan, S., Gehrels, J., 1997. Ground penetrating radar for determining volumetric soil water content; results of comparative measurements at two test sites. J. Hydrol. 197, 316–338. https://doi.org/10.1016/S0022-1694(96)03244-1.
Völkel, J., Leopold, M., Roberts, M.C., 2001. The radar signatures and age of periglacial slope deposits, Central Highlands of Germany. Permafr. Periglac. Process. 12, 379–387. https://doi.org/10.1002/ppp.402.
Walter, J., Hamann, G., Lück, E., Klingenfuss, C., Zeitz, J., 2016. Stratigraphy and soil properties of fens: geophysical case studies from northeastern Germany. Catena 142, 112–125. https://doi.org/10.1016/j.catena.2016.02.028.
Watanabe, T., Matsuoka, N., Christiansen, H.H., 2013. Ice- and soil-wedge dynamics in the Kapp Linné Area, Svalbard, investigated by two- and three-dimensional GPR and ground thermal and acceleration regimes. Permafr. Periglac. Process. 24, 39–55. https://doi.org/10.1002/ppp.1767.
Weihermüller, L., Huisman, J.A., Lambot, S., Herbst, M., Vereecken, H., 2007. Mapping the spatial variation of soil water content at the field scale with different ground penetrating radar techniques. J. Hydrol. 340, 205–216. https://doi.org/10.1016/j.jhydrol.2007.04.013.
William, X.W., Comas, 2016. Estimating methane gas production in peat soils of the Florida Everglades using hydrogeophysical methods. J. Geophys. Res. 121, 1190–1202. https://doi.org/10.1002/2015JG003246.
Winkelbauer, J., Völkel, J., Leopold, M., Bernt, N., 2011. Methods of surveying the thickness of humous horizons using ground penetrating radar (GPR): an example from the Garmisch-Partenkirchen area of the Northern Alps. Eur. J. For. Res. 130, 799–812. https://doi.org/10.1007/s10342-010-0472-2.
Wu, Y., Guo, L., Cui, X., Chen, J., Cao, X., Lin, H., 2014. Ground-penetrating radar-based automatic reconstruction of three-dimensional coarse root system architecture. Plant Soil 383, 155–172. https://doi.org/10.1007/s11104-014-2139-0.
Yeung, S.W., Yan, W.M., Hau, C.H.B., 2016. Performance of ground penetrating radar in root detection and its application in root diameter estimation under controlled conditions. Sci. China Earth Sci. 59, 145–155. https://doi.org/10.1007/s11430-015-5156-9.
Zhang, J., Lin, H., Doolittle, J., 2014. Soil layering and preferential flow impacts on seasonal changes of GPR signals in two contrasting soils. Geoderma 213, 560–569. https://doi.org/10.1016/j.geoderma.2013.08.035.
Zhu, S., Huang, C., Su, Y., Sato, M., 2014. 3D ground penetrating radar to detect tree roots and estimate root biomass in the field. Remote Sens. 6, 5754–5773. https://doi.org/10.3390/rs6065754.

9.4. Publication IV

Zajícová, K., Chuman, T. (in review). O and A soil horizons' boundaries detection using GPR under variable soil moisture conditions. Geoderma

O and A soil horizons' boundaries detection using GPR under variable soil moisture conditions

Kateřina ZAJÍCOVÁ[1,2], Tomáš CHUMAN[1,3]

[1]Charles University, Faculty of Science, Department of Physical Geography and Geoecology, Albertov 6, 128 43 Prague 2, Czech Republic

[2]Global Change Research Institute of the Czech Academy of Sciences, Bělidla 986/4a, 603 00 Brno, Czech Republic

[3]Czech Geological Survey, Klárov 3, 118 21 Prague 1, Czech Republic

katerina.zamazalova@natur.cuni.cz

Abstract

The thicknesses of organic (O) and organomineral (A) horizons are essential parameters for estimating the soil organic carbon stock. They are usually measured at sampling points distributed randomly or regularly over a site, but due to high spatial variability of the soil horizons' thicknesses, the sampling should be dense enough to estimate the carbon stock precisely. Dense soil sampling is cost, time, and labour demanding. Therefore, some studies suggest that geophysical methods such as ground-penetrating radar (GPR) can assist with a more precise estimation of the organic and organomineral horizons thicknesses without digging soil pits. This study evaluates the accuracy of the organic and the organomineral horizons thicknesses repeatedly measured under different soil moisture conditions on two contrasting soil types: Dystric Cambisol and Arenic Podzosol, using GPR with 800 MHz antenna. The results proved this method to be promising; however, we could not distinguish the boundary between organic and organomineral horizons but only the O+A horizon/subsoil boundary. The thickness of O+A horizons was estimated with an error between 25 – 35% in the Dystric Cambisol site and 18 – 24% in the Arenic Podzol site. The results were more accurate under moister conditions for both soil types, but under drier conditions, deeper parts of irregular horizon boundaries were better distinguishable.

Keywords: GPR, soil organic horizon thickness, soil stratigraphy, geophysical methods, soil moisture conditions

Introduction

Soil organic matter is an important soil constituent because it controls vital functions of the soil, i. e., nutrients' supply (Hansson et al. 2013) or water retention capacity (Bens et al., 2007). Moreover, primarily thanks to the organic matter, soils provide vital ecosystem services (Adhikari and Hartemink, 2016), i.e. carbon sequestration, nutrient supply, water filtration and storage, and biomass production (Adhikari and Hartemink, 2016; Wiesmeier et al., 2019). The thicknesses of the organic and organomineral horizons are essential parameters for modelling of soil organic carbon stocks, especially in forest soils (e. g., Kristensen et al., 2015; Muukkonen et al., 2009; Strand et al., 2016), because the models of soil organic carbon stock use the concept of equivalent soil mass (Ellert and Bettany, 1995):

$$SOC = \%C * BD * T \quad [1]$$

where SOC is soil organic carbon stock [kg/m^2], $\%C$ is organic carbon concentration in soil [kg/kg], BD is soil bulk density [kg/m^3], and T is soil/soil horizon thickness [m].

The thickness of organic and organmineral horizons in temperate forest soils is more spatially variable than the carbon concentration and the bulk density, as follows from the data published by Chuman et al. (2021). Thus, it is worth sampling the thickness in more detail than the other two parameters. The thicknesses of the organic and organomineral horizons are usually measured at sampling points distributed randomly or in a regular grid and then spatially interpolated (e.g., Muukkonen et al. 2009; Kristensen et al. 2015). However, due to the high spatial variability of the horizons' thicknesses (e. g., Šamonil et al. 2011; Valtera et al. 2013; Zajícová and Chuman 2021), the precise estimation requires dense sampling, which is time, labour, and cost consuming. Several studies, e.g. Liu et al. (2016) or Zajícová and Chuman (2019), showed that ground-penetrating radar (GPR) could help with soil surveys to reduce the time costs of the fieldwork. The GPR has already been used for the organic and organomineral horizons' thicknesses determination, for example, by Winkelbauer et al. (2011), Li et al. (2015), Voronin and Savin (2018), and (Liu et al., 2021).

GPR works on the principle of the penetration of electromagnetic waves and their reflections in a medium, soil, in the case of our study. The reflections emerge on boundaries with contrasting electromagnetic properties. The more significant difference

in electromagnetic properties on the boundary is, the more distinct is the reflection. The principle was explained in the review published by Zajícová and Chuman (2019) or Huisman et al. (2003). The dielectric permittivity is considered the dominant factor of electromagnetic waves propagation and it is usually expressed in values relative to the dielectric permittivity of a vacuum. The relative dielectric permittivity of most rocks is 3 – 5, the relative dielectric permittivity of air is close to 1, which is the value in a vacuum, and the highest permittivity has water with values reaching 80-81 (Cassidy 2009). This fact indicates that the water content directly impacts the dielectric permittivity of soils (Annan, 2009). However, Saarenketo (1998) found that soil water's permittivity differs according to the type of soil water, i.e. where it is stored in the soil. Dielectric permittivity of free water reaches the value of approximately 80, whereas permittivity of the hygroscopic water can be below 4 (Saarenketo, 1998). The permittivity of capillary water is somewhere between the value of the free water and the hygroscopic water (Saarenketo, 1998). Nevertheless, the water content is supposed to influence the soil dielectric permittivity the most. Therefore, soil moisture estimation is the most frequent application of GPR in soil surveys (Zajícová and Chuman, 2019), applying a wide variety of approaches as reviewed, e.g., by Huisman et al. (2003), Slater and Comas (2009), Klotzsche et al. (2018), or Zajícová and Chuman (2019).

Surveys of the soil stratigraphy using GPR assume that soil horizons differ in water content, thus in the dielectric permittivity. This fact should enable the detection of boundaries by GPR. Other factors determining soil dielectric permittivity also in its dry state are presence of calcite, dry mass density, related porosity, compaction (Salat and Junge, 2010), or soil organic matter content (Jonard et al., 2014; Lauer et al., 2010). The dielectric permittivity of dry undecomposed biomass was close to 1 and increased as biomass decomposition increased (André et al., 2015; Ardekani et al., 2014; Jonard et al., 2014).

In general, to be distinguished by GPR, soil horizons should differ in the proportion of three phases (solid: mineral and organic material, liquid: soil water, and gaseous: soil air) with the soil water to be of particular importance during GPR surveys of soil stratigraphy. Van Dam et al. (2002), Zhang et al. (2014), and Curioni et al. (2017) concluded that the higher moistures induce more significant differences in the dielectric permittivity between soil horizons and in consequence, higher moistures allow better distinction of individual horizons. However, Zhang et al. (2014) showed that the clear reflections representing horizon boundaries under wet conditions could be

disrupted by tree roots, which formed a preferential path for water infiltration along with the roots. Therefore, Van Dam et al. (2002) suggested that more measurements under different moisture conditions can help distinguish and characterise individual horizons better.

Hence, this study aims to estimate the soil organic and organomineral horizons thicknesses using GPR with 800 MHz antenna at two study sites with contrasting soil types: Dystric Cambisol and Arenic Podzols, and to evaluate the effect of soil moisture on the accuracy of the horizons' thicknesses determination. The aim is also to find the optimum moisture conditions for GPR measurements. The same antenna frequency as Winkelbauer et al. (2011) used in their study of mountainous karst in central Europe was chosen for this study in the temperate forest of central Europe because we expected similar thicknesses of organic and organomineral horizons.

Materials and Methods

Data collection

GPR data were collected using a shielded bistatic antenna system–type Ramac by MALÅ Geosciences (Sweden) with an 800 MHz antenna and equipped with a wheel-odometer. Signal response (hereinafter in the text "trace") was recorded every 0.75 cm with a time resolution of 0.12 ns. GPR surveys were repeatedly run on the same transects on two study sites with contrasting soil types, Dystric Cambisol site and Arenic Podzosol site, under different moisture conditions. The transects were chosen short, with the length of several meters, which allowed us to study them in more detail. In order to performe the time-depth conversion of the GPR data, the dielectric permittivity of the soil was measured simultaneously within the GPR survey using GS3 Soil moisture device by Decagon, which works on the capacitance principle. The dielectric permittivity was measured at each distinguished horizon separately at least every meter, along with the profile transects dug to validate the GPR measurements. If the individual soil horizons were not distinguished at the site, compound soil horizons were documented. Compound soil horizons were Oi+Oe and Oa+Ah in the Dystric Cambisol site and Oi+Oe+Oa in the Arenic Podzol site. The soil profile transects were not exactly overlapping with the GPR transects. However, these were dug parallel approximately 20-30 cm apart in order for the GPR transects to stay undisturbed for the following surveys. The actual horizon depth and stratigraphy along the dug transects of

each horizon or compound soil horizons were documented. Depth of soil horizons, the position of stones (with >5 cm in diameter) and tree roots (with >2cm in diameter) were recorded every 20 cm along the uncovered soil transect at the Dystric Cambisol site and every 10 cm at the Arenic Podzol site. Positions of the horizon depth measurements along the uncovered soil profile transects are referred to as checkpoints from now on in the text.

Study sites

Study site 1 – Cambisol on acid metamorphic rocks

The Dystric Cambisol survey site was located in a managed Norway spruce forest where the ground vegetation was almost absent except for several small patches covered by mosses. The GPR transect was 5.6 m long, and parallel to it the verification soil profile was dug to a depth of 25 cm (Fig. 1). The bedrock of the area is formed by metamorphic rock (paragneiss) of low alkalinity (Chuman et al., 2014). The soil is sandy but with a substantial content of silt (Tab. 1), and it is classified as loam/sandy loam according to the USDA classification.

The GPR data were collected during five surveys: twice in August 2015 (firstly under natural conditions and secondly after manual irrigation by using 10 litres of water added to the whole transect), in December 2015, in April 2016, and in August 2016. The survey in August 2015 was performed at the end of a dry summer when the sum of precipitation of the three months preceding the survey was about 140 mm, including 17 mm that precipitated during two weeks before the survey. The average temperature of the summer season in 2015 was 15°C (CHMI, 2020). The survey in December 2015 was performed at the beginning of a winter season after the first thin snow cover had melted. We expected the soil to be thoroughly wetted at this time. The sum of precipitation of the two weeks preceding the survey was 11 mm, the mean daily temperature was 2°C, and the evapotranspiration was low. The survey in April 2016 was performed after snow melting. Again, the soil profile was expected to be thoroughly wetted. The snow cover lasted from the beginning of January till the end of March in that year, and it was slowly melting down. The survey was performed a day after the snow had melted down completely. The survey in August 2016 was performed at the end of summer with heavy episodic rains. During the two weeks preceding the survey, there were several heavy rain showers with almost 80 mm in total (CHMI, 2020).

Fig. 1 Uncovered soil transect at the Dystric Cambisol site dug for verification

Table 1 Average values of selected soil physical characteristics for horizons in the Dystric Cambisol site

Horizon	Soil texture					dry soil bulk density [g/cm^3]	porosity [%]
	coarse sand 2.0 – 0.25 mm [%]	fine sand 0.25 – 0.05 mm [%]	coarse silt 0.05 – 0.01 mm [%]	fine silt 0.01 – 0.002 mm [%]	clay under 0.002 mm [%]		
O	-	-	-	-	-	0.15	90
Ah	22	25	32	11	10	0.58	75
Bv	36	24	21	11	8	0.93	63

The soil texture was determined by the hydrometer method (*ISO 11277, 2009*). *The bulk density was determined by weighting all soil excavated within a 10 x 10 cm reference frame by horizons (organic horizon O, organomineral horizon Ah, and the underlying horizon Bv separately). The thickness of each horizon within the reference frame was measured. The values represent the average values of 3 samples taken along the transect.*

Table 2 Water retention characteristics and relative dielectric permittivity for horizons in the Dystric Cambisol site

	saturation		**field capacity**		**permanent wilting point**		**dried at 105°C**
Horizon	VWC [cm^3/cm^3]	ε_r [-]	VWC [cm^3/cm^3]	ε_r [-]	VWC [cm^3/cm^3]	ε_r [-]	ε_r [-]
Oi+Oe+Oa+Ah	0.72	41.5	0.34	10.8	0.29	7	1.7
Bv	0.64	28.3	0.25	7.8	0.16	4.9	2.4

Soil samples were taken into cylinders of 16.5 cm in diameter and 5 cm high. The volumetric water content (VWC) was measured in the laboratory using the pressure plate extractor method (ISO 11274, 2009) at full saturation (suction 0 kPa), field capacity (33 kPa) and below permanent wilting point (1550 kPa). Soil relative dielectric permittivity (ε_r) was measured

simultaneously using Decagon GS3 soil moisture device (Decagon Devices, Inc., 2014). The analysis was performed in cooperation with Research Institute for Soil and Water Conservation. The values represent the average values of 3 samples taken along the transect.

Study site 2 – Arenic Podzol on sandstone

The Arenic Podzol study site was surveyed next to a 2.5 m long already uncovered profile in an old sandpit in a pine forest with sparse grass and mosses in the understory (Fig. 2). This site was measured three times, in May 2017, June 2018, and August 2018. The soil is sandy (Table 3) with low retention capacity (Table 4), and according to its particle size distribution, it is classified as sand (USDA classification). Compared to the Dystric Cambisol site, the site's climate is arider. The first survey was performed in May 2017. It was in spring with occasional light precipitation. The sum of precipitation of the month preceding the survey was 50 mm, out of which 14 mm precipitated during two weeks and 2 mm during two days preceding the survey (CHMI, 2020). The mean monthly temperature of the spring in 2017 was 7.5 °C. The survey in June 2018 was performed at the end of a relatively hot and dry spring. The average temperature of the spring in 2018 was 15°C. During one month preceding the survey, the average daily temperature was 19°C, and during the last two weeks, it was 21°C. Precipitation was relatively scarce. During the month preceding the survey, there was no precipitation. The precipitation of 41 mm came three days before the survey. The survey in August 2018 was performed during an exceptionally dry and hot summer when the total amount of precipitation since the survey in June was only 34 mm. The average temperature for the period since the survey in June was 20°C and in the last month even 25°C (CHMI, 2020).

Fig. 2 Uncovered soil profile in the Arenic Podzol site

Table 3 Average values of selected soil physical characteristics for horizons in the Arenic Podzol site

Horizon	Soil texture					dry soil bulk density [g/cm3]	porosity [%]
	coarse sand 2.0 - 0.25 mm [%]	fine sand 0.25 - 0.05 mm [%]	coarse silt 0.05 - 0.01 mm [%]	fine silt 0.01 - 0.002 mm [%]	clay under 0.002 mm [%]		
Ah	51	39	4	6	0	1.1	56
Ev	38	56	2	4	0	1.48	42
Bs	49	45	0	6	0	1.43	45

The soil texture was analysed by the hydrometer method (ISO 11277, 2009). The bulk density of the organomineral A, eluvial E and spodic Bs horizons was determined separately by weighing the oven-dry (105°C) soil samples in metal cylinders (10cm3). The values represent the average values of 3 samples taken along the transect.

Table 4 Water retention characteristics and relative dielectric permittivity for horizons in the Arenic Podzol site

	saturation		**field capacity**		**permanent wilting point**		**dried at 105°C**
Horizon	VWC [cm^3/cm^3]	ε_r [-]	VWC [cm^3/cm^3]	ε_r [-]	VWC [cm^3/cm^3]	ε_r [-]	ε_r [-]
Ah	0.43	18.1	0.11	5.3	0.08	4.2	3.0
E	0.43	16.5	0.07	4.6	0.05	3.4	2.9
B	0.34	14.1	0.07	4.4	0.05	3.4	3.0

Soil samples were taken into cylinders of 16.5 cm in diameter and 5 cm high. The volumetric water content (VWC) was measured in the laboratory using the pressure plate extractor method (ISO 11274, 2009) at full saturation (suction 0 kPa), field capacity (33 kPa) and below permanent wilting point (1550 kPa). Soil relative dielectric permittivity (ε_r) was measured simultaneously using Decagon GS3 soil moisture device (Decagon Devices, Inc., 2014). The analysis was performed in cooperation with Research Institute for Soil and Water Conservation. The values represent the average values of 3 samples taken along the transect.

GPR Data processing using one-dimensional analysis

We decided to work with raw GPR data to recognise better individual reflections of the GPR signal (electromagnetic waves) and their oscillations in 1D analysis. The thickness of the organic and organomineral horizons was estimated from the measured GPR data using the two-way travel time of the GPR signal between the soil surface and the

horizon's lower boundary. We considered the first reflection peak of the signal, more specifically the maximum of the second positive amplitude of the trace, to be the soil surface (Fig. 3a), similarly as Bristow and Jol (2003) and Winkelbauer et al. (2011) did, and the next significant reflection of the signal response to be the lower boundary of the uppermost horizon. The time of the reflection was recorded as the arrival time of the maximum of the highest positive amplitude of the oscillations composing the individual reflection because the further oscillations are often less distinct due to increasing depth or because of the so-called composite reflections. The composite reflections arise from reflections from near objects. The peak of the highest positive amplitude of the surface reflection can also be a part of a composite reflection. Here, the composite reflections arise from accidental reflections from objects on the surface, antenna jumping, or from an underground object (stone, root) near the surface. In these cases, the highest amplitude was considered the desired part of the surface reflection (Fig. 3b, 3c). Even though, we could miss some information in the case of a subsurface object, we could not distinguish these cases at this stage. The first significant oscillation was considered as the surface reflection even in instances where this non-compound reflection was somewhat smaller (Fig. 3d).

The other rules, how we interpreted the GPR data, included:

- If the reflection of the lower boundary of the organic/organo-mineral horizon was a part of a composite reflection, the maximum of the highest oscillation was considered as the reflection on the boundary.
- If the dielectric permittivity of the soil in the upper horizon was found to be lower than that in the lower horizon, the phase of the signal was probably inversed, and so the largest negative amplitude of the wavelet was used instead of the positive amplitude for characterisation of the boundary.

The depth of the eluvial (Ev) horizon at the Arenic Podzol study site was estimated using the same method. However, the lower boundary of this horizon is often not right the following reflection after the determined organomineral Ah lower boundary, because there could be layers differing in physical characteristics in the upper horizon or there could also be reflections from the upper horizon lower boundary beside the GPR actual position. There were no stones at this site, and tree roots were also scarce. We distinguished the E horizon lower boundary by the most significant

amplitude of the part of a trace after the considered uppermost horizon lower boundary (Fig. 4).

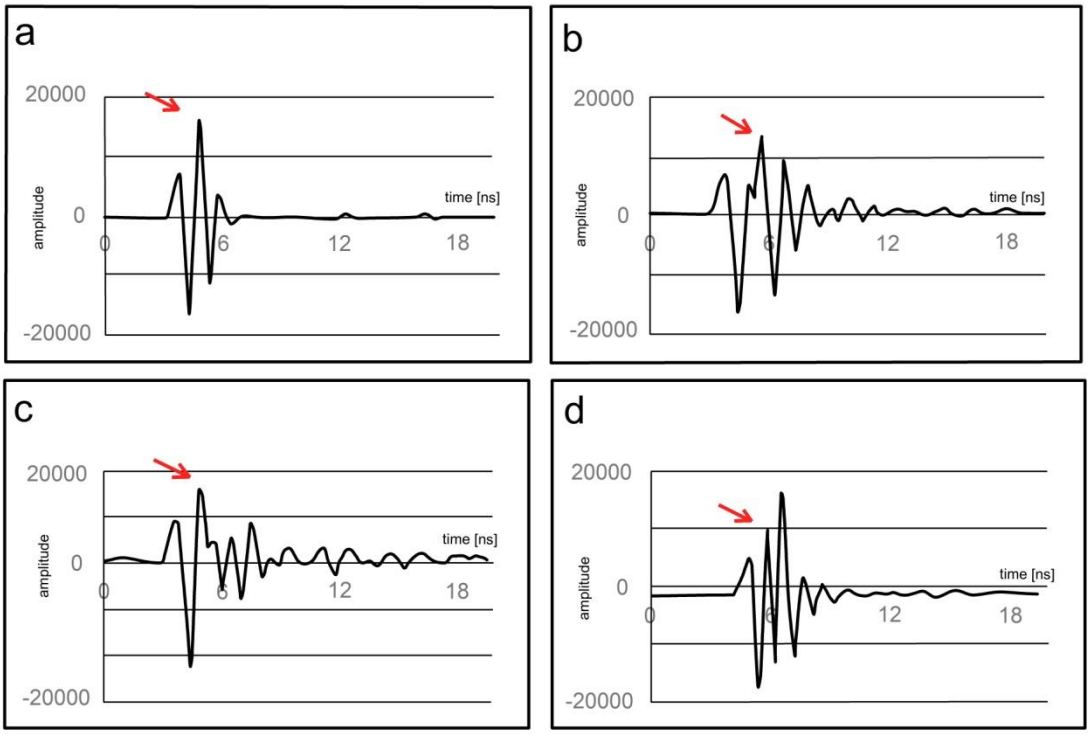

Fig. 3 Signal response from the soil *in four practical situations: a clear reflection from the soil surface (3a), composite reflection from soil surface arising from accidental reflections from surface objects, antenna jumping, or an underground object near the surface (3b, 3c), and composite reflection from the soil surface and a distinct subsurface object (3d); red arrow indicates the amplitudes considered as the soil surface.*

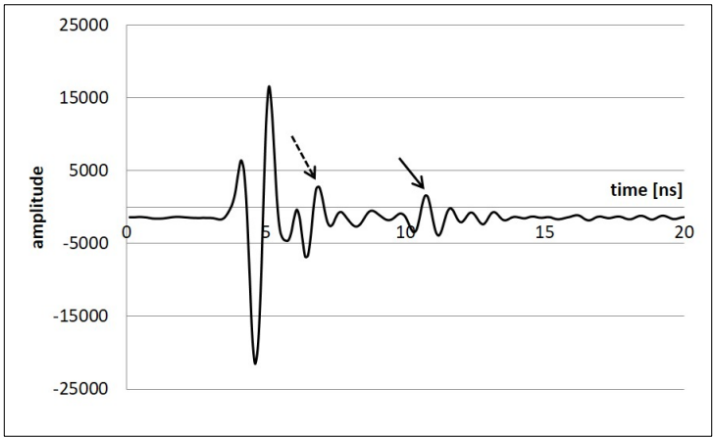

Fig. 4 Signal response from the soil with marked uppermost horizon lower boundary (dotted arrow) and E horizon lower boundary (black arrow)

The time-depth conversion was made for each trace using the velocity of electromagnetic waves calculated from the dielectric permittivity of the soil measured during the survey (Reppert et al., 2000),

$$v = \frac{c}{\sqrt{\varepsilon_r}}$$

[2]

where "v" is the velocity of electromagnetic waves of a horizon/compound horizons [m/s], "c" is the electromagnetic wave velocity in a vacuum [m/s], ε_r is soil relative dielectric permittivity of a horizon/compound horizons [-].

An average value of the dielectric permittivities recorded during a particular survey was used for the velocity calculation. The average value is a mean of the measured dielectric permittivity in a horizon weighted by the horizon thickness in case of an estimation of the thickness of compound horizons, e. g. Oi+Oe+Of+Ah for Ah lower boundary at the Dystric Cambisol site and Ah+Ev for the Ev lower boundary at the Arenic Podzol site. The calculation of the average value of dielectric permittivity originates in the mathematical expression of average velocity equal to the total distance within total time. The second prerequisite is that the dielectric permittivity is a parameter controlling the velocity of electromagnetic waves. The final formula of the average dielectric permittivity is specified in Equation *[3]*.

$$\varepsilon_r = \left(\frac{\sum_{i=1}^{h} m\sqrt{\varepsilon_{rm}}}{\sum_{i=1}^{h} m} \right)^2$$

[3]

where ε_r is the average relative dielectric permittivity of soil in a horizon/compound horizons [-], "h" is a number of horizons in case of compound horizons, "m" is a mean value of the thickness of a horizon calculated using the values at checkpoints [m], ε_{rm} is a mean value of relative dielectric permittivity of soil horizon [-].

The differences between the mean values of soil dielectric permittivity in the upper and lower horizons indicate the GPR signal phase. The thickness of a horizon or compound horizon was estimated at points of all recorded GPR traces along the transect (i.e., every 0.75 cm). The thickness of a horizon or compound horizons at a point of the trace was determined as a mean value of the thicknesses calculated from 15

neighbouring traces (the trace at the point and seven preceding and seven following traces at each side along the transect). This approach should eliminate accidental reflections, reflections from small objects, or local measurement' or processing' errors. The determined point thicknesses were used for a detailed reconstruction of the studied soil horizons thicknesses along the survey transect.

Evaluation of errors in the estimated thickness/depth of a horizon

Firstly, the horizon thicknesses recorded manually at checkpoints along the survey transect were compared with the estimation of the thicknesses determined from the GPR data. The error of the horizon or the compound horizons thickness was expressed at each checkpoint in percentage, and the mean error was calculated. For even better comparison, scatter plots with the coefficient of the determinations R^2 were created. However, it was impossible to create a scatter plot for each horizon and each survey condition separately due to the low number of points. In addition, the range of values was not wide enough. For these reasons, the data from both study sites, both studied horizons, and from different survey conditions were processed together. The depths exceeding 50 cm that represented deep tongues of Ev horizon were excluded due to the low number of points. Finally, three plots were constructed: (i) all moisture conditions, (ii) wetter conditions, including Arenic Podzol site surveyed in May 2017 together with Dystric Cambisol site surveyed in April 2016 and August 2016, and (iii) drier conditions including Arenic Podzol site surveyed in June 2018 and August 2018 together with Dystric Cambisol site surveyed in August 2015 and August 2015 after irrigation. The survey performed in December 2015 at the Dystric Cambisol site was included only in the scatter plot of all moisture conditions. It was excluded from the other two scatter plots because of medium soil moisture values.

In addition, we estimated mean horizon thicknesses at the whole transects and their sections. The soil organic carbon stock model [Eq. 1] requires information on organic carbon concentration in soil and soil bulk density, apart from soil thickness. Since these two parameters are sampled in the field but then analysed in the laboratory, they cannot be measured at every point. As a consequence, the thickness could be the most detailed parameter used in the model. The thickness could be expressed as a mean value for each section/landscape unit with available carbon concentration and bulk density data. For illustration, we estimated mean thicknesses at the whole measured transects and at one-meter long sections of the transects. The sections were created from

the start of the transect, and the last part of the transect shorter than 1 m was excluded. We compared the estimated mean thicknesses to mean thicknesses calculated from the values measured manually at the checkpoints.

Results

The most remarkable difference between soil horizons (compound horizons Oi+Oe and Oa+Ah) in dielectric permittivity at the Dystric Cambisol site was found during the survey under the driest conditions in August 2015, and then under the moist conditions after the snow melted down in April 2016. For the other surveys, the permittivity of these soil horizons (compound horizons) was very similar. The difference in soil dielectric permittivity between the compound horizons Of+Ah and horizon Bv was relatively low, despite varying precipitation before the surveys.

Table 5 Soil moisture conditions and corresponding relative dielectric permittivity of the horizons/compound horizons during the respective surveys in the Dystric Cambisol site

	Oi+Oe		Oa+Ah		Bv		O+Ah weighted average	
mean horizon depth [cm]	9.9		2.9		not measured			
survey	ε_r [-]	VWC [%]	ε_r [-]	VWC [%]	ε_r [-]	VWC [%]	ε_r [-]	EM wave velocity [m/ns]
August_15	6.0	19.5	8.5	25	9.5	21	6.6	0.117
August_15i	8	25	8.5	25	9.5	21	8.1	0.105
December_15	8.5	30	9.0	25	9.5	21	8.6	0.102
April_16	9	26	11.5	30	12	25	9.6	0.097
August_16	11.5	30	11.5	30	12.5	27	11.5	0.088

ε_r is relative dielectric permittivity measured at the field, VWC is the volumetric water content of the soil shown here for completeness and illustration and calculated from ε_r using relations provided by Decagon Devices, Inc. (2014). VWC in O and Ah horizon is calculated according to ε_r –VWC relation designed for organic soils[1], VWC in Bv according to ε_r –VWC relation for mineral soils[2] (Decagon Devices, Inc., 2014).

[1] $VWC\ [\mathrm{cm3/cm3}] = 0.118\sqrt{\varepsilon} - 0.117$

[2] $VWC\ [\mathrm{cm3/cm3}] = 5.89 \times 10^{-6} \times \varepsilon^3 - 7.62 \times 10^{-4} \times \varepsilon^2 + 3.67 \times 10^{-2} \times \varepsilon - 7.53 \times 10^{-2}$

At the Arenic Podzol site, the soil permittivity and its difference between the horizons/compound horizons were the highest in May 2017 (organic horizon "O" was not considered because its thickness did not exceed 1 cm) and decreased during dry summer in 2018. In August 2018, soil permittivities in the Ah and Ev horizons were

similar (Table 6). Due to the spodic Bhs horizon compactness, it was not possible to measure soil dielectric permittivity there using the Decagon GS3 soil moisture device. However, it was supposed to be the highest of all horizons because of the expected high concentration of the Fe-Al oxyhydroxides, which this diagnostic horizon commonly contains (IUSS Working Group WRB, 2015).

Table 6 Arenic Podzol Study site - Soil moisture conditions and corresponding relative dielectric permittivity of the horizons/compound horizons during the respective surveys in the Arenic Podzol site

mean horizon depth [cm]	O		Ah		Ev		O+Ah weighted average		O+Ah+Ev weighted average	
	1		17.5		21					
survey	ε_r [-]	VWC [%]	ε_r [-]	VWC [%]	ε_r [-]	VWC [%]	ε_r [-]	EM wave velocity [m/ns]	ε_r [-]	EM wave velocity [m/ns]
May _17	10	27.5	10	22	7	14.5	10	0.095	8.4	0.103
June_18	2.5	10	4	6	3.5	4	3.9	0.152	3.7	0.156
August_18	1.2	1	2.8	< 1	2.8	< 1	2.71	0.182	2.76	0.181

ε_r is the relative dielectric permittivity measured at the field, VWC is the volumetric water content of the soil shown here just for completeness and illustration and calculated from ε_r using relations provided by Decagon Devices, Inc. (2014). VWC in O horizon is calculated according to ε_r –VWC relation designed for organic soils[1], VWC in Ah and Ev according to ε_r –VWC relation for mineral soils[2] (Decagon Devices, Inc., 2014).

[1] $VWC\ [\mathrm{cm3/cm3}] = 0.118\sqrt{\varepsilon} - 0.117$

[2] $VWC\ [\mathrm{cm3/cm3}] = 5.89 \times 10^{-6} \times \varepsilon^3 - 7.62 \times 10^{-4} \times \varepsilon^2 + 3.67 \times 10^{-2} \times \varepsilon - 7.53 \times 10^{-2}$

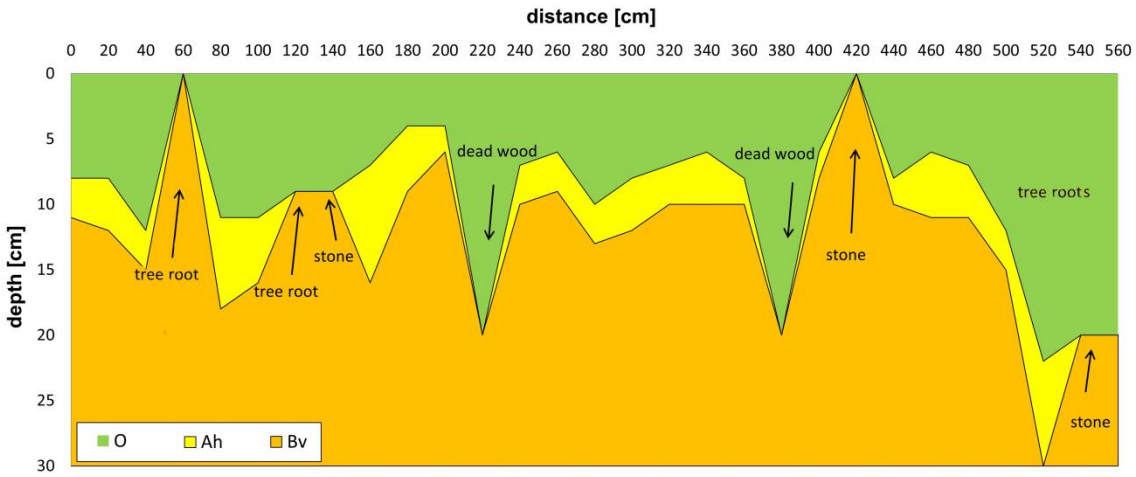

Fig. 5 Reconstruction of the soil horizons depths along the studied transect in the Dystric Cambisol site based on the manual field measurements at the checkpoints

At the end of the profile, many smaller tree roots are dispersed at a depth of between 5 and 15 cm.

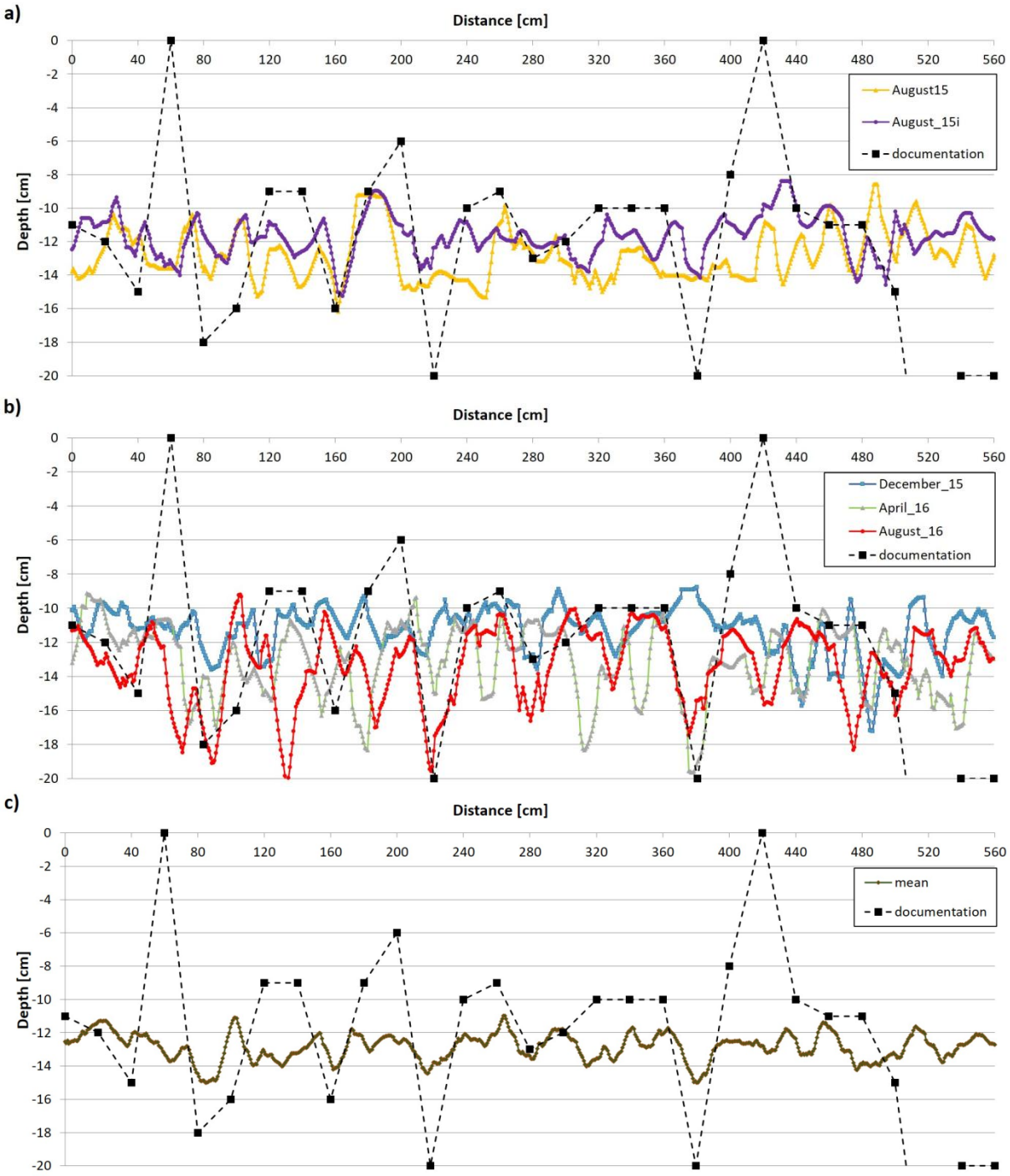

***Fig. 6 The estimation of the O+Ah horizons' depth at the Dystric Cambisol site based on the GPR measurements at different times*:** *August 2015 and August 2015 with irrigation (a), December 2015, April 2016 and August 2016 (b) and the mean value of all surveys (c).*

At the Dystric Cambisol site, the boundary between compound Oi+Oe and Of+Ah horizons was not detected under either soil moisture conditions, probably due to the low thickness of the Ah horizon (Fig. 5). The first recorded reflection of the GPR signal mainly corresponded to Ah/Bv horizons boundary. The estimation error of the organic horizons thickness at the checkpoints was found to be the lowest under the

moistest conditions in August 2016 (Table 7). The organic horizons' thickness errors vary between 25% and 35% (Table 7). The estimation errors in the mean thicknesses were even lower between 8% and 23% (Table 8) at one-meter long sections and between 3% and 9% for the whole transect. However, the error was the lowest under the driest conditions in August 2015. This is opposite to the average error at the checkpoints. The thickness distribution constructed as a mean of all measurements (from now on in text "mean curve") visually corresponds better with the field verification, but the estimation errors are significantly lower (Table 7, 8). The interpretation of the measured data and field verification also shows that some objects in the soil profile are displayed next to their actual position. Next, some objects detected in the data were not observed in the field (Fig. 6). This causes an increase in the errors observed at the checkpoints. Especially irregular horizon boundary and deep penetration of horizon tongues cause some difficulties in the interpretation. This is because the signal is not emitted just below the GPR device, but it spreads rather like a cone, and the signal reflects not only from objects vertically right under the device but also from objects to the four sides.

In most cases, tongues rich in soil organic matter or dead wood were indicated (Fig. 6a,b,c). There is an exception of a tongue at the end of the transect where some tree roots in Oi+Oe horizons were documented. They probably reflected the GPR signal and were interpreted as the first distinguished horizon boundary. However, an indication of the beginning of the tongue is noticeable. It is evident from comparing the mean curve from all measurements at the site and the thickness distribution based on the verification profile (Fig. 6c). In dry conditions (in August 2015), signal reflections were probably strongest from sides of the tongues filled with deadwood when the GPR was approaching or moving away. Consequently, the tongues appear wider at the GPR data-based thickness distribution. These tongues were displayed the best in the moistest conditions (August 2016 and April 2016). Similarly, signal reflection from a side of a tongue not recorded in the verification transect can appear in the GPR data-based output (Fig. 6b).

Table 7 Descriptive statistics of the error of O+Ah thickness at the checkpoints at the Dystric Cambisol site under different soil moisture conditions

	N	mean	median	min.	max.
August_15	29	31.4%	25.4%	1.8%	137.7%
August_15i	29	25.6%	21.9%	0.6%	83.8%
December_15	29	34.6%	30.1%	2.1%	118.9%
April_16	29	31.1%	21.5%	2.0%	91.4%
August_16	29	27.6%	15.8%	0.4%	113.4%
mean curve	29	28.6%	26.1%	2.2%	108.4%

N is the number of the points

Table 8 Average error of O+Ah mean thicknesses at the Dystric Cambisol site under different soil moisture conditions

mean thickness errors [%]	length of transect sections		
	1 m		whole transect
	mean	std	
August_15	8.5%	5.3%	3.1%
August_15i	12.5%	12.3%	5.8%
December_15	12.0%	6.7%	5.8%
April_16	19.3%	14.6%	6.2%
August_16	23.0%	12.6%	8.2%
mean curve	17.4%	12.3%	3.5%
number of points measured at a section			
verification	6		29
GPR	133		743

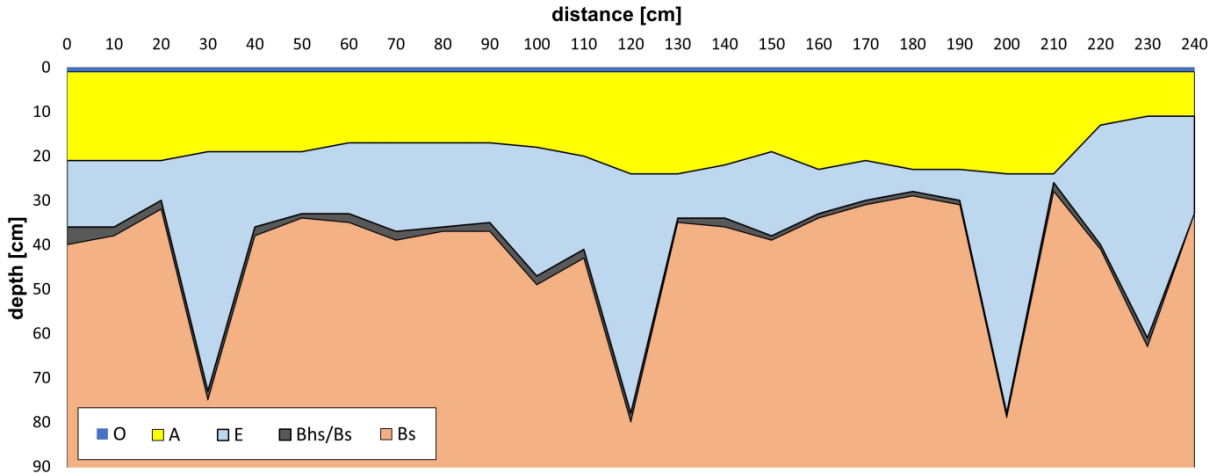

Fig. 7 Reconstruction of the studied soil profile at the Arenic Podzol site based on the verification at the checking points

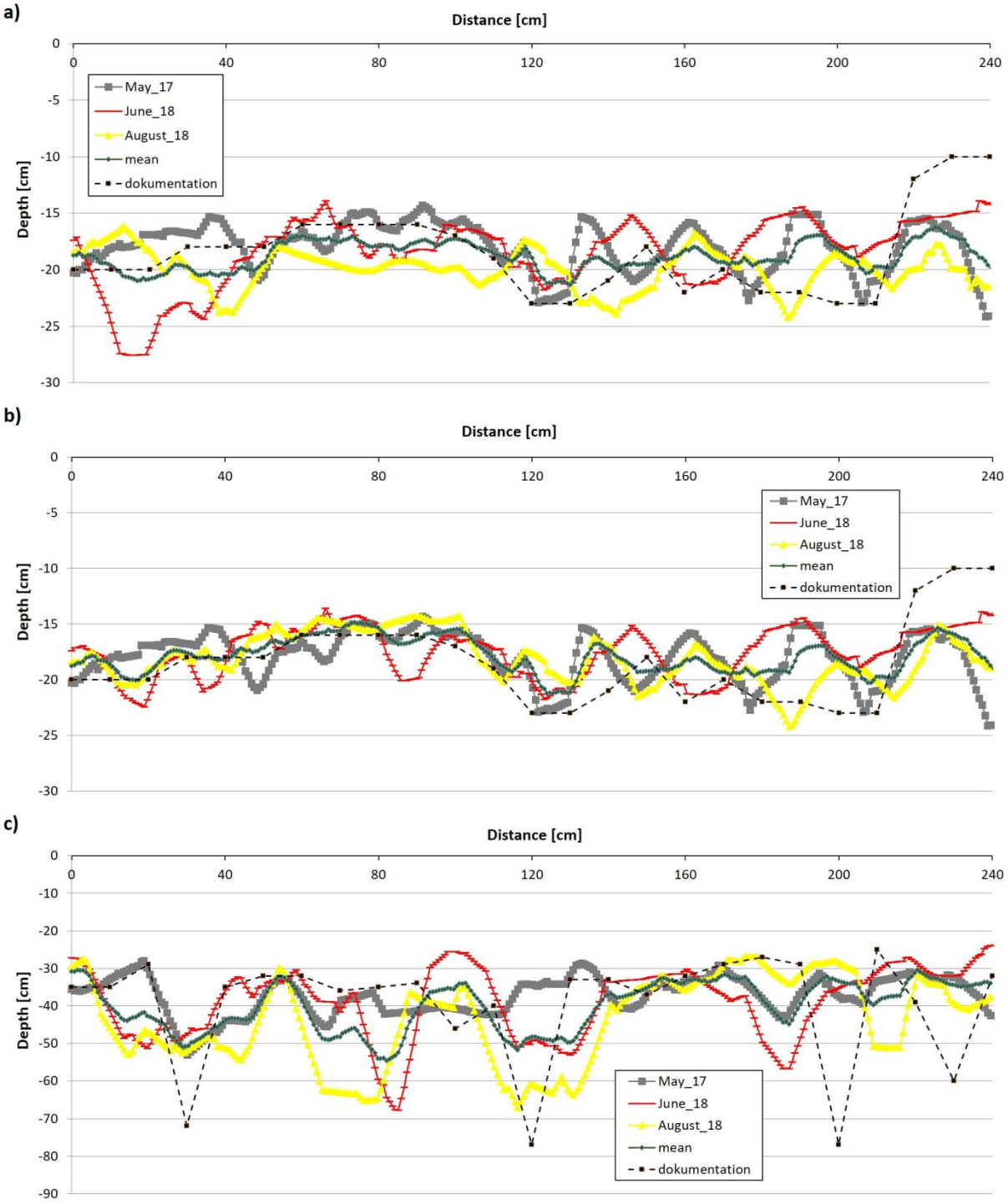

Fig. 8 The estimation of the horizons' depth at the Arenic Podzol site based on the GPR measurements*: Ah horizon (a), Ah horizon processed with the phase inversion in June 2018 and August 2018 in a part of the line (b), E horizon (c)*

At the Arenic Podzol site, organic horizons were found to be less than 1 cm thick. Thus, we estimated the thickness of O+Ah horizons together. No stones or big tree roots were present in the uncovered verification profile at the locality (Fig. 7). The errors in estimating O+Ah horizons were lower at this locality than at the Cambisol site (Table 9),

and the GPR derived boundaries corresponded better to the reconstruction made from the checkpoints (Fig. 8). Generally, at the first 120 cm of the transect length, the Ah/Ev boundary is the most clearly displayed during the moistest conditions in May 2017 (Fig. 8a), exhibiting the lowest thickness error (Table 9). The remaining length of the transect shows distinct reflections from uncovered objects or microsites with higher soil moisture (Fig. 8a).

During the driest conditions (in August 2018), the Ah/Ev boundary at the first 120 cm of the verification profile transect did not correspond with the GPR data (Fig. 8a). However, it was corrected when we supposed that the GPR signal phase was inversed during the reflection and applied this inversion to the signal (Fig. 8b). It indicates that the soil permittivity was higher in the Ah horizon than in the eluvial Ev horizon in this part of the soil profile transect. However, there was only a slight difference in the soil permittivity between the Ah and Ev horizons during the field measurements (Table 6). This phenomenon was observed in June 2018 as well. The GPR outputs of the surveys in June 2018 and August 2018, where we assumed that the signal phase was inversed at the part of the profile transect, show lower measurement errors, even lower than the output of May 2017 (Table 9). However, the ranges of measurements' errors are not large. The Ah horizon thickness differences (error) between soil profile transect and GPR data at checkpoints vary between 18% and 24%, but only up to 12% for estimating the mean thicknesses at all section lengths. The lowest error of the mean thickness was found under the driest conditions, similarly to at the Dystric Cambisol site. The mean curve improves the estimations but not substantially (Table 9, 10).

The Ev horizon depth estimation is satisfying (Fig. 8c). The tongues are slightly shifted compared to the uncovered transect, and there appears to be a tongue 80 cm from the beginning of the transect, which was not uncovered (in June 2018 and August 2018). In the driest conditions (in August 2018), the tongues of Ev horizons were probably detected from their outer side when the GPR device was approaching and when it was moving away. They are displayed wider at the output, similar to the Cambisol site's organic tongues. This phenomenon causes a big difference (error) in the Ev horizon's depth between soil profile transect and GPR data at the checkpoints and in estimating the O+Ah+Ev mean thickness in August 2018 (Table 11). The mean thicknesses estimation error was the highest during the moistest conditions in May 2017, where the tongues were only weakly detectable (Table 12, Fig. 8a).

Table 9 Descriptive statistics of the error of O+Ah thickness at checkpoints at the Arenic Podzol site under different soil moisture conditions

	N	mean	median	min.	max.
May_17	25	18.2%	9.3%	0.2%	137.0%
June_18	25	18.1%	15.1%	0.5%	52.2%
August_18	25	23.5%	16.5%	3.2%	115.2%
mean curve	25	16.8%	9.4%	1.4%	98.2%
June_18b	25	16.0%	11.7%	0.5%	52.2%
August_18b	25	16.4%	10.6%	0.3%	81.7%
mean curve_b	25	14.8%	7.0%	0.1%	87.0%

N is the number of the points; b- phase inversion is supposed to happen in a part of soil profile transect (the part interpreted during data processing)

Table 10 Average error of O+Ah mean thicknesses at the Arenic Podzol site under different soil moisture conditions

***mean thickness errors* [%]**	**length of transect sections**		
	1 m		**whole transect**
	mean	std	
May_17	6.2%	3.6%	7.5%
June_18	12.8%	0.5%	0.2%
August_18	7.6%	3.9%	3.1%
mean curve	7.1%	6.2%	5.0%
June_18b	7.0%	1.3%	2.6%
August_18b	7.6%	1.5%	1.5%
mean curve_b	7.3%	3.8%	3.6%
number of points measured at a section			
verification	11		25
GPR	133		317

b- phase inversion is supposed to happen in a part of soil profile transect (the part interpreted during data processing)

Table 11 Descriptive statistics of the error of E horizon thickness at checkpoints at the Arenic Podzol site under different soil moisture conditions

	N	mean	median	min.	max.
May_17	25	19.3%	15.9%	1.7%	55.3%
June_18	25	32.5%	27.7%	1.7%	84.2%
August_18	25	35.1%	26.6%	1.4%	84.7%
mean curve	25	23.5%	16.5%	4.1%	55.7%

N is the number of the points

Table 12 Average errors of O+Ah+Ev mean thicknesses at the Arenic Podzol site under different soil moisture conditions

***mean thickness errors* [%]**	**length of transect sections**		
	1 m		**whole transect**
	mean	std	mean
May_17	13.1%	12.0%	10.3%
June_18	5.7%	1.9%	1.7%
August_18	8.6%	5.1%	5.9%
mean curve	9.1%	2.9%	0.9%
number of points measured at a section			
verification	11		25
GPR	133		317

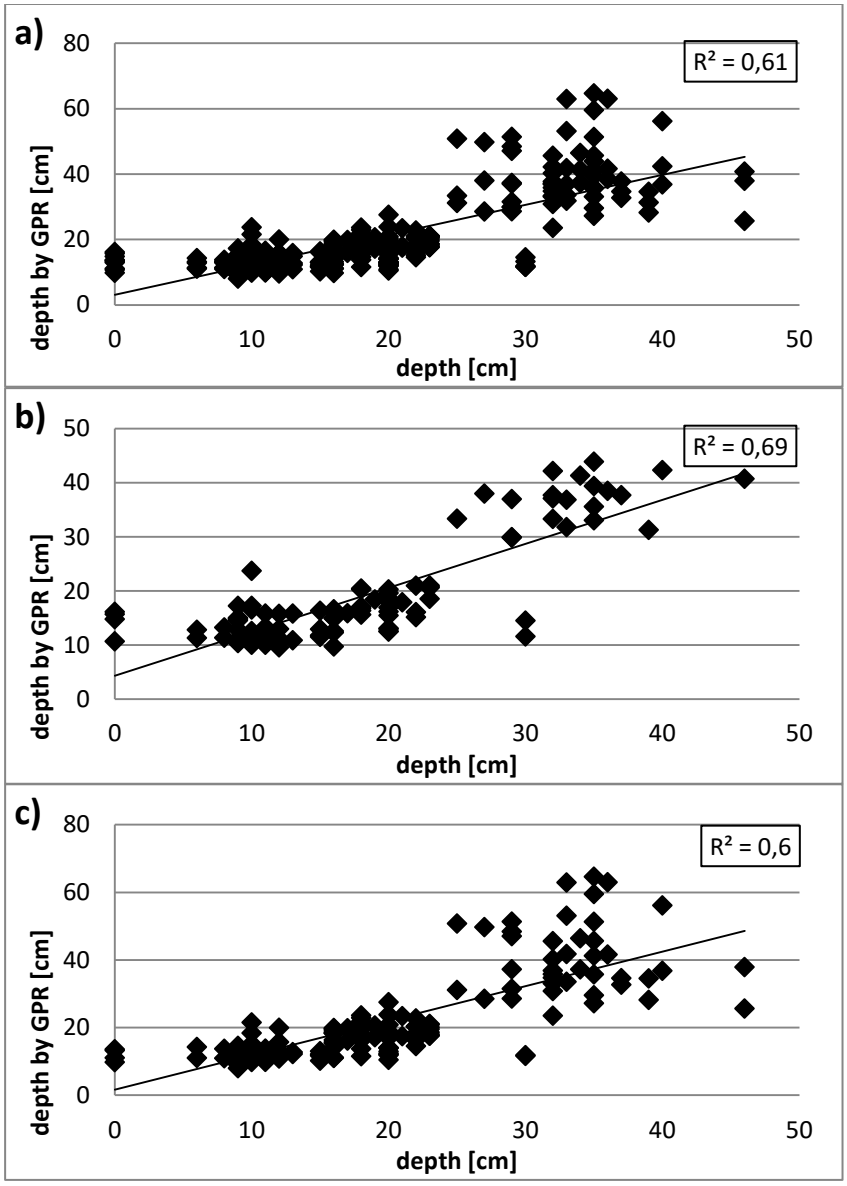

Fig. 9 The comparison of the thickness values measured manually with the thickness values estimated by GPR under all moisture conditions (a), in moist conditions (b), in dry conditions (c)

The comparison of all thicknesses estimated using GPR with the thicknesses measured manually at checkpoints (Fig. 9.) showed similar trends as those described above for the estimation errors at the checkpoints. The coefficient of determination (R^2) is about 0.6, with slightly better results under wetter conditions (Fig. 9b). The scatter plots (Fig. 9) show an offset at the depth of 0 m. It is because we were not able to identify the cases where organic and organomineral horizons were missing due to a stone near the surface. We considered the first big reflection as the surface and the following significant reflection as the organomineral horizon lower boundary at all times.

Discussion

Doolittle and Butnor (2009) reported in the review on soil stratigraphy using GPR that the mean measurement errors in estimated depths of argic, spodic, placic, R, or C horizon were between 2 and 40 %. Afshar et al. (2017) estimated the depth of cemented petrosalic horizon with an average error of 23%. In our study, the thickness of combined organic and organomineral horizons was estimated with 25 – 35% mean measurement error at the Cambisol site (for 50 % of the checkpoints the error was below 16 – 30 %), and with 16 – 24 % mean measurement error at the Arenic Podzol site (for 50 % of the checkpoints the error was below 10 – 17 %) (Table 7, 9). The fact that some edges and forms are slightly shifted on the GPR output relative to their documented position would be partly responsible for the measurement error. This occurs because the GPR signal is not emitted just below the GPR device but spreads rather like a cone and reflects from objects vertically right under the device and from objects to the sides in four directions. Therefore, the objects could be detected before or after the GPR passed over them as well as if these objects continue aside the transect. Moreover, during the survey, the GPR did not pass precisely over the excavated transect but adjacent to it.

In addition, soil moisture and in consequence soil dielectric permittivity is highly spatially variable (e. g., Gallardo 2003). It could differ in such a level that it deforms reflection hyperbolas in the 2D GPR radargrams (e. g., Igel 2008). For calculating electromagnetic signal velocity, we used the average soil dielectric permittivity at the study site at the time of each survey. Therefore, it is likely that some inaccuracy in estimating the thicknesses is caused by the spatial variability of the soil

dielectric permittivity. Determination of the dielectric permittivity at every point of the transect using GPR directly is not possible without using a multi-channel GPR system. As an alternative, the permittivity of organic horizons could be measured more precisely over the transect by the GPR ground waves approach as these layers can act as guided waves under certain moisture conditions (Strobbia and Cassiani, 2007; van der Kruk et al., 2006). Another approach could encompass the analysis of the reflection hyperbolas in the GPR radargram (e. g., Elkarmoty et al. 2017). Nevertheless, the latter method requires enough reflection hyperbolas in the GPR output.

There exist studies reporting higher accuracy of organic plus organmineral horizons thickness estimation using GPR, but there are no studies, to our knowledge, distinguishing individual organic horizons. In a similar study, Winkelbauer et al. (2011) estimated the thickness of organic plus organomineral horizons with a 15 % measurement error. Still, they could not distinguish individual organic horizons, similar to our study. The higher accuracy reported by Winkelbauer et al. (2011) is because they evaluated only the cases where the horizon boundary was detected, and they excluded transect segments with larger stones or tree roots. For the inability to distinguish organic horizons, Winkelbauer et al. (2011) argued that it resulted from the insufficient thicknesses of the respective organic horizons relative to the antenna resolution and insignificant differences in the dielectric permittivity. In our study, the differences in the dielectric permittivity between organic and organomineral horizons were even larger than those between organomineral and mineral horizons in some cases (Table 5, 6). The insufficient thickness of an organic horizon would be the main reason why its boundary was not detected in our study. The soil in Winkelbauer et al. (2011) study was predominantly of the A-C stratigraphy. The (A)B/C or soil/bedrock boundaries are the most often detected using GPR (e. g., Zhang et al. 2014; Ikazaki et al. 2018; Šamonil et al. 2020; Schaller et al. 2020; Schiavo et al. 2020). Ikazaki et al. (2018) estimate this boundary with a mean measurement error of 2.9 cm for soil shallower than 50 cm and of 5.7 cm for soil deeper than 50 cm. Schiavo et al. (2020) studied podzols as we did in our study at the Arenic Podzol study site and detected E/Bhs and Bhs/C boundaries, but they did not detect organomineral-mineral (Ah/E) horizon boundary. In our study at the Arenic Podzol site, the depth of the E/Bhs boundary was estimated with 19 – 35% mean measurement error (for 50 % of the checkpoints the error was below 16 – 29 %) (Table 9, 11). This is because of the variable depth of the E/Bhs boundary with deep tongues slightly shifted on the GPR output. There were weaker reflections above or below the

E/Bhs boundary that did not correspond to any feature observed in the field. Possibly this could be caused by variations in water content not related to soil diagnostic horizons, as also argued by Winkelbauer et al. (2011). This can be caused by micro-porosity and pores' distribution according to De Benedetto et al. (2019).

In general, the horizon boundaries were detected despite low dielectric permittivity differences between the two horizons in some cases in our study. A boundary with a very small change of dielectric permittivity was also detected by Corradini et al. (2020), but they noticed that the peak of the reflection is weak. We recognised these boundaries using the 1D analysis of individual traces, but we were not able to distinguish them in the 2D radargrams.

At the Cambisol site, surveys were performed under several different soil moisture conditions. However, the moisture finally differed less significantly than expected. The moisture conditions at field capacity, which is suggested advantageous by van Dam et al. (2002), was almost met in the Ah horizon in August 2016 and April 2016. During most surveys, conditions in the Ah horizon corresponded to the permanent wilting point, or they were even below this point in August 2015. However, the Bv horizon was wetter during all of the surveys, suggesting that it drains much slower than the Ah horizon or that roots more explore the Ah horizon to uptake water. For this reason, the dielectric permittivity between the two horizons differed only moderately (Table 5) and the same holds between horizons at the Podzol study site (Table 6). The reason is probably that the texture of soil horizons of the studied Podzol does not show a significant difference (Table 3). Surveys were performed under conditions between full saturation and field capacity in May 2017, near the permanent wilting point in June 2018 and almost dried out in August 2018.

Results with a bit lower estimation error at the checkpoints were obtained under wetter conditions at both sites (but at the Podzol study site, it is very similar), which is in line with previous studies (Curioni et al., 2017; van Dam et al., 2002; Zhang et al., 2014). However, these studies argued that they found the most significant difference in soil dielectric permittivity between horizons and the most significant reflection under wet conditions. In our study, it was true for the Arenic Podzol study site, but at the Dystric Cambisol study site, the permittivity was very similar (Table 5, 6).

By contrast, under drier conditions, we can see better deeper parts of irregular horizon boundaries (Fig. 8c) because of the limited signal attenuation. For this reason,

surveying under dry conditions was also suggested by Li et al. (2015) based on their study in a karst environment. The errors of the mean thicknesses at the measured profiles and their sections were the lowest under the driest conditions. It showed, that estimating a soil horizon thickness for soil organic carbon modelling using the concept of soil equivalent mass (Ellert and Bettany, 1995) could be advantageous under very dry conditions. It follows that both wet and dry conditions can have advantages and that their combination could bring more information, as was recommended by van Dam et al. (2002). However, our study showed that if we are not looking for particular objects and, as a result, we use the surveys under different conditions to make an average, the estimation improvement is relatively moderate and not very effective (Table 7 – 11).

Another source of uncertainties could be the presence of tree roots and stones. Tree roots and stones can be obstacles to GPR surveying of soil horizon boundaries as found at the Cambisol study site. The tree roots are usually parts of organic horizons, so they should be filtered out during the GPR data processing not to disturb the horizon boundaries. We can not distinguish either these objects from horizons' boundaries or stones from tree roots at this stage. The stones and tree roots could be distinguished from horizons' boundaries at the 2D GPR radargram if they appeared as hyperbolas. However, the spatial resolution that we used (0.75 cm) wasn't probably high enough to show the stones and tree roots appearing at the studied transects in the form of reflection hyperbolas. Alternatively, tree roots and stones could be distinguished based on dielectric permittivity. The relative dielectric permittivity of roots is between 4.5 for dry roots and 22 for water-saturated roots (al Hagrey, 2007). The relative dielectric permittivity of stones is between 3 and 5 (Cassidy, 2009). It implies that stones should be detectable better under wetter conditions and the roots under drier conditions. According to Cui et al. (2011), an antenna of 450 MHz can detect roots larger 2 cm in diameter, while an antenna of 1.5 GHz can detect even roots smaller 0.5 cm but only to the depth of 30 cm. In our study, an antenna of 800 MHz was used, which means that the roots detected can be supposed to be larger 1 cm in diameter. The diameter of 1 cm is also considered to be the smallest object's diameter most GPR devices can detect with reasonable accuracy (Borden et al., 2016; Hirano et al., 2009). However, such small roots are filtered out by the data processing method used in our study as well as bigger roots and stones near the surface. Difficulties could cause smaller roots in a bunch that appears like a big root or even wider interface on the GPR output, suggesting a boundary between soil horizons. It was observed at the end of the survey line at the

Cambisol study site (Fig. 6). Root systems are more evident when using 3D image visualisation, but these surveys require detailed measurements on small grids (Doolittle and Butnor, 2009).

The primary purpose of this study was to facilitate the estimation of soil organic carbon stock. Mean horizon thickness can serve as a base for calculating soil organic mass. In this study, the mean horizon thickness estimation error was between 8% and 23% at one-meter long sections and up to 9% at the entire transect for the Cambisol site and 6 - 13% at one-meter long sections and up to 8% at the entire transect for the Podzol site. The mean thickness seems the most accurate under the driest conditions. Therefore, it could be advantageous to survey the thickness under very dry soil conditions when targeting the average thickness. Still, to obtain a single value at a point, wet soil conditions are more suitable, as shown by a comparison of the thickness values at the checkpoints.

Conclusion

Our study showed that detecting organomineral/mineral horizon boundary is possible even if the soil dielectric permittivity of the horizons doesn't differ significantly. The mean measurement error is slightly higher than in previous studies. However, the studied Cambisol site was characterised by a highly variable organomineral/mineral horizon boundary with numerous tree roots and stones. The mean thickness estimation, which can serve as a base for mass calculation, is promising for assessing soil organic carbon stock. Results at individual points were slightly better under moister conditions, probably due to a more significant difference in the dielectric permittivity between the horizons. However, deeper forms (boundaries) were better detected under drier conditions, and the mean thickness estimation was the most accurate under the driest conditions. Both conditions can bring important information but averaging the measurements under different conditions didn't improve the results significantly.

Acknowledgement

This research was supported by the institutional resources of the Ministry of Education, Youth and Sports of the Czech Republic for the support of science and research, project no. SVV260438, and within the CzeCOS program, grant number LM2018123. We

appreciate Martina Vlčková from the Research Institute for Soil and Water Conservation for her kind cooperation with measuring water retention characteristics of studied soils.

References

Adhikari, K., Hartemink, A.E., 2016. Linking soils to ecosystem services - A global review. Geoderma 262, 101–111. https://doi.org/10.1016/j.geoderma.2015.08.009

Afshar, F.A., Ayoubi, S., Castrignanò, A., Quarto, R., Ardekani, M.R.M., 2017. Using ground-penetrating radar to explore the cemented soil horizon in an arid region in Iran. Near Surf. Geophys. 15, 103–110. https://doi.org/10.3997/1873-0604.2016049

al Hagrey, S.A., 2007. Geophysical imaging of root-zone, trunk, and moisture heterogeneity. J. Exp. Bot. 58, 839–854. https://doi.org/10.1093/jxb/erl237

André, F., Jonard, M., Lambot, S., 2015. Non-Invasive Forest Litter Characterization Using Full-Wave Inversion of Microwave Radar Data. IEEE Trans. Geosci. Remote Sens. 53, 828–840.

Annan, A. P., 2009. Ground Penetrating Radar Principles, Procedure & Applications. Gr. Penetrating Radar Theory Appl. Ground Pen, iv. https://doi.org/10.1016/B978-0-444-53348-7.00016-8

Ardekani, M.R., Nottebaeret, M., Jacques, D., 2014. GPR data inversion for vegetation layer. Proc. 15th Int. Conf. Grounds Penetrating Radar, 2014. GPR 2014. 170–175.

Bens, O., Wahl, N.A., Fischer, H., Hüttl, R.F., 2007. Water infiltration and hydraulic conductivity in sandy cambisols: Impacts of forest transformation on soil hydrological properties. Eur. J. For. Res. 126, 101–109. https://doi.org/10.1007/s10342-006-0133-7

Borden, K.A., Thomas, S.C., Isaac, M.E., 2016. Interspecific variation of tree root architecture in a temperate agroforestry system characterized using ground-penetrating radar. Plant Soil 1–12. https://doi.org/10.1007/s11104-016-3015-x

Bristow, C.S., Jol, H.M., 2003. Ground Penetrating Radar in Sediments (Geological Society Special Publication) (No. 211).

Cassidy, N.J., 2009. Electrical and Magnetic Properties of Rocks, Soils and Fluids, in: Jol, H.M. (Ed.), Ground Penetrating Radar Theory and Applications. pp. 41–72. https://doi.org/10.1016/B978-0-444-53348-7.00010-7

CHMI, 2020. Czech Hydrometeorological Institute [WWW Document]. Hist. data. URL https://www.chmi.cz/historicka-data/pocasi/denni-data/Denni-data-dle-z.-123-1998-Sb

Chuman, T., Gürtlerová, P., Hruška, J., Adamová, M., 2014. Geochemical reactivity of rocks of the Czech Republic. J. Maps 10, 341–349. https://doi.org/10.1080/17445647.2013.867418

Chuman, T., Oulehle, F., Zajícová, K., Hruška, J., 2021. The legacy of acidic deposition controls soil organic carbon pools in temperate forests across the Czech Republic. Eur. J. Soil Sci. 72, 1780–1801. https://doi.org/10.1111/ejss.13073

Conyers, L.B., 2012. Interpreting Ground-Penetrating Radar for Archaeology. Walnut Creek: Left Coast Press.

Corradini, E., Dreibrodt, S., Erkul, E., Groß, D., Lübke, H., Panning, D., Pickartz, N., Thorwart, M., Vött, A., Willershäuser, T., Wilken, D., Wunderlich, T., Zanon, M., Rabbel, W., 2020. Understanding wetlands stratigraphy: Geophysics and soil parameters for investigating ancient basin development at lake duvensee. Geosci. 10, 1–35. https://doi.org/10.3390/geosciences10080314

Cui, X.H., Chen, J., Shen, J.S., Cao, X., Chen, X.H., Zhu, X.L., 2011. Modeling tree root diameter and biomass by ground-penetrating radar. Sci. China Earth Sci. 54, 711–719. https://doi.org/10.1007/s11430-010-4103-z

Curioni, G., Chapman, D.N., Metje, N., 2017. Seasonal variations measured by TDR and GPR on an anthropogenic sandy soil and the implications for utility detection. J. Appl. Geophys. 141, 34–46. https://doi.org/10.1016/j.jappgeo.2017.01.029

De Benedetto, D., Montemurro, F., Diacono, M., 2019. Mapping an agricultural field experiment by electromagnetic induction and ground penetrating radar to improve soil water content estimation. Agronomy 9. https://doi.org/10.3390/agronomy9100638

Decagon Devices, Inc., 2014. GS3 Water Content, EC and Temperature Sensors: Operator ’s Manual, 2014.

Doolittle, J., Butnor, J., 2009. Soils, peatlands, and biomonitoring, in: Jol, H.M. (Ed.), Ground Penetrating Radar Theory and Applications. pp. 179–202. https://doi.org/10.1016/B978-0-444-53348-7.00006-5

Elkarmoty, M., Colla, C., Gabrielli, E., Papeschi, P., Bonduà, S., Bruno, R., 2017. In-situ GPR test for three-dimensional mapping of the dielectric constant in a rock mass. J. Appl. Geophys. 146, 1–15. https://doi.org/10.1016/j.jappgeo.2017.08.010

Ellert, B.H., Bettany, J.R., 1995. Calculation of organic matter and nutrients stored in soils under contrasting management regimes. Can. J. Soil Sci. 75, 529–538. https://doi.org/10.4141/cjss95-075

Gallardo, A., 2003. Spatial Variability of Soil Properties in a Floodplain Forest in Northwest Spain. Ecosystems 6, 564–576. https://doi.org/10.1007/s10021-003-0198-9

Hirano, Y., Dannoura, M., Aono, K., Igarashi, T., Ishii, M., Yamase, K., Makita, N., Kanazawa, Y., 2009. Limiting factors in the detection of tree roots using ground-penetrating radar. Plant Soil 319, 15–24. https://doi.org/10.1007/s11104-008-9845-4

Huisman, J. A., Hubbard, S.S., Redman, J.D., Annan, A. P., 2003. Measuring Soil Water Content with Ground Penetrating Radar A Review. Vadose Zo. J. 2, 476–491. https://doi.org/10.2113/2.4.476

Igel, J., 2008. The Small-Scale Variability of Electrical Soil Properties − Influence on GPR Measurements. 12th Int. Conf. Gr. Penetrating Radar 10.

Ikazaki, K., Nagumo, F., Simporé, S., Barro, A., 2018. Soil toposequence, productivity, and a simple technique to detect petroplinthites using ground-penetrating radar in the Sudan Savanna. Soil Sci. Plant Nutr. 64, 623–631. https://doi.org/10.1080/00380768.2018.1502604

ISO 11274, 2009. Soil quality — Determination of the water-retention characteristic — Laboratory methods, INTERNATIONAL STANDARD.

ISO 11277, 2009. Soil quality — Determination of particle size distribution in mineral soil material — Method by sieving and sedimentation, INTERNATIONAL STANDARD.

IUSS Working Group WRB. 2015. World Reference Base for Soil Resources 2014, update 2015 International soil classification system for naming soils and creating legends for soil maps. World Soil Resources Reports No. 106. FAO, Rome.

Jonard, F., Demontoux, F., Bircher, S., Razafindratsimat, S., Schwank, M., Weillermuller, L., Lambot, S., Wigneron, J.-P., Kerr, Y., Vereecken, H., 2014. Electromagnetic characterization of organic-rich soils at the microwave L-band with ground-penetrating radar , radiometry and laboratory measurements. Proc. 15th Int. Conf. Grounds Penetrating Radar 202–207.

Klotzsche, A., Jonard, F., Looms, M.C., van der Kruk, J., Huisman, J.A., 2018. Measuring Soil Water Content with Ground Penetrating Radar: A Decade of Progress. Vadose Zo. J. 17, 0. https://doi.org/10.2136/vzj2018.03.0052

Kristensen, T., Ohlson, M., Bolstad, P., Nagy, Z., 2015. Spatial variability of organic layer thickness and carbon stocks in mature boreal forest stands—implications and suggestions for sampling designs. Environ. Monit. Assess. 187. https://doi.org/10.1007/s10661-015-4741-x

Lauer, K., Albrecht, C., Salat, C., Felix-Henningsen, P., 2010. Complex effective relative permittivity of soil samples from the taunus region (Germany). J. Earth Sci. 21, 961–967. https://doi.org/10.1007/s12583-010-0149-2

Li, L., Xia, Y., Liu, S., Zhang, W., Chen, X., Zheng, H., Qiu, H., He, X., Su, Y., 2015.

Modified Method for Estimating Organic Carbon Density in Discontinuous Karst Soil Using Ground-Penetrating Radar and Geostatistics. J. Mt. Sci. 12, 1229–1240. https://doi.org/10.1007/s11629-015-3431-z

Liu, C., Liu, G., Li, H., Wang, X., Chen, H., Dan, C., Shen, E., Shu, C., 2021. Using ground-penetrating radar to investigate the thickness of mollic epipedons developed from loessial parent material. Soil Tillage Res. 212, 105047. https://doi.org/10.1016/j.still.2021.105047

Liu, X., Dong, X., Leskovar, D.I., 2016. Ground penetrating radar for underground sensing in agriculture: A review. Int. Agrophysics 30, 533–543. https://doi.org/10.1515/intag-2016-0010

Muukkonen, P., Häkkinen, M., Mäkipää, R., 2009. Spatial variation in soil carbon in the organic layer of managed boreal forest soil-implications for sampling design. Environ. Monit. Assess. 158, 67–76. https://doi.org/10.1007/s10661-008-0565-2

Reppert, P.M., Morgan, F.D., Toksoz, M.N., 2000. Dielectric constant determination using ground-penetrating radar reflection coefficients. J. Appl. Geophys. 43, 189–197. https://doi.org/10.1016/S0926-9851(99)00058-0

Saarenketo, T., 1998. Electrical properties of water in clay and silty soils. J. Appl. Geophys. 40, 73–88. https://doi.org/10.1016/S0926-9851(98)00017-2

Salat, C., Junge, A., 2010. Dielectric permittivity of fine-grained fractions of soil samples from eastern Spain at 200 MHz. Geophysics 75, J1–J9. https://doi.org/10.1190/1.3294859

Šamonil, P., Phillips, J., Daněk, P., Beneš, V., Pawlik, L., 2020. Soil, regolith, and weathered rock: Theoretical concepts and evolution in old-growth temperate forests, Central Europe. Geoderma 368, 114261. https://doi.org/10.1016/j.geoderma.2020.114261

Šamonil, P., Valtera, M., Bek, S., Šebková, B., Vrška, T., Houška, J., 2011. Soil variability through spatial scales in a permanently disturbed natural spruce-fir-beech forest. Eur. J. For. Res. 130, 1075–1091. https://doi.org/10.1007/s10342-011-0496-2

Schaller, M., Dal Bo, I., Ehlers, T.A., Klotzsche, A., Drews, R., Fuentes Espoz, J.P., Van Der Kruk, J., 2020. Comparison of regolith physical and chemical characteristics with geophysical data along a climate and ecological gradient, Chilean Coastal Cordillera (26 to 38° S). Soil 6, 629–647. https://doi.org/10.5194/soil-6-629-2020

Schiavo, J.A., Pessenda, L.C.R., Buso Júnior, A.A., Calegari, M.R., Fornari, M., Secretti, M.L., Pereira, M.G., Mayle, F.E., 2020. Genesis and variation spatial of Podzol in depressions of the Barreiras Formation, northeastern Espírito Santo

State, Brazil, and its implications for Quaternary climate change. J. South Am. Earth Sci. 98, 102435. https://doi.org/10.1016/j.jsames.2019.102435

Slater, L., Comas, X., 2009. The Contribution of Ground Penetrating Radar to Water Resource Research, First Edit. ed, Ground Penetrating Radar Theory and Applications. Elsevier. https://doi.org/10.1016/B978-0-444-53348-7.00010-7

Strand, L.T., Callesen, I., Dalsgaard, L., de Wit, H.A., 2016. Carbon and nitrogen stocks in Norwegian forest soils — the importance of soil formation, climate, and vegetation type for organic matter accumulation. Can. J. For. Res. 1473, 1–15. https://doi.org/10.1139/cjfr-2015-0467

Strobbia, C., Cassiani, G., 2007. Multilayer ground-penetrating radar guided waves in shallow soil layers for estimating soil water content. Geophysics 72, J17. https://doi.org/10.1190/1.2716374

Valtera, M., Šamonil, P., Boublík, K., 2013. Soil variability in naturally disturbed Norway spruce forests in the Carpathians: Bridging spatial scales. For. Ecol. Manage. 310, 134–146. https://doi.org/10.1016/j.foreco.2013.08.004

van Dam, R.L., van den Berg, E.H., van Heteren, S., Kasse, C., Kenter, J. a. M., Groen, K., 2002. Influence of Organic Matter in Soils on Radar-Wave Reflection: Sedimentological Implications. J. Sediment. Res. 72, 341–352. https://doi.org/10.1306/092401720341

van der Kruk, J., Streich, R., Green, A.G., 2006. Properties of surface waveguides derived from separate and joint inversion of dispersive TE and TM GPR data. Geophysics 71, K19. https://doi.org/10.1190/1.3467444

Voronin, A.Y., Savin, I.Y., 2018. GPR Diagnostics of Chernozem Humus Horizon Thickness. Russ. Agric. Sci. 44, 250–255. https://doi.org/10.3103/s1068367418030199

Wiesmeier, M., Urbanski, L., Hobley, E., Lang, B., von Lützow, M., Marin-Spiotta, E., van Wesemael, B., Rabot, E., Ließ, M., Garcia-Franco, N., Wollschläger, U., Vogel, H.J., Kögel-Knabner, I., 2019. Soil organic carbon storage as a key function of soils - A review of drivers and indicators at various scales. Geoderma 333, 149–162. https://doi.org/10.1016/j.geoderma.2018.07.026

Winkelbauer, J., Völkel, J., Leopold, M., Bernt, N., 2011. Methods of surveying the thickness of humous horizons using ground penetrating radar (GPR): An example from the Garmisch-Partenkirchen area of the Northern Alps. Eur. J. For. Res. 130, 799–812. https://doi.org/10.1007/s10342-010-0472-2

Zajícová, K., Chuman, T., 2021. Spatial variability of forest floor and topsoil thicknesses and their relation to topography and forest stand characteristics in managed forests of Norway spruce and European beech. Eur. J. For. Res. 140, 77–

90. https://doi.org/10.1007/s10342-020-01316-1

Zajícová, K., Chuman, T., 2019. Application of ground penetrating radar methods in soil studies: A review. Geoderma 343, 116–129. https://doi.org/10.1016/j.geoderma.2019.02.024

Zhang, J., Lin, H., Doolittle, J., 2014. Soil layering and preferential flow impacts on seasonal changes of GPR signals in two contrasting soils. Geoderma 213, 560–569. https://doi.org/10.1016/j.geoderma.2013.08.035